INVESTIGATION INTO A NEW CPT-BASED DESIGN METHOD FOR LARGE DIAMETER MONOPILES IN SAND

Willemijn Foursoff

TU Delft

FUGRO

MSc in Offshore and Dredging Engineering, Bottom Founded Offshore Structures

MSc thesis

"Investigation into a new CPT-based design method for large diameter monopiles in sand"

Willemijn Foursoff

Delft University of Technology

Offshore and Dredging Engineering &

Geo Engineering

Prof. K.G. Gavin	TU Delft
Dr. L.J. Prendergast	TU Delft/ University of Nottingham
Dr. F. Pisanò	TU Delft
Ir. B.F.J. van Dijk	Fugro
Ir. J.M.C. Lascols	Fugro

Preface

This thesis is written as final requirement in order to obtain the MSc degree in Offshore- and Dredging Engineering with a specialization in Bottom Founded Offshore structures. The research has been conducted during the past 12 months at Fugro in Nootdorp, The Netherlands. During this period, I have been supervised by Luke Prendergast from TU Delft, Bas van Dijk and Judith Lascols from Fugro.

Fugro is a global leader in offshore survey, offshore geotechnical and seabed geophysical services, and has significant experience in the design and installation of foundations and infrastructure for numerous global offshore wind projects. They acquire the technical data and information required to design, construct and maintain (offshore) structures and add value through processing, interpretation and visualisation.

The research that is described in this thesis is interesting for anyone who would like to develop an improved design method for offshore wind turbines based on cone penetration test- (CPT) and pile load test (PLT) data. For this thesis, the PISA (PIle Soil Analysis) project made CPT- and PLT data available that was recorded in Dunkirk. Without this data it would not have been possible to evaluate the performance of existing (CPT-based) *p-y* methods and to investigate the development of a new *p-y* method.

During this thesis, I have been helped by many people. First of all, I would like to thank everyone of the Client Delivery Department at Fugro. I have enjoyed the friendly and helpful environment that I experienced during the 12 months I have spent at this department. Specifically, I would like to thank my supervisors at Fugro, Bas van Dijk and Judith Lascols, for providing me with daily guidance and their extensive knowledge of soil characteristics and pile-soil interaction. From the TU Delft, I would like to thank Luke Prendergast, who provided me with academic guidance and the MATLAB skills needed for conducting this thesis. We have had many interesting discussions on the research topic. I would also like to thank the rest of my graduation committee, Federico Pisanò and Ken Gavin for taking the time to study my thesis and listen to my presentation.

Last but not least, I would like to thank family and friends for proof-reading, commenting and providing mental support during the entire research. This has been very valuable to me and I am grateful to have had such good support. In particular, many thanks to Mathijs van Schaik for helping me to correct, shape and finetune the report.

Executive summary

The API RP 2GEO (2011) *p-y* method is an industry standard approach to predict the lateral pile behaviour of slender oil platform piles with length (L) over diameter (D) ratios > 10. However, offshore wind turbines are founded on large diameter monopiles with an *L/D* ratio < 8, which are rather rigid piles. There are concerns about the applicability of the standard *p-y* approach to piles that have low *L/D* ratios and it is expected that other soil reaction terms such as base shear, base moment and distributed moment also play a role in rigid pile behaviour (Davidson & Donovan, 1983).

Due to the increasing demand for renewable energy, the offshore industry is taking a leap when it comes to the development of offshore wind parks. Because power generated by a wind turbine is directly related to rotor diameter and thus to monopile dimensions, it is expected that monopiles with even lower *L/D* ratios will become standard. With the prospect that 27 % of European energy should be generated by renewable energy sources by 2030 (EUCO 169/14, 2014), efficient design methods for offshore wind turbine foundations are desired. Therefore, in this thesis, the performance of the current design approach is analysed and an investigation is conducted into the development of a new design method for large diameter piles in sand that are tailored to the offshore wind industry.

In 2013, the PISA (PIle Soil Analysis) project, a joint industry research project, has been established to develop a new design method for large diameter monopiles under lateral loading. As part of the project, pile load tests (PLTs) and cone penetration tests (CPTs) were performed in Dunkirk, in sand. This new (unpublished) design method includes the derivation of soil springs, that represent the additional soil reaction terms, by using complicated Finite Element Method (FEM) calculations which require input from advanced laboratory tests. Even though these calculations are accurate, they are also time-consuming. In the past two decades, several cone penetration test (CPT)-based *p-y* methods have been published. With these methods, *p-y* soil springs are derived directly from CPT data and used as input in a pile-response model, avoiding the necessity of advanced laboratory testing and FEM calculations.

In this thesis, the performance of CPT-based *p-y* methods, compared to the current approach is evaluated by using the API RP 2GEO *p-y* method (2011) together with CPT-based *p-y* methods published by Novello (1999), Dyson & Randolph (2001), Li, Igoe & Gavin (2014) and Suryasentana & Lehane (2016) to simulate the pile behaviour of short (*L/D*=3), medium (*L/D*=5.25) and large (*L/D*=8) piles that were tested in Dunkirk during the PISA project. A pile-response model is built in MATLAB to perform these calculations quickly and accurately. It is found that the API *p-y* method generally overestimates the pile response compared to results of CPT-based *p-y* methods and PLT measurements, especially for the short pile. Therefore it can be concluded that the current API *p-y* approach is not sufficient for predicting short pile behaviour. The CPT-based *p-y* methods predict stiffer responses, yet not stiff enough to match PLT measurements of the short pile. This strengthens the expectations that for short pile behaviour, apart from the *p-y* term, also other soil reaction terms play a role.

Still, the largest contribution to pile displacement *y* is determined by the lateral soil pressure *p* (Byrne, et al., 2015a). Therefore, the development of a new *p-y* method based on the longest pile (*L/D*=8) that was available from the PISA PLT data set is investigated first. This investigation involves processing PISA PLT data into pile displacement- and soil pressure

profiles. During this process, it is found that the direct differentiation of raw PISA measurement data comes with problems and results into wiggly soil pressure profiles. Curve fitting the moment profile has been applied in an attempt to overcome this issue. In this thesis, all 'simple' MATLAB curve fitting techniques have been analysed for the pile with *L/D*=8. The curve fitting techniques that have been investigated can be separated into four different types: global polynomials, interpolation splines, smoothing splines and least-squares splines. The 'simple' MATLAB curve fitting techniques in combination with the PISA PLT data did not result in a trustworthy pressure profile. Hence it was not feasible to continue the research into a new CPT-based *p-y* method based on the 'simple' MATLAB curve fitting techniques and the PISA data that was available.

However, a future work approach is presented that can be used as a guideline for further research into the development of a new CPT-based design method for large diameter monopiles. A step-by-step approach is given for the complete derivation of CPT-based *p-y* curves from PLT data, together with the first steps for deriving springs for the additional soil reaction terms. The future work approach elaborates on data gathering, PLT testing, PLT data processing, curve fitting, how to the link *p-y* curves to *qc* data, and what formulas can be used as a preliminary basis for the derivation of the base shear, base moment and distributed moment. Following the future work approach created in this thesis, an accurate and cost efficient design method for offshore wind turbines could be developed that positively contributes to the energy transition and a sustainable environment.

List of abbreviations

API	American Petroleum Institute
CPT	Cone penetration test
FEM	Finite element analysis
FLS	Fatigue limit state
LVDT	Lateral velocity displacement transducers
PISA	PIle Soil Analysis
PLT	Pile load test
OWT	Offshore wind turbine
SLS	Serviceability limit state
ULS	Ultimate limit state

C1, C2, C3	Coefficients function of soil friction angle φ' (API)
D	Diameter
Dr	Relative density
E	Youngs' modulus
F	Force
fs	Sleeve friction
Gmax	Max shear modulus
HG	Laterally applied load
I	Second moment of area
K0	Coefficient of earth pressure at rest
ki	Initial spring stiffness
Ks	Spring stiffness
L	Pile length
Δl	Beam element length
M	Moment
MB	Base moment
MG	Ground moment
p	Lateral soil pressure at pile lateral displacement y
pu	Ultimate unit lateral soil resistance
pud	Ultimate unit lateral soil resistance for deep failure mode
pus	Ultimate unit lateral soil resistance for shallow failure mode
qc	Cone friction
r	Radius of the instrument from the neutral axis of the pile section
t	Wall thickness
ug	Water pressure at ground level
y	Displacement
y0	Ground displacement

yB	Base displacement
z	Depth
γ	Unit weight
γ'	Effective unit weight
ϵ	Extension
ε	Strain
θ	Rotation
θ_0	Ground rotation
θ_B	Base rotation
σ_v	Vertical stress
σ_v'	Effective vertical stress
υ	Poisson ratio
ϕ	Curvature
φ_{cv}	Constant friction angle
φ_{peak}	Peak friction angle
φ'	Effective angle of internal friction

Table of Contents

Part 3: Investigation into a new CPT-based *p-y* method

Part 4: Future work

Part 1:

Introduction and literature study

This thesis starts with an introduction of the current situation and introduces the problem statement along with the research structure for this thesis. Subsequently an extensive literature study is performed on all subjects that are relevant for the development of a CPT-based design method for large diameter monopiles in sand.

1. Introduction

In the design of offshore wind monopile foundations, lateral pile behaviour is often investigated by means of *p-y* curves. *p-y* curves are based on a Winkler modelling approach and are developed from field tests on long slender piles. However, offshore wind turbines are often founded on short and rigid monopiles, and therefore it is concerned that the current *p-y* approach may not be accurate enough to predict the behaviour of offshore wind turbines. In this chapter, the current situation and some promising developments are discussed, after which the aims and objectives of this thesis are formulated.

1.1 Current situation

Based on the Winkler assumption, the soil surrounding laterally loaded foundation piles is usually modelled as independent non-linear lateral springs. The lateral soil springs represent the soil stiffness and are called *p-y* curves, where *p* is the soil pressure per unit length of the pile [MN/m] and *y* is the pile displacement [m]. In Figure 1-1 is shown how the soil response is modelled by a series of non-linear *p-y* curves that vary with depth and soil type.

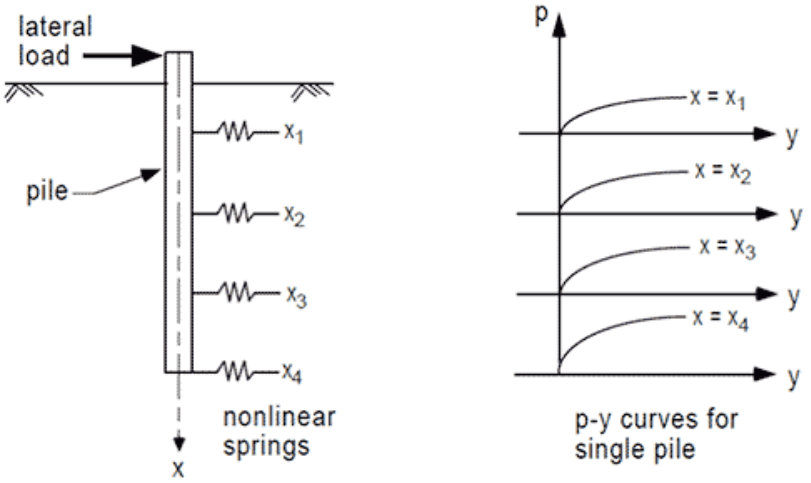

Figure 1-1: Model representing lateral pile behaviour (Lemnitzer, 2013)

Several *p-y* design methods for laterally loaded piles were first developed between the 1940's and 1950's when oil and gas companies were building offshore structures that had to sustain heavy horizontal loads during storm loading conditions. The standard *p-y* curve methods used in the offshore oil & gas practice are based on empirical studies of pile load tests performed on piles with an outer diameter of less than 1 m and a length *L* over diameter *D* ratio of 34 (Reese, et al., 1974; O'Neill & Murchison, 1983). These *p-y* methods are included in the API RP 2GEO guideline (API, 2011) and have become the current industry standard approach to predict the lateral displacement of piles with an *L/D* ratio > 10. In this thesis this standard *p-y* design method will be referred to as the API method.

Offshore wind turbines are often founded on large diameter monopiles that have an $L/D < 8$, which are rather called intermediate or short pile foundations, see Table 1-1 and Table 1-2. When piles with such *L/D* ratios (or lower) are simulated according to the API method, the resulting pile head deflections are larger than actually measured (Davidson & Donovan, 1983). Therefore it is concerned that the API method may underestimate the soil stiffness of piles with low *L/D* ratios and that when applied to monopiles for offshore wind turbines, it leads to overly conservative foundation designs than required for the limit state criteria.

Table 1-1: Typical pile dimensions

Foundation type	Diameter [m]	Production of
Jacket pile foundation	2	Oil & gas
Monopile foundation	4-6	5 MW wind power
Monopile foundation expected	10	10 MW wind power

Table 1-2: Pile definition

L/D	Pile defined as
<3	Short
3-6	Intermediate
8-10	Long
>10	Very long

During the United Nations Climate Change Conference is agreed on the target that 27% of the total energy consumed in the EU must be renewable by 2030 (EUCO 169/14, 2014). With this prospect, more significance is given to the development of offshore wind parks. At this moment a net total of 169 GW wind energy is installed in Europe from which 15.8 GW is produced by offshore wind (Windeurope, 2018). It is estimated that in 2030 320 GW wind is installed, of which 66 GW comes from offshore wind (Corbetta, et al., 2015). The efficiency of offshore wind power is related to the rotor diameter of a wind turbine, see Figure 1-2. Rotor diameters, and consequently required monopile diameters, increased considerably over the past decades and are expected to grow further in the future (Figure 1-3). This also means that typical *L/D* ratios for monopiles will decrease even more.

The costs for monopile foundations can accumulate to 35% of the installation costs, in contrast to oil and gas platforms for which the foundation costs contribute to a much smaller portion. (Byrne & Houlsby, 2004). On top of that, an offshore wind park generally includes a number of turbine locations (50-200), therefore an optimised foundation design for wind turbines (leading to shorter required pile lengths) may considerably reduce the total costs of an offshore wind project.

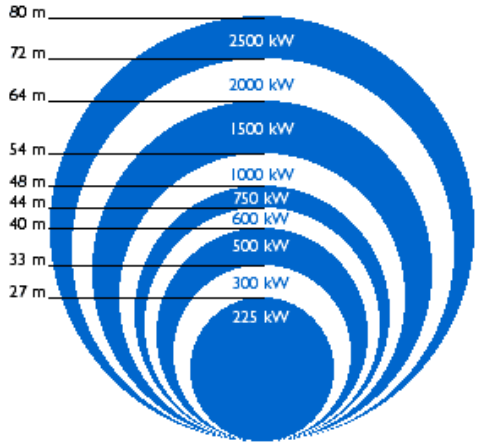

Figure 1-2: Wind power vs. rotor diameter (Bussel, 2008)

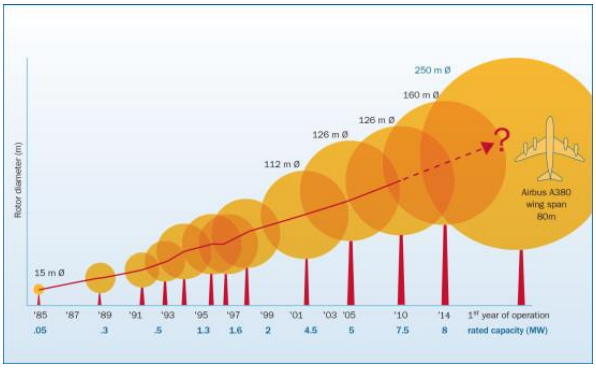

Figure 1-3: Rotor diameters vs. time

1.2 Promising developments

1.2.1 PISA project

In 2013, the Pile Soil Analysis (PISA) project was launched to get a better insight in the lateral soil response of large diameter monopiles and to develop optimised design methods. The project focused on lateral monotonic loading of piles in the North Sea. As part of the project, pile load tests (PLTs) and cone penetration tests (CPTs) were performed in Dunkirk (sand) and Cowden (clay), as these two sites that were found to be representative for North Sea soil conditions. (Byrne, et al., 2017)

The PISA project included the three following steps:

(i) *Numerical Finite Element Modelling (FEM) and laboratory testing*

With a 3D numerical FEM model, pile deformation under monotonic lateral loading was investigated and it showed that apart from the lateral soil pressure (*p-y*), also the base moment (M_b), base shear (F_b) and vertical shear stresses (τ) contribute to laterally pile behaviour for short piles. In Figure 1-4 (left) the current situation is depicted in which is accounted for *p-y* curves only, Figure 1-4 (right) shows the findings of the PISA project, in which all soil reaction terms are included. Because the FEM model requires information about soil characteristics as input, intensive laboratory- and field tests were performed prior to the numerical investigation.

(ii) *Development of a new design method*

In the second phase of the project a relation for each contributing soil reaction term has been developed.

(iii) *On-site pile load testing*

In the third phase of the project several pile load tests (PLT) were performed on a range of pile geometries on both field test sites. During these pile load tests among other things, the pile head displacement and rotation was measured to validate the new design method.

The new design method showed good resemblance to the measured displacements. However, the PISA project developed new design methods based on the results of extensive on-site and advanced laboratory testing which fed into the 3D FEM analyses. To perform this for an entire offshore wind park with a large number of wind turbines this would be a time-consuming and expensive operation.

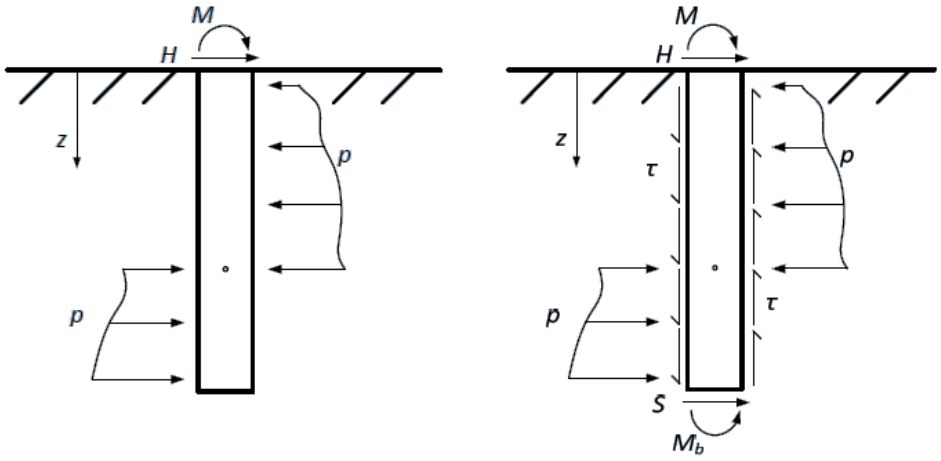

Figure 1-4: Current and new method with additional soil reaction terms short pile

1.2.2 Cone penetration tests

Apart from laboratory tests, in-situ field tests such as cone penetration tests (CPT) are common ways to investigate soil characteristics. During a CPT, a cone is pushed vertically into the soil, while the cone resistance, *qc*, is constantly measured. The cone resistance is related to the in-situ horizontal effective stress and therefore it can be convenient to express *p-y* curves in terms of *qc* (Houlsby & Hitchman, 1988; Novello, 1999). CPT measurements are much cheaper and less time consuming to perform compared to advanced laboratory testing. A CPT-based *p-y* method is therefore a potentially interesting method to determine the soil stiffness and lateral behaviour of piles as it also avoids the need of finite element modelling. In the last two decades, four different relations for CPT-based *p-y* spring have been published, that can be used directly into a pile response model. Novello (1999) and Dyson & Randolp (2001) both published a CPT-based *p-y* method that was derived by means of regression analysis and PLT results of on small scale centrifuge model piles in calcareous sands (Novello, 1999; Dyson & Randolph, 2001). Recent CPT-based *p-y* methods have been proposed that are developed from FEM analysis and PLTs on rigid piles in siliceous sand (Li, et al., 2014; Suryasentana & Lehane, 2016). These CPT-based *p-y* methods are discussed in more detail in Subsection 2.4, Literature Study.

1.3 Aims and objective

The current API *p-y* method may be overly conservative and may not provide the most optimised foundation for offshore wind turbines. Using *p-y* springs derived from FEM analysis lead to a better match with PLT measurements, but it is an expensive and time consuming method. A cheaper and quicker method may be to use soil springs that are directly derived from CPT measurements. Therefore, the aim of this thesis is to evaluate the performance of the current API *p-y* method compared to existing CPT-based *p-y* methods on short piles and to investigate an approach for the development of a new CPT based design method for large diameter monopiles in sand.

1.3.1 Objective

Evaluation of existing (CPT-based) *p-y* methods in sand and investigation into an approach for the development of a new CPT-based design method for large diameter monopiles in sand typically used in the offshore wind industry.

1.3.2 Scope

The focus of this thesis is on lateral pile behaviour of large diameter monopiles (L/D<8) subject to static loading in sand soil conditions that are typically found in the North Sea .

The investigation is based on data from pile load tests (PLTs) and cone penetration tests (CPTs) that have been performed at the Dunkirk site during the PISA project. CPT data gives information about the soil characteristics in Dunkirk and PLT data gives information on the loading and deformation of the piles during the tests. Chapter 3 elaborates further on the measurements that have been recorded during the PISA project, a summary of the data that is provided for this thesis, is presented in Table 3-1.

1.3.3 Research structure

An overview of the research structure is presented in Table 1-3. This research starts with an extensive literature study that is the theoretical backbone for the development of a new CPT-based method. In the second research part, the performance of existing (CPT-based) *p-y* methods is evaluated for a range of pile geometries that were tested in Dunkirk, during the PISA project. In order to perform this evaluation, the Dunkirk site conditions and characteristics are analysed first, after which a pile-response model is developed in MATLAB and validated with Fugro inhouse software. The pile-response model is used to calculate pile head displacements according to each of the (CPT-based) *p-y* methods and to compare the results with displacements measured during pile load tests at the Dunkirk site. In the third research part, an approach to develop a new (CPT-based) method is investigated. PLT data of the longest pile that has been tested in the PISA project is processed into pile displacement and soil pressure profiles. This part also addresses uncertainties in pile load test measurements and the pitfalls inherent to the development of such profiles. In the final part of this research, recommendations for further research are given and a future work approach is presented which can be used as a guideline to develop a new CPT-based design method for large diameter piles.

Table 1-3: Research structure

Part 1: Introduction and literature study

1. Introduction
2. Literature study

Part 2: Evaluation of existing *p-y* methods

3. Soil and site analysis
4. Pile-response model
5. Evaluation of *p-y* methods

Part 3: Investigation into a new CPT based *p-y* method

6. PLT data processing
7. Curve fitting assessment
8. Conclusions

Part 4: Future work

9. Recommendations & Future work approach

2. Literature study

This chapter treats the literature that is available on the subject of design principles for offshore foundations, lateral pile behaviour and . It introduces important facets of pile behaviour in sand, the critical differences between long and short pile failure types and presents the history, development and shortcomings of existing (CPT-based) pile design methods.

2.1 Design principles of offshore structures

Because the API *p-y* method is initially developed for the lateral pile behaviour of the jacket pile foundation of oil and gas platforms, it is relevant to compare the design principles of an offshore jacket platform with an offshore wind turbine. In Figure 2-1 and Figure 2-2, a typical offshore jacket platform and wind turbine are shown.

Figure 2-1: Offshore oil platform (Chen , 2016)

Figure 2-2: Offshore wind turbine (4 C Offshore, 2018)

The foundation of both offshore structures has to sustain horizontal loads from wind, waves and current (environmental loading) and the vertical weight of the structure itself. Though, the way in which the load is transferred to the structure's foundation is different. The weight of the heavy topside of the oil platform is carried on a multiple jacket pile foundation, while the light weighted wind turbine is founded on just one monopile. As a consequence, vertical loading is generally governing in the foundation design of a jacket platform, whereas for an offshore wind turbine its behaviour is mostly determined by horizontal loading and a large overturning moment, see Figure 2-3 (Hoving, 2016).

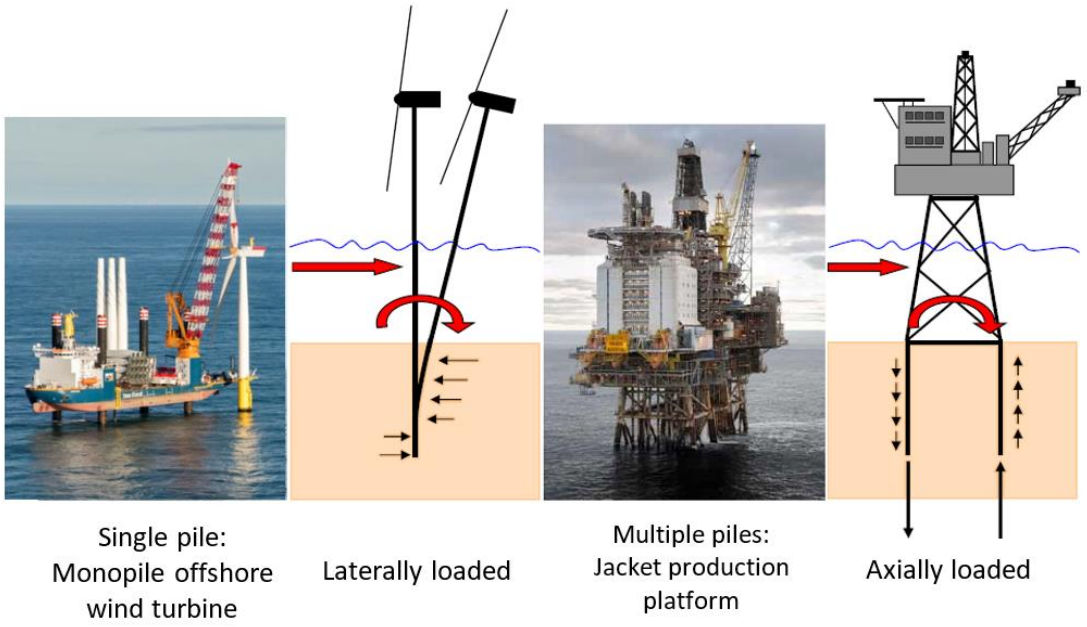

Figure 2-3: Behaviour monopile vs. jacket piles after (Hoving, 2016) and (Lourens, 2016)

Furthermore, a wind turbine has to withstand rotational loads coming from the rotor blades (operational loading). Wind, wave and blade rotation have a repetitive character, called cyclic loading, bringing the turbine into a dynamic response. When the frequency of the cyclic loads comes close to the natural frequency of the turbine, the system may resonate which causes severe damage to the wind turbine. The monopile should therefore be designed in such a way that its natural frequency is outside of the frequency ranges of the various considered cyclic environmental loads as shown in Figure 2-4. The natural frequency of the turbine is highly dependent on the material properties of the monopile and stiffness of the soil surrounding the pile. Therefore, it is important that the soil stiffness is predicted accurately to prevent premature failure.

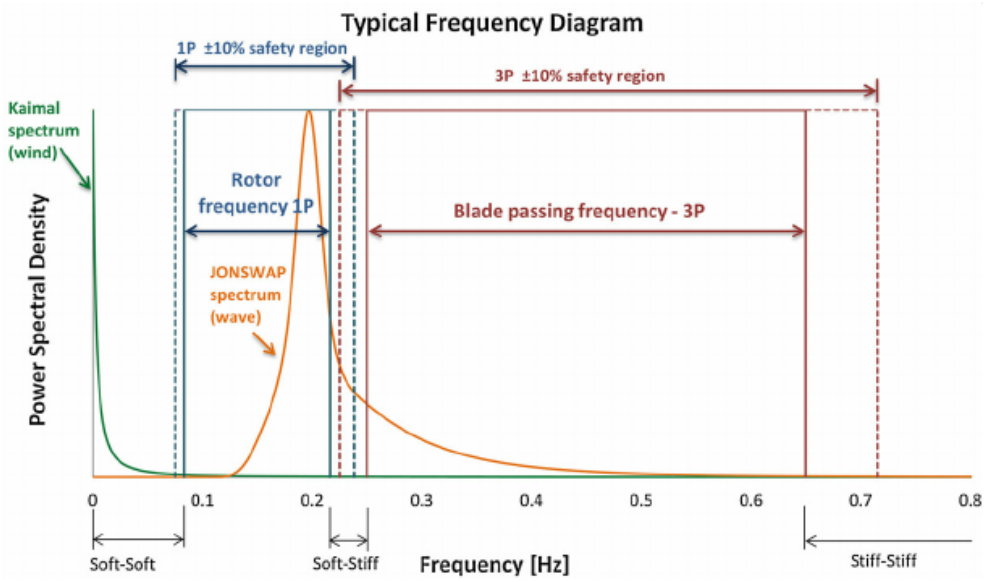

Figure 2-4: Frequency range of typical loads on OWT (Arany, et al., 2014)

To ensure that an offshore structure satisfies the design requirements regarding safety and performance, there are several design limit states that have to be taken into account (DNV-OS-J101, 2014). A design limit state describes specific criteria, about for example maximum loads or displacements, and are dependent on the structure's function, foundation type and load situations. The limit states that are considered the most significant for an offshore wind turbine are described in Table 2-1.

Table 2-1: Significant design limit states

Ultimate limit state (ULS)
The ultimate limit state corresponds to the maximum load capacity that a structure foundation can withstand before failure occurs.
Serviceability limit state (SLS)
The serviceability limit state corresponds to the usability of the structure and usually is related to maximum displacements or rotations of the foundation. Normally for a monopile, the pile head displacement, y_0, must not exceed a value that is 10% of the diameter $(y_0 < 0.1D)$ and the pile head rotation, θ_0, must not exceed 2° $(\theta_0 < 2^o)$ (Byrne, et al., 2015b).
Fatigue limit state (FLS)
The fatigue limit state corresponds to cumulative damage from repeated loading of the offshore structure. It is not related to the maximum load capacity, because repetitive loading can cause the structure to fail long before the maximum load capacity is reached. The maximum fatigue limit stress depends on the magnitude and frequency of the loads (number of load cycles).

The API *p-y* method is mainly concerned with avoiding the ultimate failure of offshore platforms. Nevertheless, the condition of an offshore wind turbine is dominated by cyclic loading and lateral displacements, and therefore the serviceability and fatigue limit states are extremely important too.

The first step in the development of cyclic loading methods involves an accurate base method for static loading. Therefore a good understanding of static behaviour is essential upon analysing cyclic behaviour. In this thesis is focused on static lateral pile behaviour only and cyclic loading is not examined further.

2.2 Lateral pile behaviour

In this section, the basics of static lateral pile behaviour is discussed, which involves the interaction between the pile and soil that occurs under lateral loading.

When a pile is loaded in horizontal direction (H), the soil behind the pile is under pressure and reacts with a force in opposite direction against the pile (passive soil reaction). The soil stresses on this side of the pile increase, while on the other side of the pile, soil stresses decrease due to the extra space that is provided by the displaced pile (active soil reaction). In a theoretical case where the pile is in a perfect vertical position, the mechanism is shown in Figure 2-5.

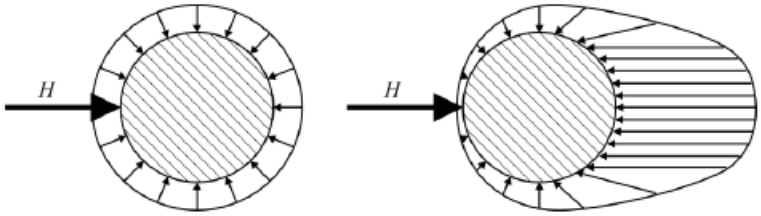

Figure 2-5: Soil stresses acting on the pile before (left) and after lateral loading (right) (Janoyan & Whelan (2004) top view of the pile

The (radial) passive soil stress can be decomposed in normal stresses acting on the frontal side and shear stresses acting on the side, this is shown in Figure 2-6 (left). Compared to the passive stress, the active stress is often so small that it is completely neglected. In current methods that are used to calculate the pile displacement, the soil stress *p* is regularly simplified to the model depicted in Figure 2-6 (right).

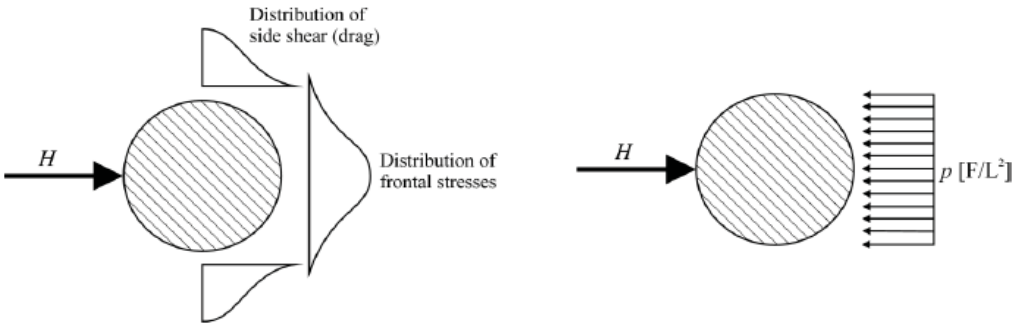

Figure 2-6: (left) Actual distribution of stresses (Baguelin, et al., 1977), (right) simplified soil stress.

The soil stress profile that is built up along the whole pile depth is called the lateral distributed soil pressure or soil resistance and should be in equilibrium with the applied load to ensure foundation stability. In Figure 2-7, the soil resistance profile according to Broms (1964) is shown for a slender pile.

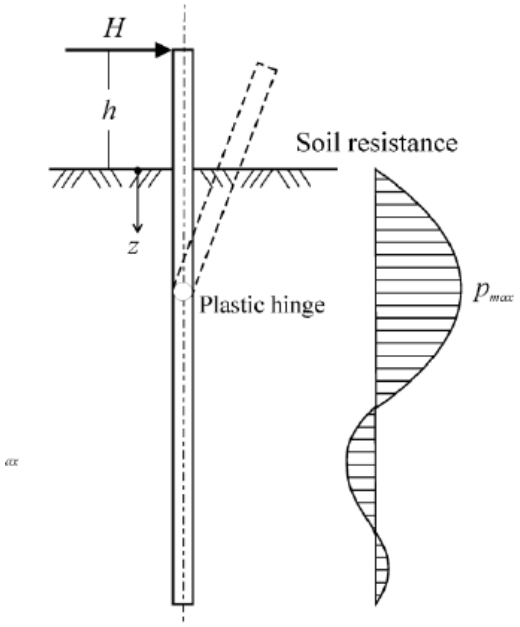

Figure 2-7: Soil resistance distribution for flexible piles (Broms, 1964)

2.3 *p-y* method

As explained Section 2.1, it is essential that the pile displacements under expected environmental and operational loads do not exceed the limit state criteria. In a pile-response model, a relation for the soil reaction can be incorporated in order to calculate the pile displacement under a certain load. A well-known method to simulate the soil reaction, is by means of the Winkler method, developed in 1867.

In the Winkler method, the soil reaction profile is modelled as a set of springs, see Figure 2-8 (left). The pile is simplified as a beam and divided in several 'beam elements'. Each of the local springs is assumed to act independently on a beam element and is referred to as the *p-y* curve or *p-y* spring, in which *p* is the soil pressure and *y* is the corresponding pile displacement. The spring stiffness, also called the sub-grade reaction modulus (K_{py}), represents the soil strength. Originally, the springs had an elastic character and the spring stiffness could easily be calculated by $K_{py} = p/y$ which is the constant slope of the *p-y* curve, shown in Figure 2-8 (right).

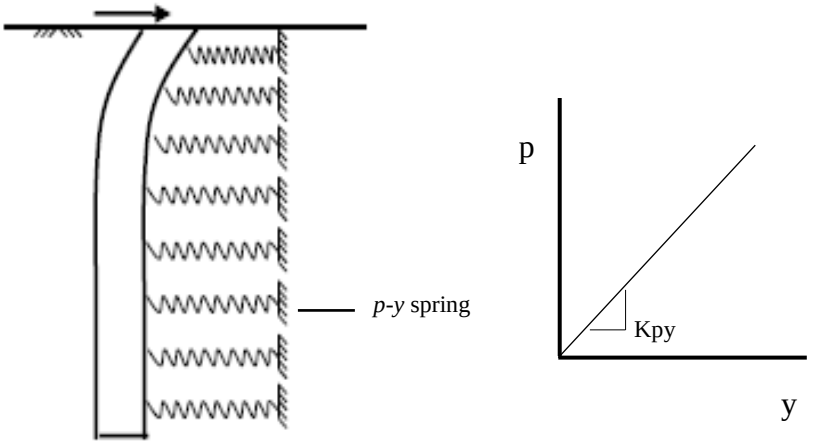

Figure 2-8: Winkler method applied to monopile (left) after (Huang, 2011) and linear stiffness curve (right)

However, soil does not have an elastic character and in 1958, McClelland & Focht proposed a *p-y* method in which non-linear soil behaviour is taken into account. Beyond a certain pile displacement the soil pressure reaches a maximum soil pressure p_u and instead of a constant spring stiffness, the stiffness thus decreases gradually with increasing pile displacement. p_u depends on local soil parameters and hence the *p-y* curves are depth specific. For an offshore wind turbine, the load-displacement method by means of non-linear *p-y* curves is depicted in Figure 2-9.

The pile itself is usually modelled as a beam by means of the Euler-Bernoulli beam theory. According to this theory, the lateral load induces lateral pressures and internal pile bending moments and do not include vertical shear forces in the model. For long slender piles (L/D>10), the vertical shear displacements induced by lateral loading are relatively small compared to pile bending moments (Byrne, et al., 2017) and can therefore be neglected. In a Timoshenko beam, the vertical shear force can be incorporated. The difference between the two beams can be seen in Figure 2-10. The beam equations for a small beam element by means of both theories are presented in Figure 2-11. Where *y* is the pile displacement at a depth *z*, *p* is the soil resistance per unit length, *Q* is the shear force, *M* is the moment and θ the rotational slope, κ is the Timoshenko shear coefficient and *G* is the shear modulus and *A* the cross sectional area.

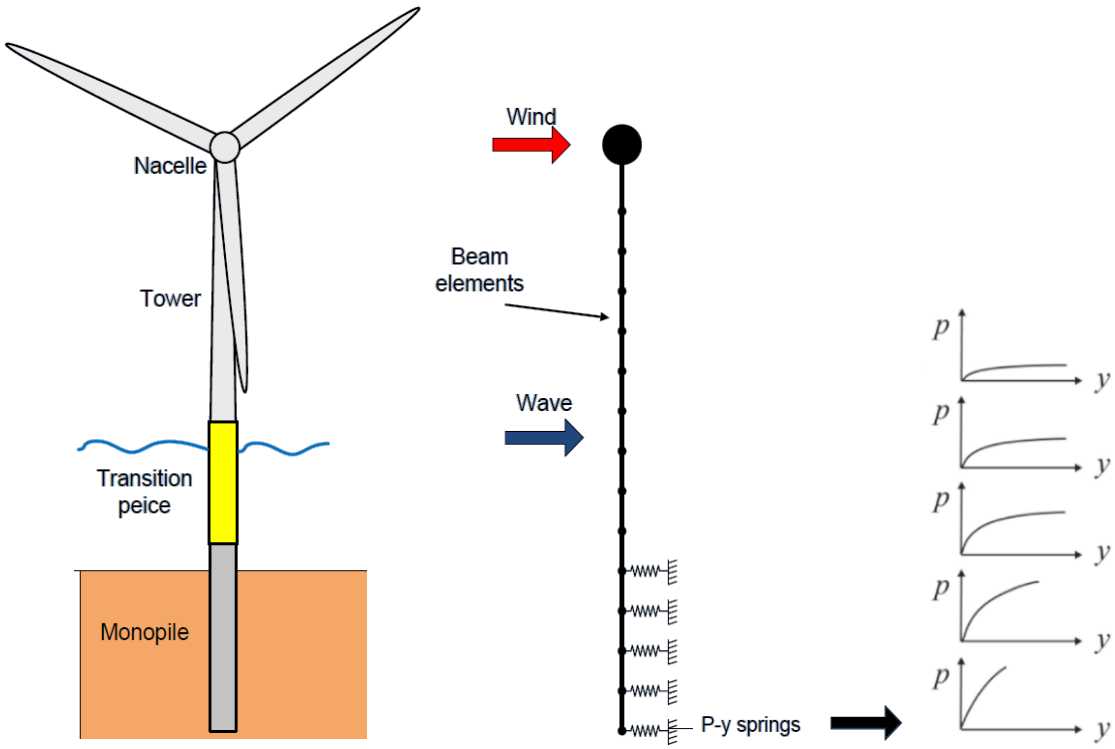

Figure 2-9: non-linear p-y method applied to offshore wind turbine after Liingaard (2013)

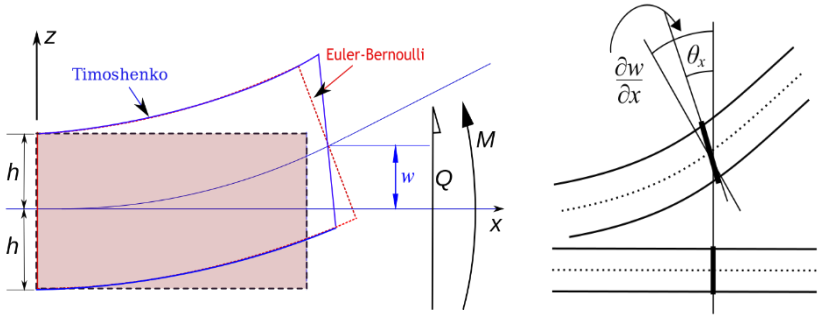

Figure 2-10: Deformation of an Euler beam and Timoshenko beam

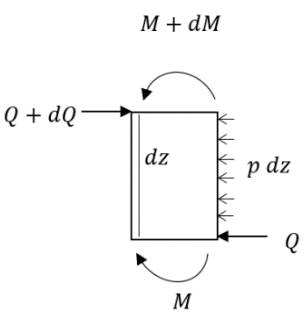

1. $EI\frac{d^4y}{dz^4} = -K_{py}\,y = -p$
2. $EI\frac{d^3y}{dz^3} = -Q$
3. $EI\frac{d^2y}{dz^2} = -M$
4. B: $\frac{dy}{dz} = \theta$

   T: $\frac{dy}{dz} = \theta - \frac{1}{\kappa AG}\frac{d^3y}{dz^3}$

Figure 2-11: Beam equation for small beam element with length dz

2.3.1 Derivation *p-y* springs

To make accurate predictions for a specific site, *p-y* curves are ideally derived from pile load tests performed on large scale piles. During a pile load test (PLT), the pile is subjected to known horizontal load increments while internal instruments measure the pile deformation, see Figure 2-12. When for a range of load increments the corresponding pile displacement and soil pressure (along the whole pile depth) are known, it is possible to construct depth-dependent *p-y* curves for a specific site.

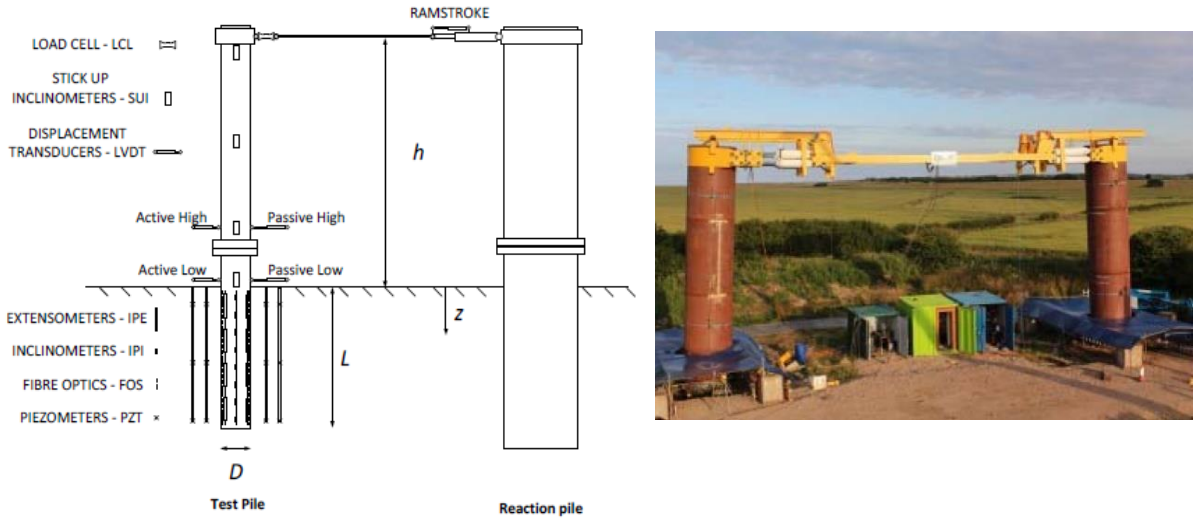

Figure 2-12: A fully instrumented pile for monotonic loading tests during the PISA project (Byrne, et al., 2015b) and (Liingaard, 2013)

In Figure 2-13, a typical loading plan is presented in which 9 load steps can be identified: a certain load step, H_G, is applied to the pile and remains constant until a desired pile head displacement is reached (creep), then the load is increased further to a new load step and the procedure continues until the pile has ultimately failed (e.g. reached displacements ($\frac{V_G}{D} >$ 10%)). (Byrne, et al., 2015b)

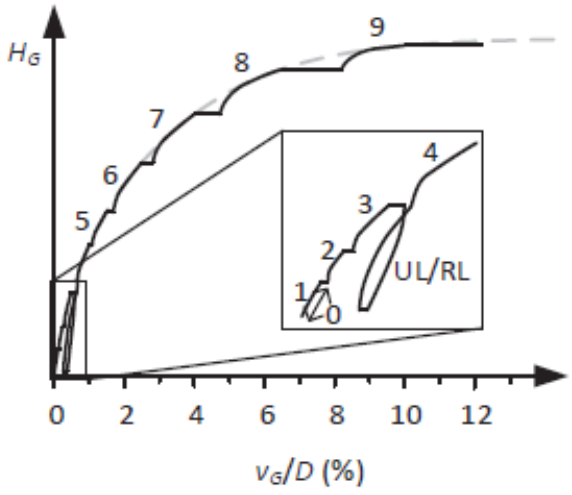

Figure 2-13: Typical loading procedure (Byrne, et al., 2015b)

Figure 2-12 (left) shows also all the instruments that are used during monotonic pile load testing in the PISA project. Instruments that are commonly used to gather information about the pile deflection are:

- Load cells: measure the load that is applied by the reaction pile to the test pile
- Inclinometers: measure the pile rotation from neutral line at front and back side of the pile
- Linear variable differential transformers (LVDTs): measure above ground displacements from which rotations can be determined
- Extensometers: measure the vertical extension that occurs due to pile bending
- Fibre optic strain gauges: measure the vertical strain that occurs due to pile bending

Strain can be derived from the extension data, but (if possible) it is better to use strain gauges as they give more accurate data results for the pile curvature (Byrne, et al., 2017). From strain data, the curvature and bending moment can be calculated with the following formulas:

1. *Curvature*

$$\phi = \frac{\varepsilon_{compression} - \varepsilon_{tension}}{D} \tag{2.1}$$

2. *Moment*

$$M = \phi\, EI \tag{2.2}$$

The displacement- and pressure profile are obtained by double integration and differentiation:

1. *Displacement*

$$y = \iint \phi dz + \theta_0 z + y_0 \tag{2.3}$$

2. *Pressure*

$$p = -\frac{d^2M}{dz^2} \tag{2.4}$$

ε is the strain measured at both sides of the pile (compression and tension), *EI* is the pile bending stiffness, *z* is the pile depth and θ_0 and y_0 are the ground- rotation and displacement. θ_0 and y_0 can be derived from above ground inclinometers or LVDT measurements. A schematization of the total approach is shown in Figure 2-14.

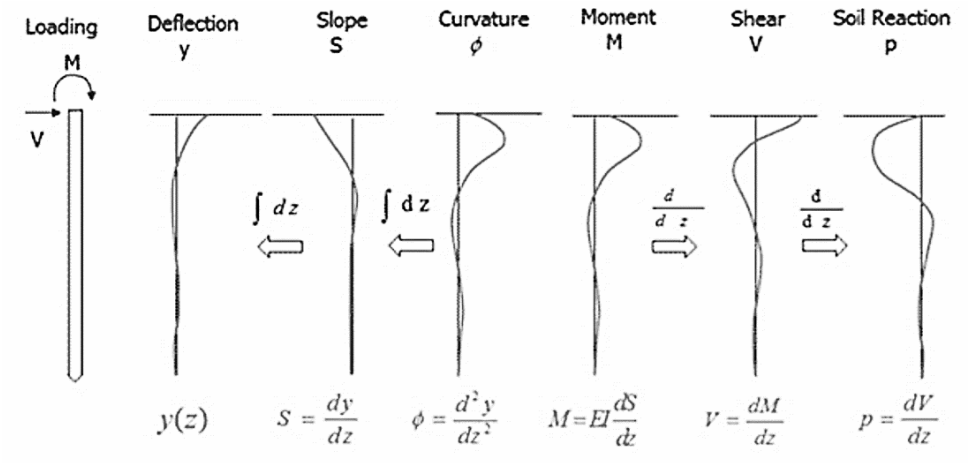

Figure 2-14: derivation of pile displacement and soil pressure from curvature data (Lemnitzer, 2013)

2.3.2 API method

Because it would be a time consuming and expensive operation to do pile load tests for each project, usually empirical *p-y* methods are used to predict the lateral pile displacement. Because of its easy to employ character, the API *p-y* method developed by (Reese, et al., 1974) and later simplified by (O'Neill & Murchison, 1983), is the most used method.

Originally (Reese, et al., 1974)proposed a *p-y* curve that consisted of four parts: an initial straight line, a parabolic part and two straight lines, see Figure 2-15. This *p-y* method is based on the results of pile load tests performed at Mustang Island, USA.

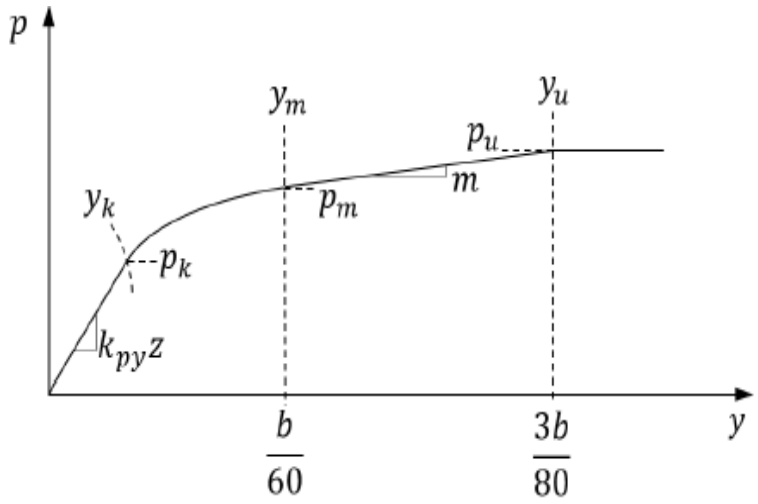

1. $p = K_{py}\, z\, y$
2. $p = C\, y^{\frac{1}{n}}, \quad C = \frac{p_m}{y_m^{\frac{1}{n}}}, \quad n = \frac{p_m}{m y_m}$
3. $m = \frac{p_u - p_m}{y_u - y_m}$
4. Beyond $y = \frac{3b}{80}$, $p = p_u$

Figure 2-15: p-y curves for sand (after Reese, Cox and Koop (1974).

The ultimate soil pressure p_u in the *p-y* curve is depth dependent, because failure modes for soil at deeper depth and near the surface are different. Near the surface, the soil fails in a wedge failure mode, while at deeper depths block failure mode is more likely to occur, see Figure 2-16.

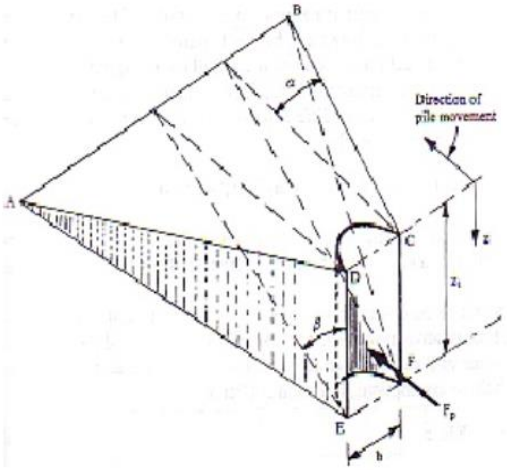

(a) Wedge failure mode

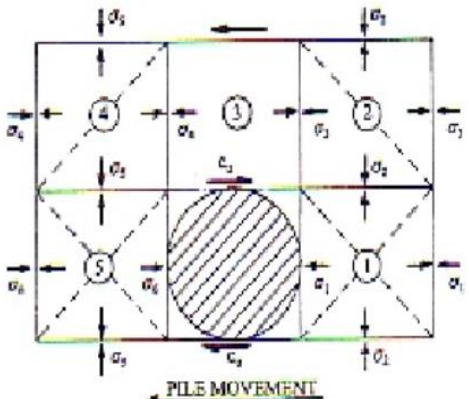

(b) Block failure mode

Figure 2-16: Two types of soil failure (Reese, et al., 1974)

Borgard & Matlock (1980) published Equations (2.5)-(2.7) to calculate the ultimate soil pressure in cohesionless soils at any given depth z in which γ' is the effective soil unit weight. The smallest value determines the ultimate soil pressure and shall be used in the *p-y* method. Functions to calculate an exact value for *C1*, *C2* and *C3* can be found in (API, 2011) or the coefficient can also be derived from Figure 2-17.

$$p_{us} = (C_1 z + C_2 D)\gamma' z \tag{2.5}$$

$$p_{ud} = C_3 D \gamma' z \tag{2.6}$$

$$p_u = \min[p_{us};\ p_{ud}] \tag{2.7}$$

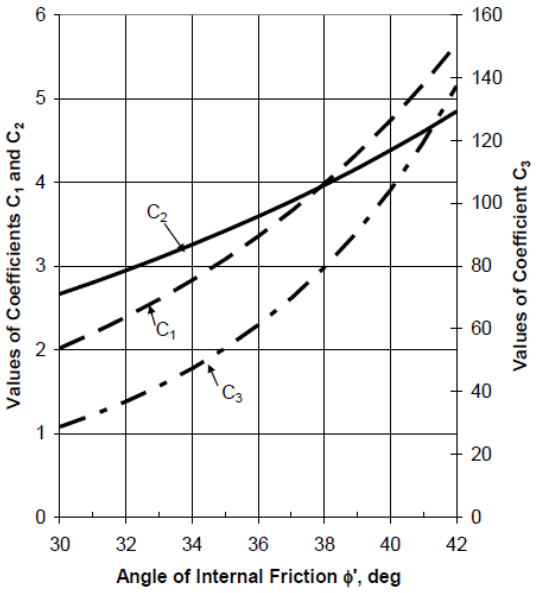

Figure 2-17: Coefficients for C1, C2 and C3 as function of the internal friction angle φ' (API, 2011)

In 1983, O'Neill & Murchison suggested a simplified version of the *p-y* curve that is described by just one hyperbolic tangent function, see Equation (2.8). The p_u is calculated with the Equations from above and the initial tangent stiffness k_1 from Table 2-2.

$$p = A \cdot p_u \left[\frac{k \cdot z}{A \cdot p_u} y\right] \tag{2.8}$$

$$A = \left(3.0 - 0.8 \frac{z}{D}\right) \geq 0.9 \text{ for static loading} \tag{2.9}$$

Table 2-2: Initial stiffness (API, 2011)

φ' [degrees]	k_1 [MN/m3]
25°	5.4
30°	11
35°	22
40°	45

The latter *p-y* method is included in the API guideline (API, 2011) and therefore became the current standard approach for deriving lateral pile displacement in cohesionless soils. An overview of the API *p-y* method is shown in Table 2-3.

The method is based on pile diameters <1m, but is found to give good predictions for piles with a diameter <2m and in comparable field test conditions (Peralta, 2010). However for piles with large diameters, the results can be less accurate. This statement has been made clear by a revision (F2.4.1) to the DNV guidance on the design of monopiles in DNV-OS-J101 (2014).

Table 2-3: Overview API method (Reese, et al., 1974), (O'Neill & Murchison, 1983), (API, 2011)

	API/ DNV
Date	O'neill and Murchinson 1983
Based on	Rees, Cox and Koop 1974;
Soil	Submerged dense fine sands, Mustang Island
L/D	D= 0.6m, *L/D*= 34

2.4 CPT- based *p-y* method

Worldwide, cone penetration tests (CPTs) are the most used in situ tests to determine the soil parameters and soil layers. The test consists of pushing an instrumented cone into the soil while forces on the tip and along the sleeve are measured. In Figure 2-18 the cone is illustrated. The total tip resistance q_c is the soil resistance acting on the tip of the cone and the sleeve friction f_s is the resistance developed between the soil and the sleeve of the cone (Titi & Abu-Farsakh, 1999). The cone resistance is related to the in-situ horizontal effective stress and therefore it can be convenient to express *p-y* curves in terms of qc (Houlsby & Hitchman, 1988; Novello, 1999)

Figure 2-18: Cone penetrometer with resistance parameters from (Lunne, et al., 1997)

As distinguished by (Ardalan, et al., 2009) the cone penetrometer can be seen as a mini-pile foundation, because the mean effective stress, compressibility and rigidity of the soil medium have a comparable influence on the pile as on the cone (Wrana, 2015). The q_c value is therefore widely used to make assumptions for the effective soil stress as the q_c value can be used to normalize site specific soil parameters, (Novello, 1999).

The CPT-based *p-y* methods that are mentioned in the introduction are discussed further in the next paragraphs.

2.4.1 Novello (1999)

In 1999, Novello researched the procedure for developing *p-y* curves for calcareous sands based on CPT measurements and continued on the research of Wesselink, et al (1988). In this research, empirical *p-y* curves were developed based on centrifuge models and small scale pile tests performed in Bass Strait calcareous sands and used CPT data and PLT data from a free-headed 2.137m diameter pile driven in 31.5 and a 0.356m diameter pile driven in 31.5 and 6.1m embedment. Novello found Equation ((2.10)) to describe a good fit to the pile load test results. An overview of the method is given in Table 2-4.

$$p = \min(\ 2\ \cdot D \cdot (\gamma' \cdot z)^{0.33}\ \cdot {q_c}^{0.67} \cdot \left(\frac{y}{D}\right)^{0.5}, D \cdot q_c) \tag{2.10}$$

Table 2-4: Overview CPT based p-y method Novello(1999)

	Novello
Date	1999
Based on	CPT, model PLT (Williams, et al., 1988), model centrifuge tests (Wesselink, et al., 1988)
Soil	Calcareous Bass Strait sands, dredged from Kingfisher B and Halibut A location
Pile	Driven steel pipe, free headed
Geometry	D= 21.37, *L/D* 14.7 and D= 0.356, *L/D*= 17.1

2.4.2 Dyson and Randolph (2001)

In 2001, Dyson and Randolph researched a method in which the *p-y* curve is linked to q_c plus is accounted for installation method, pile head restraint conditions and rate of loading. Their method used results from centrifuge tests on calcareous sand recovered from North-West Shelf of Australia (Dyson & Randolph, 2001), see Table 2-5. The *p-y* curve is based on the same power model proposed by (Wesselink, et al., 1988). Dyson & Randolph found Equation ((2.11)) to give a reasonable fit for a pile with free head conditions (Dyson & Randolph, 2001).

$$p = 2.84 \cdot D \cdot (\gamma' \cdot D) \cdot \left(\frac{q_c}{\gamma' \cdot D}\right)^{0.72} \cdot \left(\frac{y}{D}\right)^{0.64} \tag{2.11}$$

Table 2-5: Overview CPT based p-y method Dyson and Randolph(2001)

	Dyson & Randolph
Date	2001
Based on	CPT, centrifuge tests (N=160), small scale PLT
Soil	Calcareous sands recovered from seabed on North-West Shalf of Australia
Pile	Driven piles, free headed
Geometry	D= 13mm, *L/D*=26.15

2.4.3 Suryasentana & Lehane

The use of cone penetration testing became more popular and stimulated the research to *p-y* methods that were linked directly to q_c. Because previous published CPT-based *p-y* methods were derived from flexible piles in calcareous sands, Suryasentana and Lehane researched a new CPT-based *p-y* method that was numerically derived from both flexible and rigidpiles in siliceous sand (Suryasentana & Lehane, 2014a).

The research used Plaxis 3D Foundation to predict the response to lateral loads of the piles and to generate a CPT q_c profile. The output of this 3D FEM analysis comprised bending moment (M) and displacement (y) data for a given lateral load (Suryasentana & Lehane, 2014b). As explained above, by taking the double derivative of the moment profile the soil pressure profile could be derived. A model comparable to (Novello, 1999) method was used in a regression analysis to find an equation that relates the displacement, pressure and q_c parameters. This lead to the Equation (2.12).

$$p = 4.2 \cdot \gamma' \cdot z \cdot D \cdot \left(\frac{q_c}{\gamma' \cdot z}\right)^{0.68} \cdot \left(\frac{y}{D}\right)^{0.56} \quad (2.12)$$

Because the equation above overpredicted the soil stiffness for large loads, it was adjusted to give it a limiting character. This led to the exponential relation in Equation (2.13).

$$p = 2.4 \cdot \gamma' \cdot z \cdot D \cdot \left(\frac{q_c}{\gamma' \cdot z}\right)^{0.67} \cdot \left(\frac{z}{D}\right)^{0.75} \cdot \left[1 - exp\left(-6.2 \cdot \left(\frac{z}{D}\right)^{-1.2} \cdot \left(\frac{y}{D}\right)^{0.89}\right)\right] \quad (2.13)$$

Because the method was derived from computer simulated pile load tests, the method was also analysed for a set of historic cases, see Table 2-6. The results were good, encouraging the potential for CPT-based methods for laterally loaded piles. (Suryasentana & Lehane, 2014b).

Table 2-6: Overview CPT based p-y method (Suryasentana & Lehane, 2014a), (Suryasentana & Lehane, 2014b)

	Suryasentana & Lehane
Date	2014
Based on	CPT cavity expansion analogue, CPT, 3D FEM
Soil	10 hardening soil model parameters: ϕ'=36^o-51^o relative density= 28%-97%
Pile	10 piles: D=0.5-5m, L=21m, *L/D*= 42-4.2
Validation cases	1. Hampton, Virginia, Pando, et al., (2006) Sand deposit in Hampton, Virginia: Medium dense calcareous sands PC, PP, FRP D=0.6, *L/D*=28.3 2. Shenton Park, Perth, Luff (2007) Loose-medium dry dense dune sand at Shenton Park D=0.225m, *L/D*=15.6 3. C-Core, Canada (centrifuge scale test), Ramadan et al. (2013) Fully saturated dense sand at C-Core, Canada (centrifuge scale test: 70g) Open-ended aluminum pile D=1.4m, *L/D*= 12.5 4. Dry dense sand and deposit North Perth, Venville (2004) CFA, D=0.34m, *L/D*=17.6
Software	Plaxis 3D, Oasys ALP

2.4.4 Li, Igoe and Gavin (2014)

In 2014, Li, et al. investigated the performance of the previous developed CPT-based *p-y* curves: Equations (2.10)-(2.13) on rigid and flexible piles and presented an update to power-law model for rigid monopiles in siliceous sand. The model was based on a set of lateral pile load tests that was performed on six open-ended steel pipe piles driven in dense siliceous sand in Blessington, Ireland, an overview is given in Table 2-7. 5. This lead to the following *p-y* formulation in Equation (2.14).

$$p = 3.6 \cdot D \cdot (\gamma' \cdot D) \cdot \left(\frac{q_c}{\gamma' \cdot D}\right)^{0.72} \cdot \left(\frac{y}{D}\right)^{0.66} \tag{2.14}$$

Their research showed that for the flexible piles in siliceous sand Equation (2.10) from Novello (1999) and Equation (2.11) from Dyson and Randolph (2001) predict reasonable results. However, these methods overestimate the displacements for rigid piles.

The results predicted by the method of Li, et al (2014) was comparable to the results predicted with Equation (2.13) from Suryasentana & Lehane (2014a) and resembled the measured response for all six piles quite accurate. Therefore Li, et al (2014) recommended further studies to the performance of Equation (2.13) on a larger set of sand characteristics and pile geometries

Table 2-7: Overview CPT based p-y method Li, Igoe and Gavin (Li, et al., 2014)

	W. Li, D. Igoe, & K. Gavin
Date	2014
Based on	CPT
Soil	Blessington C. Wicklow, Ireland
	Site 1:UCD dense siliceous sand, water table -15m Igoe et al. (2011)
	Site 2: UCD dense siliceous sand, water table= -2.3m Gavin et al. (2013)
	RD= 100%
	Unit weigth= 20 kN/m^3
	ϕ_{cv} = 37^o, ϕ_{peak}= 54^o decreasing to 42^o
	q_c= 10 MPa decreasing to 25 MPa
Pile	Driven open-ended
Geometry	PS1: L= 2.20 m, *L/D*=6.5, PS2: L= 2.20 m, *L/D*=6.5, PS3: L= 4.35 m, *L/D*=12.8, PS4: L= 3.10 m, *L/D*=9.1. , PS5: L= 5 m, *L/D*=14.7, PS6: L= 7 m, *L/D*=20.6

2.4.5 Suryasentana & Lehane updated method

In 2016, Suryasentana & Lehane published another update to their previously derived CPT-based *p-y* method. Equation (2.13), showed some uncertainties related to the influence of pile bending stiffness, presence of water table, cross-sectional shape of the pile and soil non-homogeneities (Suryasentana & Lehane, 2016). These four effects were investigated by means of numerical experiments and led to a new CPT-based *p-y* method in Equation (2.15)-(2.18).

This updated Formulation is validated against 3D finite element calculations and data from a full-scale large diameter monopile foundation (Suryasentana & Lehane, 2016). The $q_c$profiles were derived with the spherical cavity expansion procedure just as is done for the first published CPT-based *p-y* Formulation (Suryasentana & Lehane, 2014a). An overview is given in Table 2-8.

The calculated pile head load-displacements differ less than 10% compared to the pile head load-displacements from the FE calculations. For the full scale offshore wind turbine, the measured bending moment profile is compared to the bending moment profile derived after using the updated Formulation in a standard *p-y* load transfer program. A good agreement was found (Suryasentana & Lehane, 2016).

$$p = G_{max} \cdot y; \qquad {}^{y}/_{D} \leq 0.0001 \tag{2.15}$$

$$p = p_u \cdot f(y); \qquad {}^{y}/_{D} \geq 0.01 \tag{2.16}$$

$$p_u = 2.4 \cdot \sigma_v' \cdot D \cdot \left(\frac{q_c}{\sigma_v'}\right)^{0.67} \cdot \left(\frac{z}{D}\right)^{0.75}, \qquad \sigma_v' = \gamma' \cdot z \tag{2.17}$$

$$f(y) = \left[1 - exp\left(-8.9 \cdot \left(\frac{y}{D}\right)^{-1.2} \cdot \left(\frac{\sigma_v - u_g}{\sigma_v'}\right)^{-1.2} \cdot \left(\frac{z}{D}\right)^{-1.25}\right)\right] \tag{2.18}$$

Table 2-8: Overview CPT based p-y method (Suryasentana & Lehane, 2016)

	Suryasentana & Lehane
Date	2016
Based on	CPT cavity expansion analogue, CPT, 3D FEM and Horns Rev field study (Hald et al. 2009)
Validation cases	Development numerical case studies same as taken in (Suryasentana & Lehane, 2014a) 1. Uniform loose sand (dry and with water table) D=2, *L/D*=20 2. Uniform dense sand over uniform loose sand (dry and with water table) D=2, *L/D*=20 3. Horns Rev: dense sand D= 4m, *L/D*= 5.5
Pile	D=2, *L/D*=20
Software	Plaxis 3D, Oasys ALP

2.4.6 Conclusion

From the literature study on CPT-based *p-y* methods, it can be concluded that the methods overall showed good results with (numerical) pile load test results from which they have been derived. Especially the (updated) method from Suryasentana & Lehane (2016) showed promising results with numerical simulations and one history case on an offshore wind monopile with moderate *L/D* ratio. This gives confidence in the research to a CPT-based *p-y* method for monopiles with large diameters. However, further studies to evaluate the methods for other sand conditions and pile dimensions is recommend. In Chapter 5, the performance of Equations (2.8), (2.10), (2.11), (2.14) and (2.16) is evaluated.

2.5 Short piles

The application of *p-y* curves to long piles, in which pile behaviour is only influenced by the lateral distributed pressure, is largely discussed. However, for short piles other soil reaction terms may play a role as well, which is discussed in this section.

2.5.1 Short vs. long piles

In Figure 2-19, the soil reaction profile that occurs along a laterally loaded rigid pile (left) and flexible pile (right) are shown. The distribution of the lateral soil resistance and deflection is quite different for each pile. When a lateral load is applied to a long flexible pile, the pile bends and therefore the displacement is dependent on the piles bending stiffness and moment capacity. A perfectly flexible pile has a length that is such long, that the pile toe does not deflect. Therefore it can be assumed that the base moment and base shear are zero and the pile behaviour is dependent on lateral soil pressures.

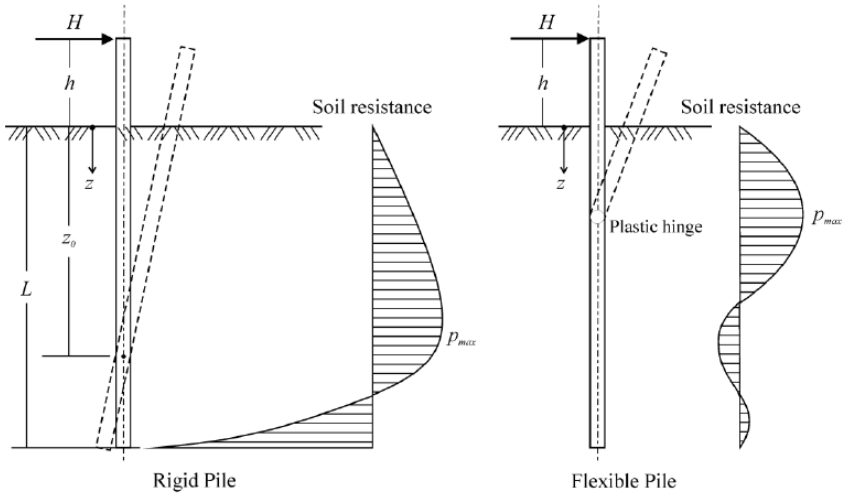

Figure 2-19: short pile behaviour (left) vs. long pile behaviour (right) (Broms, 1964)

A short pile rather rotates around one rotation point and behaves as a rigid body that does barely bend. This rigid behaviour comes with larger displacements at the end of the pile and therefore assumptions for a zero base moment and base shear could lead to inaccurate predictions for pile head displacements of rigid piles (Peralta, 2010).

2.5.2 Additional soil springs

In history, several researches have been conducted to investigate short pile behaviour and found that also other soil reaction terms than the lateral soil pressure play a significant role. In 1983, Davidson & Donovan suggested a four-spring subgrade modulus model to account for these soil reaction components, see Figure 2-20. The model was based on laterally loaded drilled pier foundations with *L/D* ratios of 3.2 (in sand) and 6.7 (in clay) that have comparable *L/D* ratios to offshore monopile dimensions.

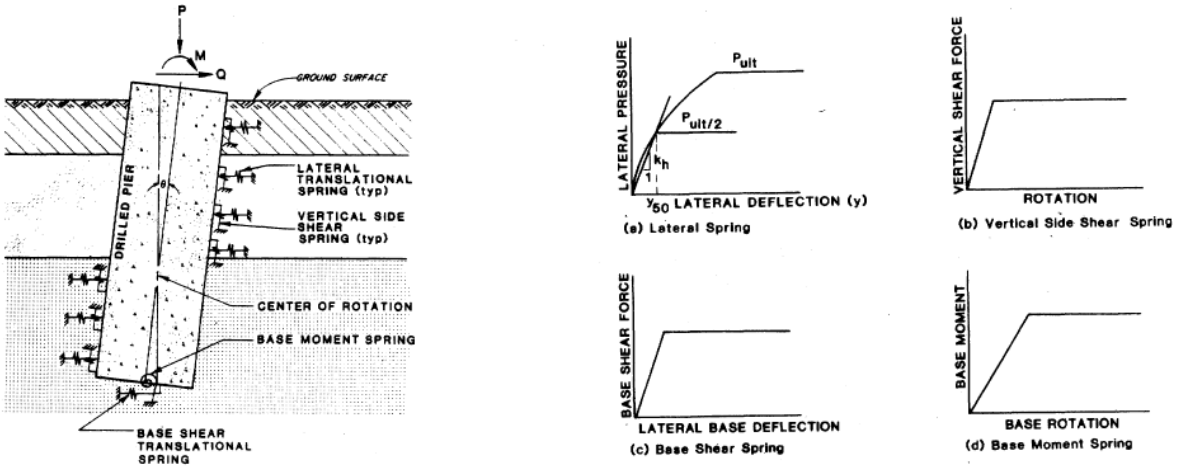

Figure 2-20: Four-spring subgrade modulus model with representation of non-linear springs from (Davidson & Donovan, 1983)

In the PISA Project a new design method is researched in which the *p-y* approach is extended with these additional soil reaction terms. In Figure 2-21 (left) all soil reaction terms that are important for monopiles that are loaded by a lateral force H_G and moment M_G are presented in Figure 2-21 (right), the concept is simplified in a 1D finite element model that is similar to the proposed design method of Davidson & Donovan (1983).

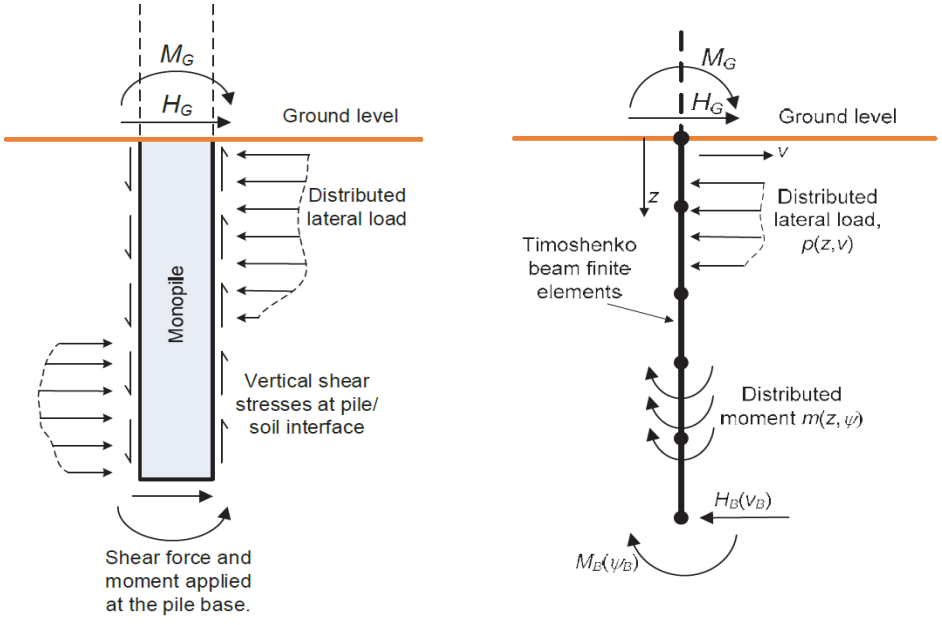

Figure 2-21: 1D spring model adopted in the PISA Project (Byrne, et al., 2017)

- *Distributed load curve $p(z, v)$*:

  The distributed load curve describes the local relation at depth *z* between the distributed lateral load, p in units of force per length, and lateral pile displacement *y (v* in the figure*)*. (Byrne, et al., 2017)

- *Distributed moment curve $m(z, \theta)$:*

  The distributed moment curve describes the relation between the distributed moment applied to the pile, *m* in units of moment per length, and the pile cross-section rotation, θ. The rotations are induced by vertical shear tractions that act on the pile perimeter. These shear tractions are caused by vertical- and horizontal loading of the pile, though for offshore wind turbines the vertical load is much smaller compared to lateral loading, as explained at the beginning of this chapter. Close to the surface on the passive side of the pile, vertical shear tractions become more significant when the pile is loaded close to failure, this is because of the wedge-type mechanism that is expected to develop. (Byrne, et al., 2017)

- *Base shear curve H_B (v_B):*

  The base shear curve describes the lateral relation between the base shear force H_B and the displacement of the pile toe v_B. (Byrne, et al., 2017)

- *Base moment curve M_B (θ_B):*

  The base moment curve describes the relation between the base moment, M_B, and the rotation of the pile toe θ_B. (Byrne, et al., 2017)

In the finite element model the pile is represented by a number of beam elements, based on Timoshenko beam theory (Byrne, et al., 2017). As discussed before, an Euler-Bernoulli beam cannot incorporate the vertical shear tractions. However, the contribution of vertical shear increases with increasing pile diameters and should therefore be accounted for piles with a reduced *L/D* ratio, (Burd, et al., 2017). In a Timoshenko beam the shear tractions can be incorporated and gives therefore a more reliable representation of the pile response.

2.5.3 Soil reaction curves from 3D FEM

In the PISA Project the soil reaction curves from Figure 2-21 were obtained by performing first an extensive 3D finite element analysis (FE analysis) on a large set of piles. From FE results, data about the applied load, distributed lateral load, distributed moment and base reactions can be extracted. The numerically derived soil reactions terms have been parameterized with variables from Figure 2-23 and fitted in a four-parameter conic function by means of a regression analysis. In Figure 2-22, the function is shown, where $\bar{x}$ is the parameter for normalized displacement or rotation and $\bar{y}$ is the parameter for equivalent normalized soil reaction component, $\bar{n}$ determines the shape of the curve. (Burd, et al., 2017). Figure 2-24 shows the contribution of each soil reaction term to short pile behaviour that was found in the PISA Project.

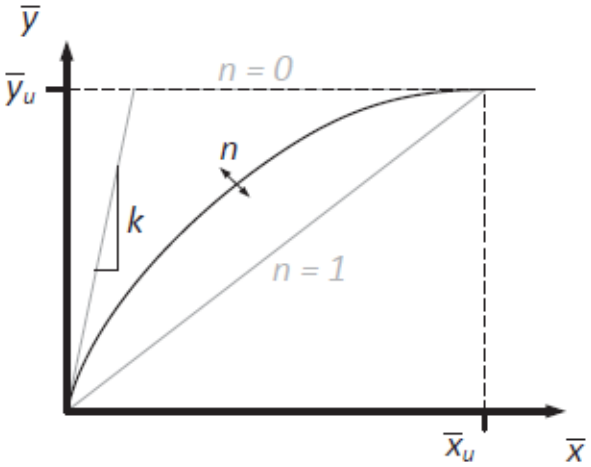

Figure 2-22. four-parameter conic function (Burd, et al., 2017)

Normalized variable	Non-dimensional form
Distributed lateral load, $\bar{p}$	$\frac{p}{\sigma'_{vi}D}$
Lateral displacement, $\bar{v}$	$\frac{vG}{D\sigma'_{vi}}$
Distributed moment, $\bar{m}$	$\frac{m}{pD}$
Pile rotation, $\bar{\psi}$	$\frac{\psi G}{\sigma'_{vi}}$
Base shear load, $\bar{H}_B$	$\frac{H_B}{\sigma'_{vi}D^2}$
Base moment, $\bar{M}_B$	$\frac{M_B}{\sigma'_{vi}D^3}$

Figure 2-23. Normalized variables to be used in soil reaction curves (Burd, et al., 2017)

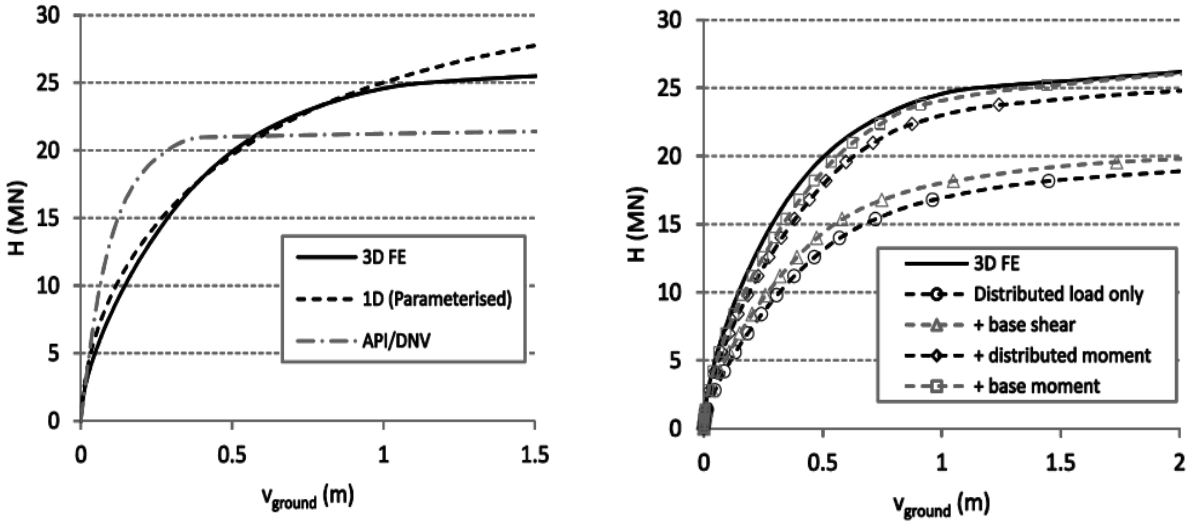

Figure 2-24: Short pile response in sand predicted with API p-y curves only (left) and cumulative breakdown component with additional numerical soil reaction curves (Byrne, et al., 2015a)

2.5.4 Conclusion

The research of Davidson & Donovan (1983) and Burd, et al (2017) showed that for piles in sand with $L/D \approx 3$, the soil stiffness is underestimated by the API method and that other soil reaction become important as well. During the PISA project, relationships for the additional terms have been developed and prove to give more reliable predictions for the displacement of short piles. However, the soil reaction curves were obtained after intensive 3D FEM modelling and laboratory -and field testing, to repeat this approach for every future offshore wind park this would be a time consuming and expensive operation. Earlier it was concluded that the cone resistance (q_c) is an accurate measure for the soil effective stress and is also relatively quickly and cheaply recorded during a cone penetration test.

By linking the expression of the additional soil reaction curves from the PISA Project to q_c, an easy to employ and possibly promising method could be developed that accounts for all soil reactions that are important for short pile behaviour.

However, the relations for the additional soil reaction curves were not published at the start of this thesis yet. Though, the API and DNV guideline describe the following methods to determine a preliminary assumptions for the base rotation, base shear and vertical shear stresses in the research to appropriate soil reaction for large diameter monopiles.

Distributed rotational moment (API, 2011)**:**

$$\tau(z)_{compression} = 0.043 \cdot q_c(z) \cdot \left(\frac{p_o'(z)}{p_a}\right)^{0.05} \cdot {A_r}^{0.45} \cdot \left[\max\left(\frac{L-z}{D}, 2\sqrt{A_r}\right)\right]^{-0.9} \left[\min\left(\frac{L-z}{D} \cdot \frac{1}{2\sqrt{A_r}}, 1\right)\right] \quad (2.19)$$

$$\tau(z)_{tension} = 0.025 \cdot q_c(z) \cdot \left(\frac{p_o'(z)}{p_a}\right)^{0.15} \cdot {A_r}^{0.42} \cdot \left[\max\left(\frac{L-z}{D}, 2\sqrt{A_r}\right)\right]^{-0.85} \quad (2.20)$$

$$F_\tau(z,\theta) = \int \tau(z) \cdot y(z,\theta)\, dz \quad (2.21)$$

$$M_\tau(z,\theta) = F_\tau(z,\theta) \cdot R \quad (2.22)$$

Base rotation (DNV, 2017)**:**

$$M_b = K_r \cdot \theta_b \quad (2.23)$$

$$K_r = \frac{8 \cdot G \cdot {r_o}^3}{3(1-v)} \quad (2.24)$$

$r_o =$ radius of foundation

$G, v\ and\ p =$ shear modulus, Poisson's ratio and mass density

Base shear (DNV, 2017)**:**

$$H_b = {\sigma'}_v \cdot \tan\varphi' \cdot A \quad (2.25)$$

Part 2:

Evaluation of existing *p-y* methods

In this part of the research, the concern that the API *p-y* method is not applicable to short piles is investigated. The API *p-y* method along with four existing CPT-based *p-y* methods are used to calculate the pile head displacement of several piles and are compared to pile head displacements and rotations that have been measured during the PISA field lateral load tests in Dunkirk. The goal of this part is to evaluate the performance of existing *p-y* methods for different pile geometries in cohesionless soils. In order to perform this evaluation, a pile-response model is developed. The *p-y* formulas used in this model require site specific soil parameters, which are determined in the first chapter: Soil and site analysis.

3. Soil and site analysis

The Dunkirk site, located in the North of France (Figure 3-1), is the reference location for which existing (CPT-based) *p-y* methods are evaluated. This chapter starts with a brief description of the field tests that were performed by the PISA project in Dunkirk, along with some site specific back ground information. Subsequently the data that was gathered an made available for this thesis, is analysed by means of several methods to determine the values for the soil parameters.

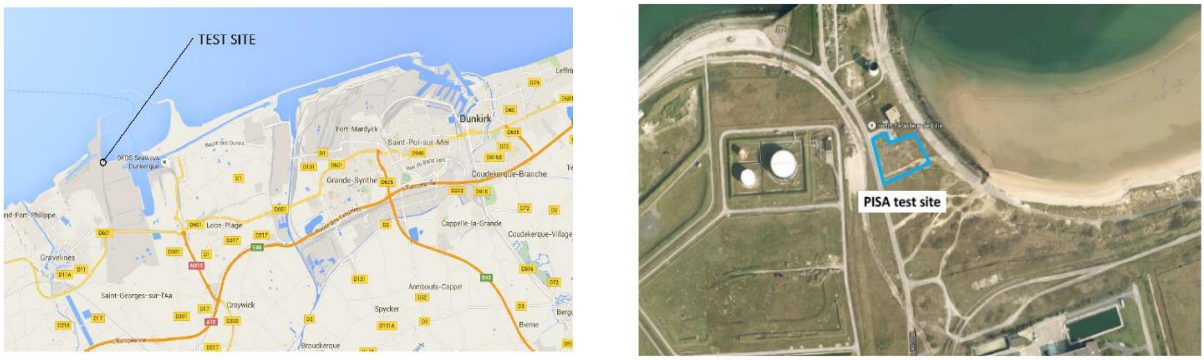

Figure 3-1: Site location (taken from PISA field report)

3.1 PISA Project

In the PISA project several lateral pile load tests (PLTs) were performed at the Dunkirk site. The site was originally chosen because the ground conditions are considered typical when compared with offshore sands in the North Sea. The PLTs were performed at locations DL1-DL2, DM1-9 and DS1-4 (Figure 3-2). *DL* refers to large diameter piles, *DM* to medium diameter piles and *DS* to small diameter piles. DR1 is the reaction pile.

The pile geometries that were tested are listed in Table 3-1.The PLTs comprised monotonic static loading and were executed as constant velocity tests. At some intervals during the loading procedure, the load was maintained to investigate the creep effect. The procedure for pile load testing has been discussed in Subection 2.3.1.

As part of the project, the soil at each pile location was investigated by means of Cone Penetration Tests (CPTs). During the CPT tests, the cone resistance q_c, sleeve friction f_s and pore water pressure u_2 were measured every 0.01m in depth. Based on this data also interpretations were given for the unit weight γ', relative density D_r and the friction angle φ' see Appendix A. D_r was determined with the method of Mayne & Kulhawy (1990) and φ' was determined with the method of Mayne (2007).

Table 3-1 gives an overview of the measurements data per pile location that was made available for this thesis. Because PLT data is required for the comparison of existing *p-y* methods, pile location DM7, DM9 and DM3, are selected for the evaluation in Chapter 5.

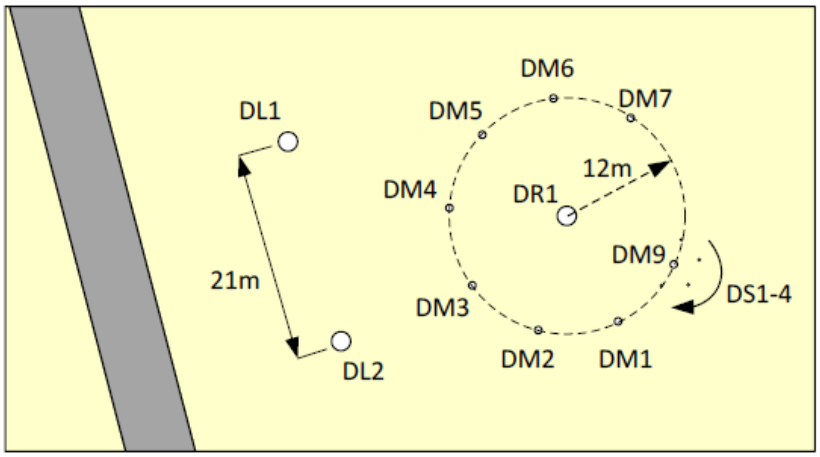

Figure 3-2: Dunkirk site layout(taken from PISA field report)

Table 3-1: Pile geometries tested in Dunkirk

Pile location	D [m]	L [m]	*L/D*	T [mm]	PLT data available	CPT data available
DS1	0.273	1.43	5.25	7		yes
DS2	0.273	1.43	5.25	7		yes
DS3	0.273	2.18	8	7		yes
DS4	0.273	2.73	10	7		yes
DM5	0.762	2.29	3	10		yes
DM7	0.762	2.29	3	10	yes	yes
DM2	0.762	4	5.25	14		yes
DM4	0.762	4	5.25	14		yes
DM9	0.762	4	5.25	14	Only above ground	yes
DM1	0.762	4	5.25	14		yes
DM6	0.762	4	5.25	19		yes
DM3	0.762	6.1	8	25	yes	yes
DL1	2	8	5.25	25		yes
DL2	2	10.5	5.25	38		yes

3.2 Site specific back ground information

The PISA PLT and CPT data were accompanied by a document that contained back ground information including the soil stratigraphy, geology and water table.

3.2.1 Stratigraphy

The ground conditions of the site are described in Table 3-2. The first two layers can be described as fine to medium sands with a mean particle size of D_{50}= 0.25mm. The sand particles are sub-rounded to rounded in shape.

Table 3-2: Soil stratigraphy Dunkirk

	Depth from	Depth to	Geological formation	Description
Layer 1	0m	3m	Hydraulic Fill	Sand fill that was dredged from the offshore Flandrian deposits, and placed to raise the ground level. No compaction or surcharging has taken place.
Layer 2	3m	30m	Flandrian Sand	Marine sand deposited during three local marine transgressions. These sands are often separated by organic layers which accumulated between transgressions. A 600mm thick organic layer is found at around 8m depth, separating the Flandrain sand into upper and middle units.
Layer 3	30m	> 10.5m	Yprésienne Clay	An Eocene marine clay (also known as London Clay and Argile de Flandres) which extends beneath the southern North Sea.

3.2.2 Geology

Between 1972 and 1975 the local ground level was raised with sand fill. The sand fill was dredged from the adjacent western port and has therefore the same geological origin as the Flandrian sand beneath it. The sand fill was allowed to drain naturally without artificial compaction or surcharging. Flandrian sand refers to marine sand that has been deposited during the Flandrian Transgression. This means the sand is deposited after the latest Weichsel glaciation which is in the Holocene epoch (12.000 years ago- present). Based on this, it can be assumed that the sand is normally consolidated and that the coefficient of earth pressure at rest K_0 has a value of 0.5.

3.2.3 Water table

In Figure 3-3 the water table with tidal variation is shown. The water table was found at around 4.8 m depth below the ground with small variations over time. The water table was derived from borehole pressure sensors that took measurements between the period June 2014 and April 2015.

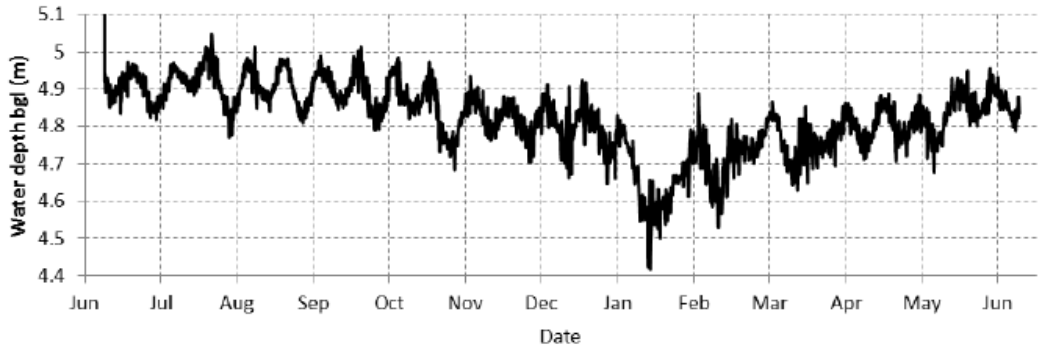

Figure 3-3: Water table depth below ground level

3.3 Soil parameter analysis

During the evaluation of existing (CPT-based) *p-y* methods, the formulas from Equation (2.8), (2.10), (2.11), (2.14) and (2.16) are compared for pile location DM7, DM9 and DM3. Table 3-3 shows the soil parameter input that is required per *p-y* formula and thus has to be determined for all pile locations. For the API method that is the effective unit weight γ' and the internal friction angle φ'. The CPT-based *p-y* formulas generally need the unit weight and cone resistance q_c as input.

Table 3-3: Required soil parameters per p-y method

API (2011)	Novello (1999)	Dyson & Randolph (2001)	Li, Igoe, Gavin (2014)	Suryasentana & Lehane (2016)
γ'	γ'	γ'	γ'	γ'
φ'	q_c	q_c	q_c	q_c

Although assumptions for γ' and φ' were made by PISA, to make an optimal estimation for the soil parameters also other methods are analysed in this section. The cone resistance is obtained from CPT data. Figure 3-4 shows an overview of the methods that are used to determine γ' and φ'. First, the unit weight γ' is selected after comparing the results of three different methods. The internal friction angle is compared for two methods that use the vertical effective stress σ_v' ($\gamma' z$) as input. Because one of the methods also needs the relative density as input, two methods to calculate the relative density are compared as well. In this section the soil parameter analysis is shown for DL2, because this is the longest pile in the data set and therefore penetrates all soil layers.

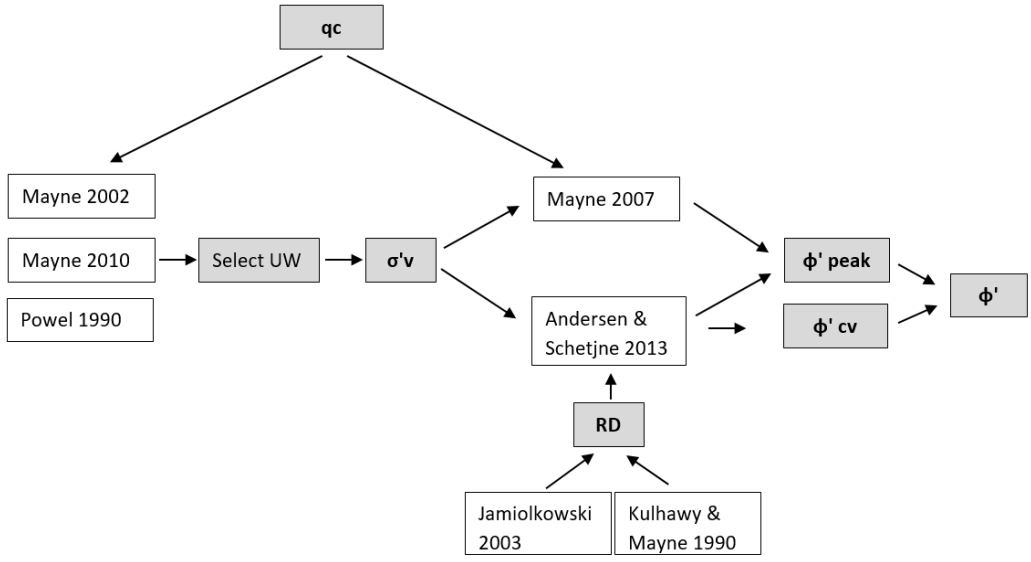

Figure 3-4: Methods used for soil parameter analysis

3.3.1 Unit weight

The unit weight is determined by means of three different methods, and is plotted in Figure 3-5.

The unit weight obtained with Powel (1990) is based on classification zones. The Ic profile falls mainly in zone number 6 (clean sand to silty sand) according to Robertson (2009) and therefore leads to an almost constant unit weight of 20 kN/m^3.

The relative density profile that was assumed in the PISA project, shows a relative density of 100% in the top layer, indicating that the soil must be very dense. A unit weight of 18.5 kN/m^3 is selected for the sand layers above the water table, this is based on general Fugro experience for very dense sands and the Dutch Eurocode that recommends values ranging between 18 kN/m^3 and19 kN/m^3 for unsaturated silty sand (Eurocode7, NEN-EN 1997-1).

Below the water table a unit weight value of around 20.5 kN/m^3 is selected, following Mayne (2010) correlation and corresponding well with the Eurocode 7 recommendations for dense clean to silty sand.

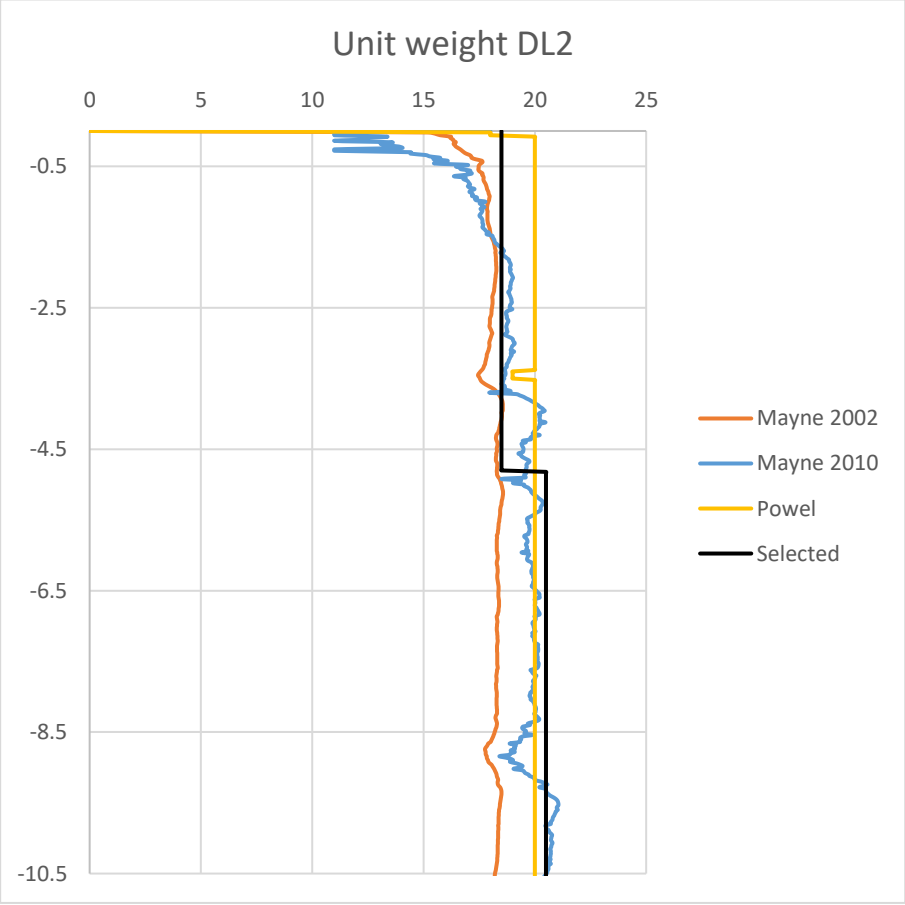

Figure 3-5: Unit weight methods and selected unit weight

3.3.2 Relative density

For the calculation of the constant- and peak friction angle by means of the Andersen & Schnetje (2013) method, an assumption for the relative density is required. Based on the selected unit weight, the relative density (D_r) is calculated according to Jamiolkowski (2003) and Kulhawy & Mayne (1990). For the Mayne method, the relation for dry relative density was used above the water table and the relation for saturated relative density was used below the water table.

The relative density according to Jamiolkowski in the top sand layer is approximately 100% which is similar to the value assumed in the PISA project. The bottom layer has a relative density of about 90%. Above the water table, the Mayne & Kulhawy method gives even higher relative density values that go beyond 100%. Below the water table, the Mayne & Kulhawy's relative density is comparable to Jamiolkowski.

Being the most recent method, the Jamiolkowksi method is used to calculate the relative density for Andersen & Schnetje's friction angle . The profile is also plotted in a discrete manner as the soil springs to be modelled in MATLAB can be seen as discrete soil reaction points along the pile.

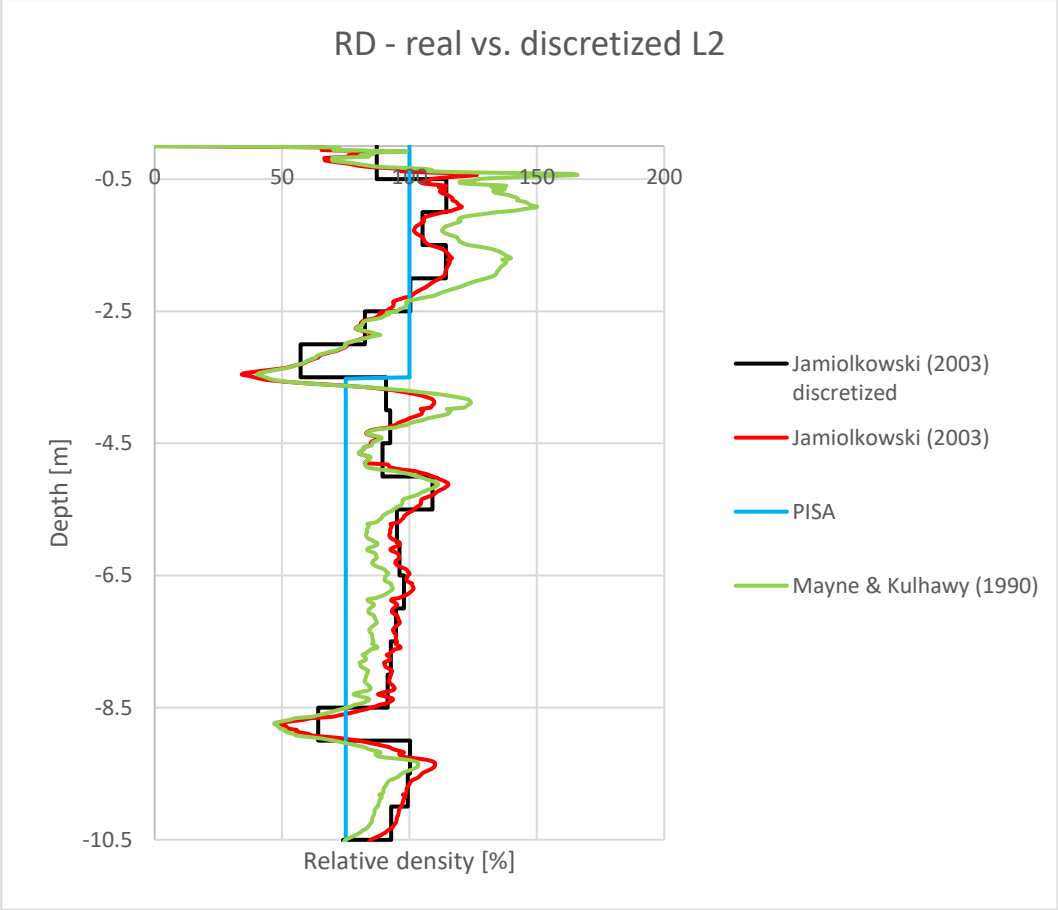

Figure 3-6: Relative density methods and selected discretized relative density

3.3.3 Peak effective angle of internal friction

The constant volume and peak effective angles of internal friction are derived from Andersen & Schetjne based on the selected relative density profile The peak effective friction angle or internal friction (φ') was calculated with Mayne (2007) and Andersen & Schetjne (2013).. There is a good agreement between the Mayne and Andersen method for the peak friction angle. The selected design profile for the φ' values is based on the average between Andersen's peak and constant volume friction angles. The φ' values are used as inputs for the *p-y* data assessments following API (2014), which recommends a limiting value of 42°. Therefore, the selected design profile for the φ' values are limited to 42° for the numerical analysis.

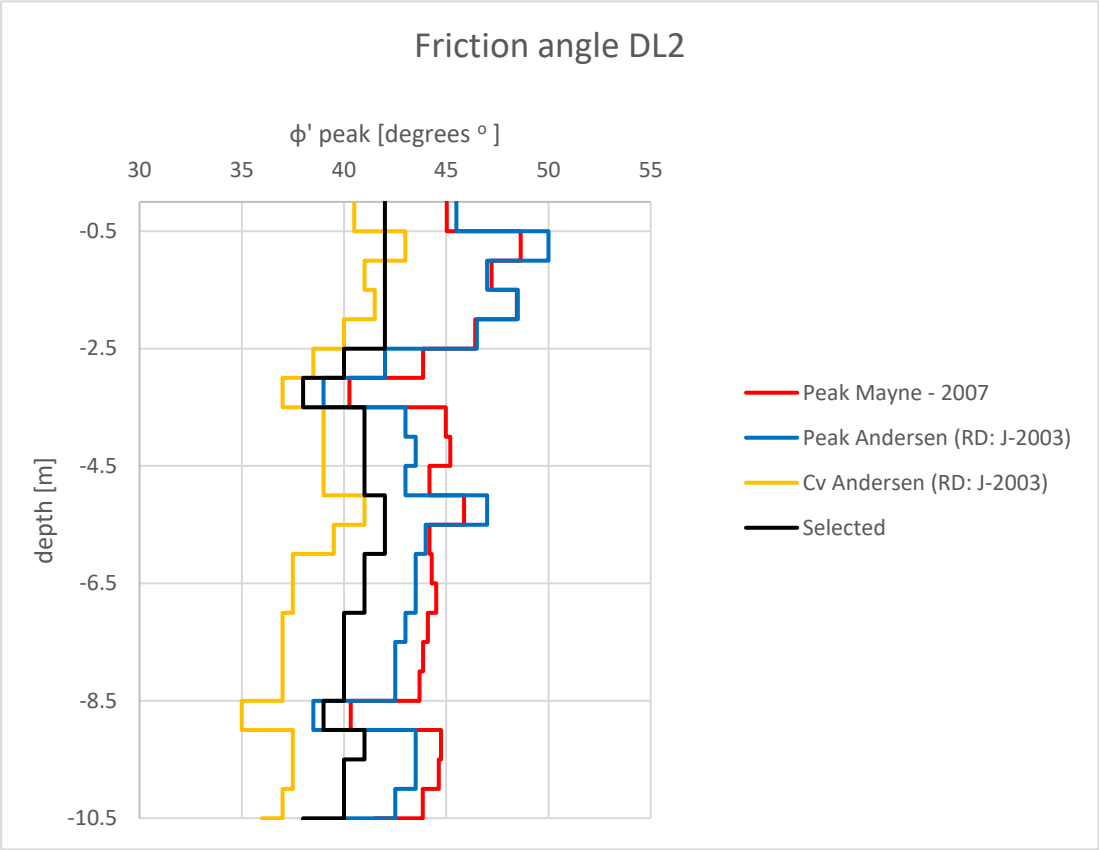

Figure 3-7: Friction angle methods and selected friction angle

3.4 Summary

The unit weight at all pile locations is assumed to have a value of 18.5 kN/m^3 until 4.8m depth (water table). For deeper depths the unit weight estimated at 20.5 kN/m^3. For each individual pile location the friction angles are obtained by calculating first the relative density based on q_c and Jamiolkowski (2003). From the relative density and effective unit weight, the constant and peak friction angle is derived with Andersen & Schetjne (2013) from which then the average is taken with a maximum value of 42°. In Appendix B the soil parameter profiles for location DM7, DM9 and DM3 are shown that result from this approach.

4. Pile-response model

To predict the pile response by means of a certain *p-y* method, a computational model is needed to perform the calculations. A pile response model is built in MATLAB, as part of the model was already made available by L.J. Prendergast (2015) and because changes to the model are easier to adjust in a MATLAB environment than in a standard pile response software program.

4.1 Model characteristics

4.1.1 Beam model

The pile is modelled as a beam divided in '*n'* beam elements. The ends of each beam element have nodes which can move in two degrees of freedom: rotation and displacement (2-DOF). Because the beam is continuous, the nodes of each two adjacent beam elements have the same displacement. The beam elements are thus 'sharing' a node, this is shown in Figure 4-1.

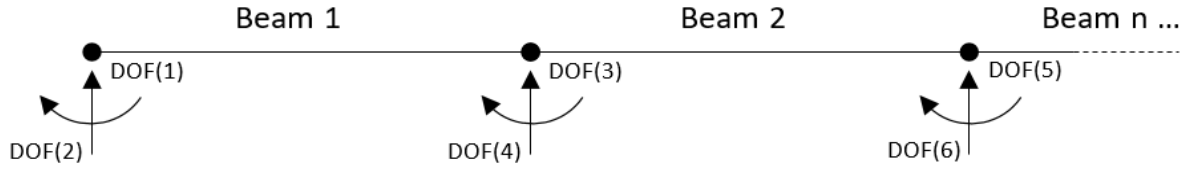

Figure 4-1: Two beam elements 'sharing 'a node, with 2 DOF's per node

$$\begin{pmatrix} \frac{12EI}{L^3} & \frac{6EI}{L^2} & -\frac{12EI}{L^3} & \frac{6EI}{L^2} \\ \frac{6EI}{L^2} & \frac{4EI}{L} & -\frac{6EI}{L^2} & \frac{2EI}{L} \\ -\frac{12EI}{L^3} & -\frac{6EI}{L^2} & \frac{12EI}{L^3} & -\frac{6EI}{L^2} \\ \frac{6EI}{L^2} & \frac{2EI}{L} & -\frac{6EI}{L^2} & \frac{4EI}{L} \end{pmatrix} \begin{pmatrix} x_1 \\ \theta_1 \\ x_2 \\ \theta_2 \end{pmatrix}$$

DOF number: 1, 2, 3, 4

Figure 4-2: Euler-Bernouilli local beam stiffness matrix

The pile displacement is calculated with Hooke's law: $\{Y\} = \frac{\{F\}}{[K]}$. The force vector $\{F\}$ and stiffness matrix $[K]$ are given as input and $\{Y\}$ is the resulting vector that contains the angle of rotation and displacement of each node. The stiffness matrix is composed of a beam stiffness matrix and a spring stiffness matrix. The beam stiffness matrix follows the rules of the beam theory, which has been selected to describe pile behaviour. In Figure 4-2, the global stiffness matrix according to Euler-Bernoulli beam theory is shown for one beam element.

For the total system with 'n' beam elements, the global stiffness matrix adds up according to Figure 4-3.

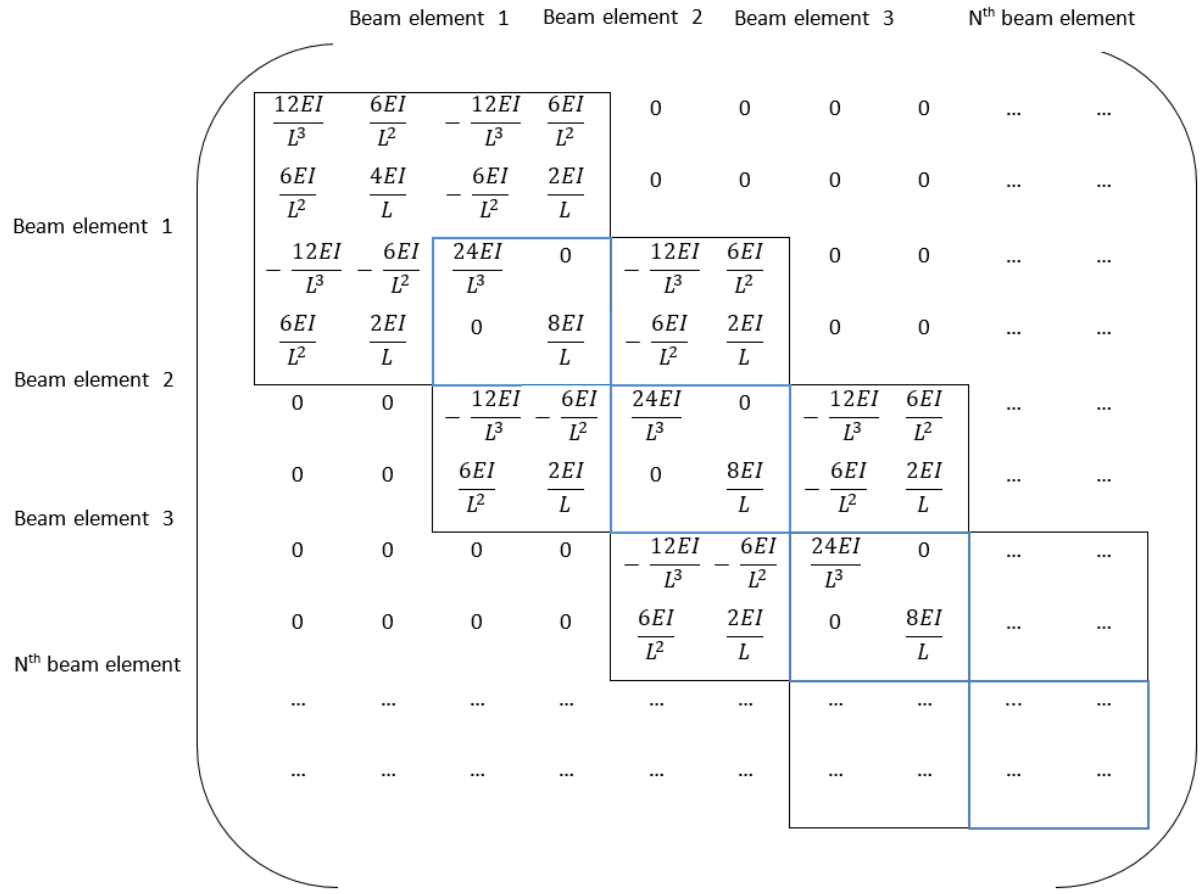

Figure 4-3: Global beam stiffness matrix for 'n' beam elements. Blue squares indicate the shared nodes between two beam elements

In Figure 4-4 is shown that one translational spring is attached to each node, thereby representing the soil strength. The spring is elongated or compressed in the lateral direction, hence adding extra stiffness, k_s to the node. DOF 3 and 6 will be added to DOF 1 and DOF 2 respectively, and the total result for the global stiffness matrix is depicted in Figure 4-5. The input for the soil reaction is described by one of the *p-y* formulas Equation (2.8), (2.10), (2.11), (2.14) and (2.16).

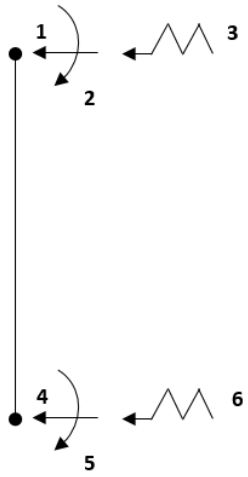

Figure 4-4: Beam element with spring attached to the nodes

		Beam element 1		Beam element 2		Beam element 3		Nth beam element		
	DOF	**1**	**2**	**3**	**4**	**5**	**6**	**7**	**8**	**...**
Beam element 1	**1**	$\frac{12EI}{L^3}+Ks$	$\frac{6EI}{L^2}$	$-\frac{12EI}{L^3}$	$\frac{6EI}{L^2}$	0	0	0	0	...
	2	$\frac{6EI}{L^2}$	$\frac{4EI}{L}$	$-\frac{6EI}{L^2}$	$\frac{2EI}{L}$	0	0	0	0	...
Beam element 2	**3**	$-\frac{12EI}{L^3}$	$-\frac{6EI}{L^2}$	$\frac{24EI}{L^3}+Ks$	0	$-\frac{12EI}{L^3}$	$\frac{6EI}{L^2}$	0	0	...
	4	$\frac{6EI}{L^2}$	$\frac{2EI}{L}$	0	$\frac{8EI}{L}$	$-\frac{6EI}{L^2}$	$\frac{2EI}{L}$	0	0	...
Beam element 3	**5**	0	0	$-\frac{12EI}{L^3}$	$-\frac{6EI}{L^2}$	$\frac{24EI}{L^3}+Ks$	0	$-\frac{12EI}{L^3}$	$\frac{6EI}{L^2}$	...
	6	0	0	$\frac{6EI}{L^2}$	$\frac{2EI}{L}$	0	$\frac{8EI}{L}$	$-\frac{6EI}{L^2}$	$\frac{2EI}{L}$	...
Nth beam element	**7**	0	0	0	0	$-\frac{12EI}{L^3}$	$-\frac{6EI}{L^2}$	$\frac{24EI}{L^3}+Ks$	0	...
	8	0	0	0	0	$\frac{6EI}{L^2}$	$\frac{2EI}{L}$	0	$\frac{8EI}{L}$	...

Figure 4-5: Global stiffness matrix including spring stiffness at the nodes (red squares)

4.1.2 Iteration loop

For the API *p-y* method, a *p-y* curve would for example look like the graph in Figure 4-6. The stiffness of a soil spring is the secant slope of the *p-y* curve: $k_s = \frac{p}{y}$, in which p, the soil pressure, is calculated with one of the *p-y* methods.

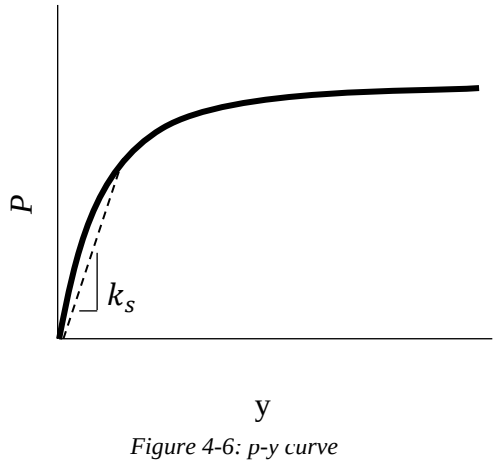

Figure 4-6: p-y curve

A problem with *p-y* curves is their non-linear aspect, and the value k_s thus varies with pile displacement. This means that the pile displacement has to be calculated in an iterative way. This is done in a force applied manner: the load is held constant while the spring stiffness is updated (and thus the entire global stiffness matrix as well) at each iteration step. The iteration process continues until the pile head displacement converges to a certain displacement.

In more detail, the following steps are taken in the iteration process and executed by MATLAB:

1. First, a horizontal load *F* is applied to the pile head.
2. Then, the spring stiffness is added to the global stiffness matrix.

   In the first iteration step the pile is not displaced yet and thus an initial value for the spring stiffness is used: k_1(from Table 2-2)
3. The pile displacement is computed with Hooke's law.

   If the pile head displacement differs less than 0.01% compared to the displacement calculated in the previous iteration step, the iteration process is finished.

   If the displacement has not reached convergence yet, the soil pressure is calculated with one of the *p-y* formulas from Equation (2.8), (2.10), (2.11), (2.14) and (2.16).
4. Now that soil pressure is known, the spring stiffness is updated for the next iteration step is by taking the secant slope through the pile displacement and soil pressure of the current step: k(n+1) = p(n)/ y(n). This is also displayed in Figure 4-7
5. In the next iteration step the applied load is still kept constant, while the global stiffness matrix is updated with the new spring stiffness.

These steps are repeated until the pile head displacement has converged, which is shown in Figure 4-8.

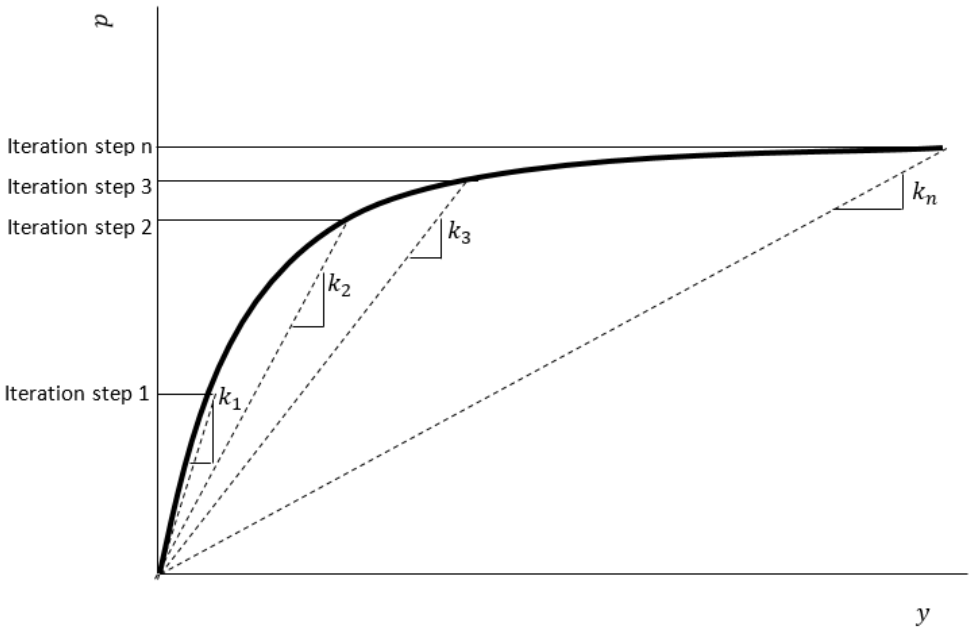

Figure 4-7: Updating the spring stiffness

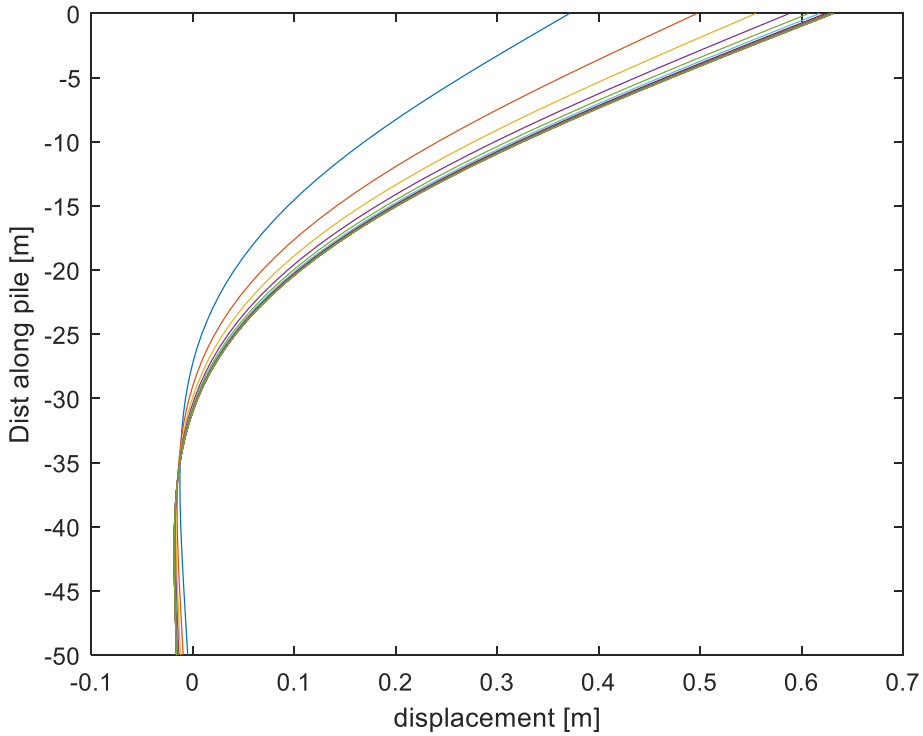

Figure 4-8: Convergence of pile displacement in MATLAB

4.2 Validation of the model

To determine whether the above described steps are correctly implemented in the model, the displacements computed by MATLAB are compared to displacements computed by FEBMCL (Finite Element Beam Column, a Fugro in-house software program for pile response). The MATLAB model is validated for uniform sand first. The pile displacement is calculated by means of the API *p-y* method for four different cases, the soil and pile properties are displayed in Table 4-1.

Table 4-1: Test cases for uniform sand

Cases		Ratio	Diameter	length	Effective unit weight	Friction angle	Initial stiffness
Dense sand	Long pile	*L/D*= 10	D= 5m	L= 50m	΄ϒ= 10 kN/m^3	φ'= 40^o	42226307
	Short pile	*L/D*= 3	D= 5m	L= 15m	΄ϒ= 10 kN/m^3	φ'= 40^o	42226307
Loose sand	Long pile	*L/D*= 10	D= 5m	L= 50m	΄ϒ= 8 kN/m^3	φ'= 29^o	2584176
	Short pile	*L/D*= 3	D= 5m	L= 15m	΄ϒ= 8 kN/m^3	φ'= 29^o	2584176

4.2.1 MATLAB model

In MATLAB, all piles are divided in beam elements of 1m length, l, with one soil spring attached to each node. The spring represents the soil that is one half beam element length above- and below the spring (Figure 4-9). The spring stiffness is derived from exact API curves. The force is applied as a concentrated nodal force at the pile head at ground level (Figure 4-10) and all nodes along are allowed to move freely without constraints.

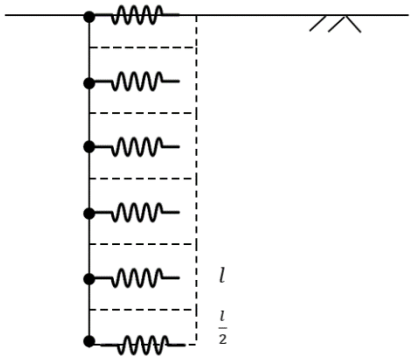

Figure 4-9: MATLAB beam model

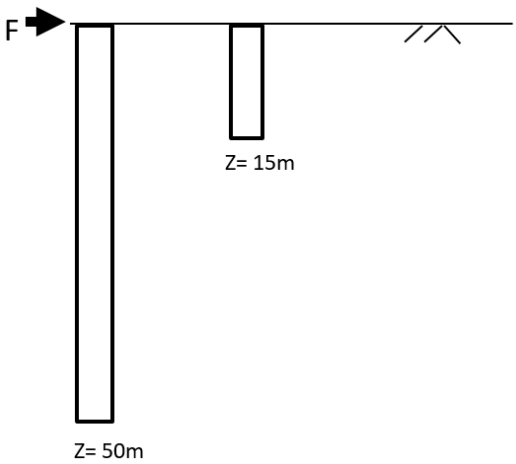

Figure 4-10: Horizontal loading

4.2.2 Fugro in-house software

The pile displacement is calculated using the FEBMCL software. In this program the pile displacement is calculated in an iterative way as well and uses *p-y* curves that are generated with another Fugro software program: GERRIT.

In GERRIT, the pile and soil characteristics soil properties from Table 4-1 are inserted to get *p-y* curves per meter depth. The *p-y* curve is not an exact curve, but a discretized curve that consists of five exact points in-between which the curve is linearly interpolated. The load is applied in the same manner as in the MATLAB model and the nodes are also made not-constrained.

4.2.3 Results in uniform sand

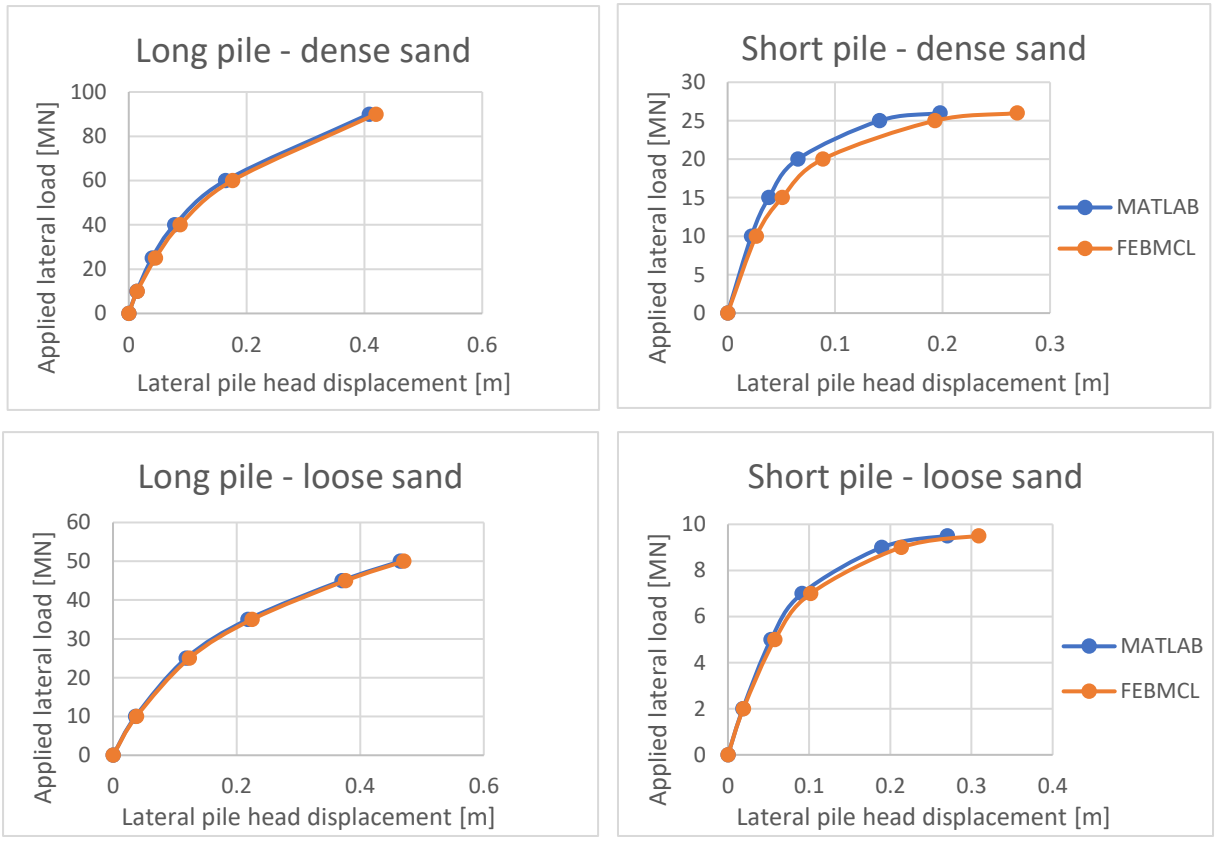

Figure 4-11: FEBMCL and MATLAB pile head displacements for four cases

The pile head displacement of long piles modelled in MATLAB is almost similar to FEBMCL results. However, for short piles in loose sand there is a difference of 10% between the ultimate pile head displacement calculated in MATLAB and the pile head displacement calculated in FEBMCL. For short piles in dense sand the difference is even 30%.

This difference could be explained by the *p-y* curve that is modelled in a discretized form in FEBMCL and modelled in an exact form in MATLAB.

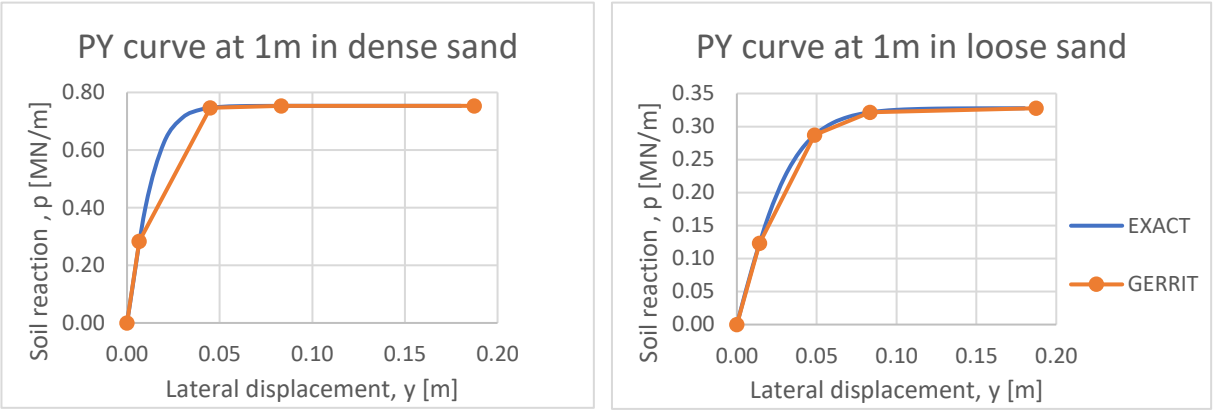

Figure 4-12: exact vs. discrete p-y curve

From Figure 4-12 it can be seen that the discretized *p-y* curves do not perfectly fit the exact *p-y* curves. In the case of dense sand, the discretized *p-y* curve even skips a large part of the exact curve. This observation could be the reason that the pile behaviour for short piles in dense sand is modelled differently by the MATLAB model compared to FEBMCL. To conclude whether this indeed is the case, the discretized approach is adopted in MATLAB after which the displacement is compared again.

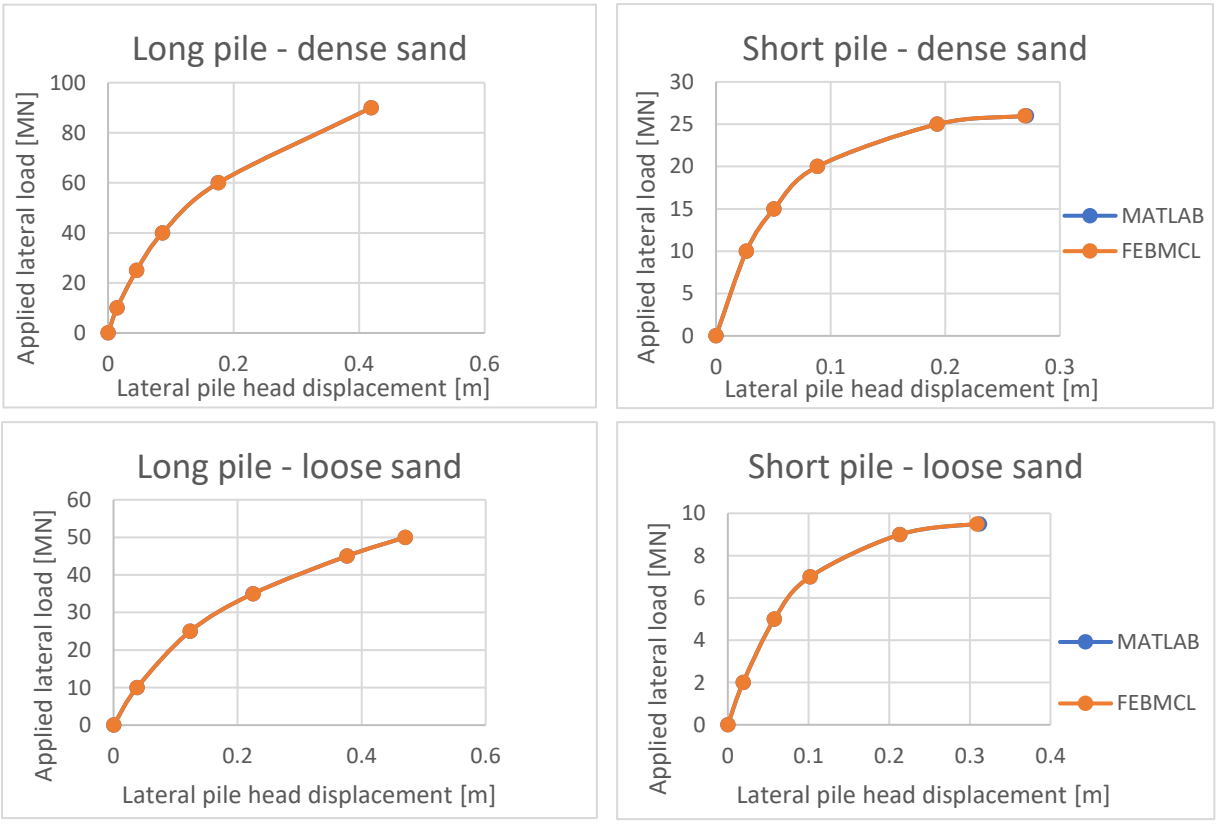

Figure 4-13: Pile head displacements FEBMCL and MATLAB (discrete p-y curve)

Conclusion

The pile behaviour computed by MATLAB and FEBMCL is similar in all cases if discrete *p-y* curves are adopted in MATLAB. This means that the MATLAB model calculates the displacements accurately. It can be concluded that the pile head displacement is rather dependent on the form of the *P-Y* curve. For long piles the use of a discrete curve is sufficient, whereas for short piles the closed-form is advised.

4.2.4 Results in layered sand

However, the Dunkirk site for which the *p-y* methods are evaluated does not have uniform soil properties. Therefore it should be checked whether the MATLAB model is also capable of simulating layered sand properly.

Because the iterative approach taken in MATLAB is already proven, it is sufficient to check whether MATLAB simulates the layered soil correctly. The biggest difference between layered and uniform soil modelling is that in layered soil the average unit weight and average friction angle are used to calculate the ultimate soil pressure instead of the exact values of the soil parameters at these depths. To verify whether the application of soil layering in MATLAB is performed correctly, the effective vertical stresses and the ultimate soil resistance per spring depth is compared to the values from GERRIT. For this validation case the DL2 pile from the PISA Project is taken, because it has the largest pile length among all the piles tested and therefore penetrates the most soil layers. The comparison is shown in Table 4-2.

Table 4-2: comparison soil parameters for layered soil modelling

	GERRIT		**MATLAB**	
Depth [m]	Pu [MN/m]	σ'_v [kPa]	Pu [MN/m]	σ'_v [kPa]
0.001	0	0.018	0.0002	0.0185
0.5	0.115	9.25	0.1153	9.25
1	0.282	18.5	0.2817	18.5
1.5	0.499	27.75	0.4994	27.75
2	0.768	37	0.7682	37
2.5	1.088	46.25	1.0883	46.25
3	1.256	55.5	1.2562	55.5
3.5	1.391	64.75	1.3907	64.75
4	2.356	74	2.3557	74
4.5	2.662	83.25	2.6618	83.25
5	3.397	90.9	3.3968	90.9
5.5	3.859	96.15	3.8591	96.15
6	3.702	101.4	3.7018	101.4
6.5	4.14	106.65	4.14	106.65
7	4.603	111.9	4.6025	111.9
7.5	5.089	117.15	5.0893	117.15
8	5.6	122.4	5.6004	122.4
8.5	5.212	127.65	5.2119	127.65
9	6.167	132.9	6.1668	132.9
9.5	7.911	138.15	7.9107	138.15
10	7.887	143.4	7.8874	143.4
10.499	8.519	148.64	8.5198	148.65

The parameters from GERRIT are fairly close to the values computed by MATLAB. All other soil parameters in the API *p-y* formula for sand do not need special adjustments in case of layering, therefore it can be concluded that the *p-y* curves for layered soil in MATLAB are simulated correctly.

4.2.5 Results Suryasentana & Lehane

To verify whether the MATLAB model also works for other *p-y* methods than API, the model is checked for one case presented in the updated paper from Suryasentana and Lehane (2016). A circular 40m long pile, with a 2m diameter (in the paper referred to as 'F1') was loaded in a dense sand layer overlying loose sand (case b) and a water table at 3m depth. The pile head displacement obtained by FE analysis is represented by the black dotted line in Figure 4-14.

The same case is simulated with the MATLAB model. The results are shown in Figure 4-15 and are quite similar to the pile head displacement computed by Suryasentana & Lehane. Therefore it can be concluded that the MATLAB model is capable of predicting the pile response for different *p-y* methods.

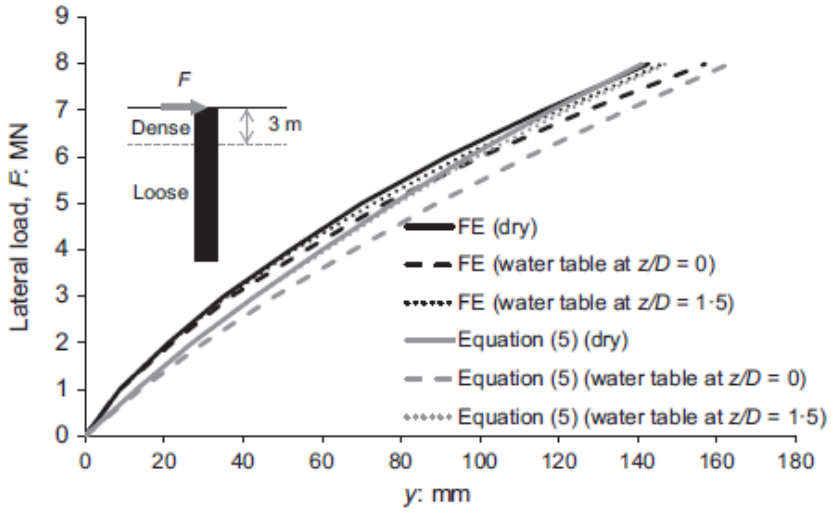

Figure 4-14: pile head displacement/ load from Suryasentana paper

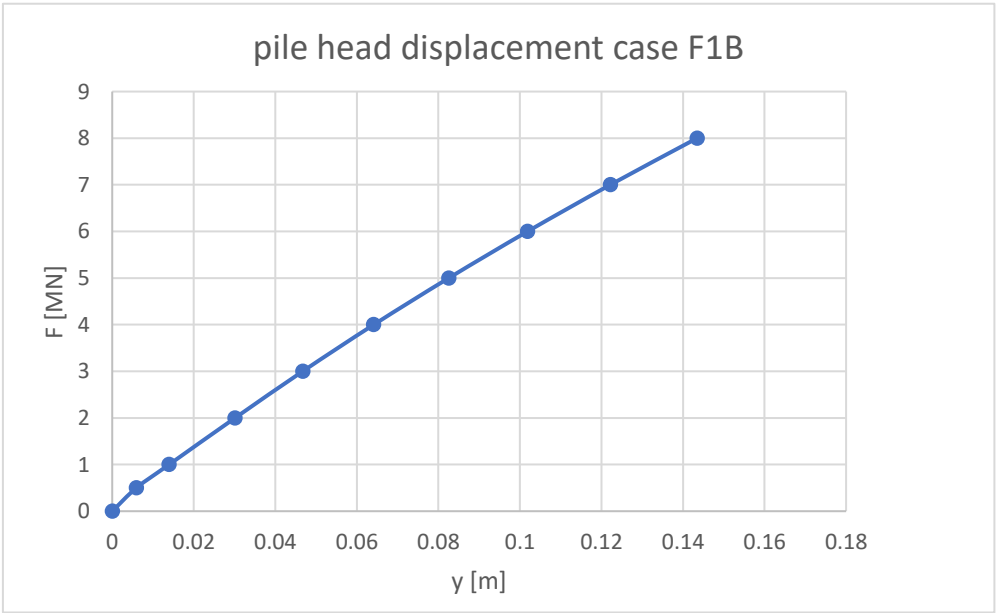

Figure 4-15: MATLAB pile head displacement for case F1b

5. Evaluation of *p-y* methods

Now the pile response model is validated for layered sand conditions, the model can be used to assess the performance of existing (CPT-based) *p-y* methods. The overall procedure for this evaluation is presented Figure 5-1.

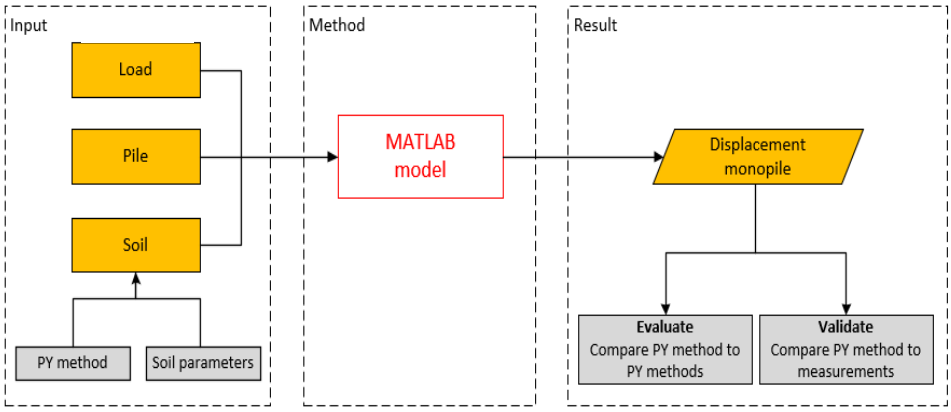

Figure 5-1: Evaluation process

The pile geometries for which the evaluation is performed are listed in Table 5-1. Based on their *L/D* ratios, the piles can be considered as short, medium and long. The soil is simulated according to either of the *p-y* formulas presented in Equation (2.8), (2.10), (2.11), (2.14) and (2.16). The soil parameters required for these formulas are derived according to the approach described in Chapter 3. The soil parameter profiles of the piles can be found in Appendix B. To incorporate possible shear tractions that can occur in short pile behaviour, the pile response is according to Timoshenko beam theory.

Table 5-1: piles selected for evaluation

Pile location	D [m]	L [m]	*L/D*	T [mm]	eccentricity [m]	Geometry
DM7	0.762	2.29	3	10	10	Short
DM9	0.762	4	5.25	14	10	medium
DM3	0.762	6.1	8	25	10	long

5.1 Results

In Figure 5-2 and Figure 5-3 the PISA PLT measurements are displayed together with the predictions of the *p-y* methods. As explained in Section 3.1, at each load increment the load was held constant for a period of time. During this period, the pile displaces further which is called the creep-effect. This effect can be observed in the horizontal parts of the graphs. The existing *p-y* methods are not capable of simulating the creep effect, therefore also a second line is drawn in which the creep is ignored. This graph is obtained by deleting the horizontal parts and compressing the remaining curve.

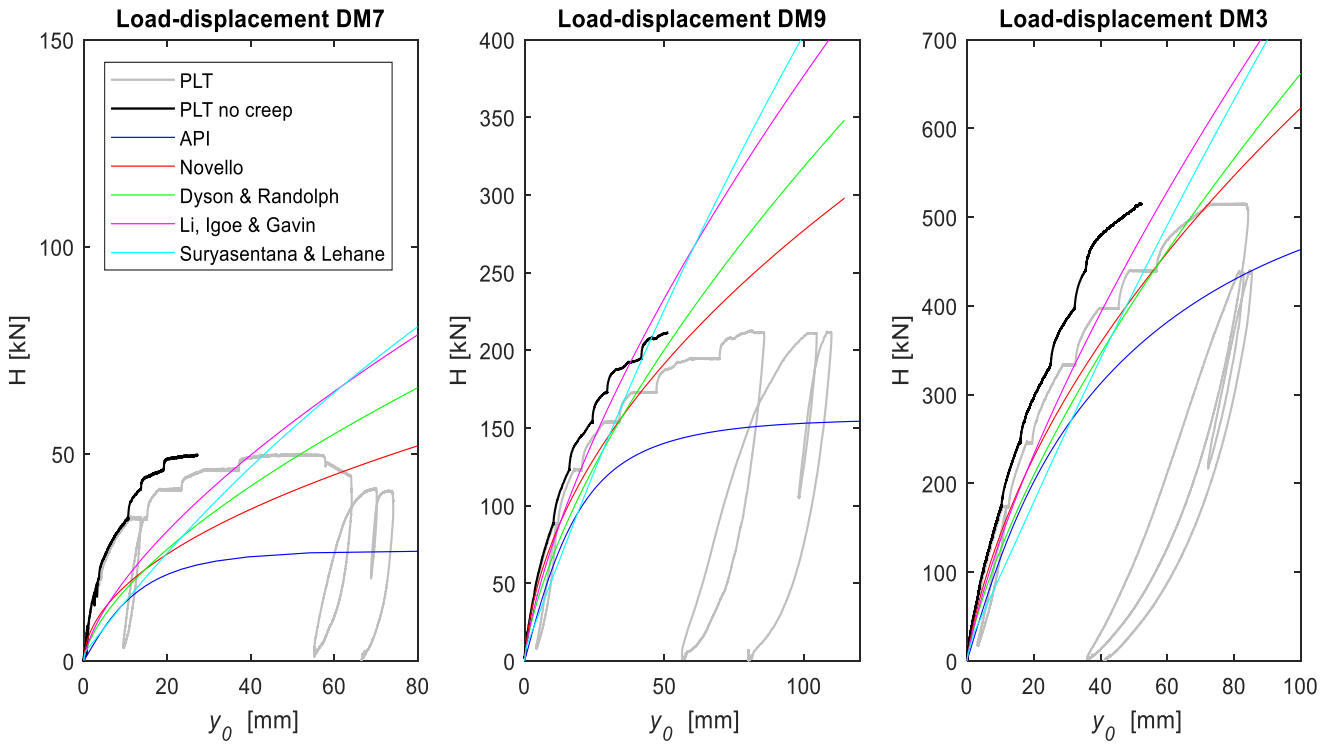

Figure 5-2: Load-displacement response per p-y method for short, medium and long pile

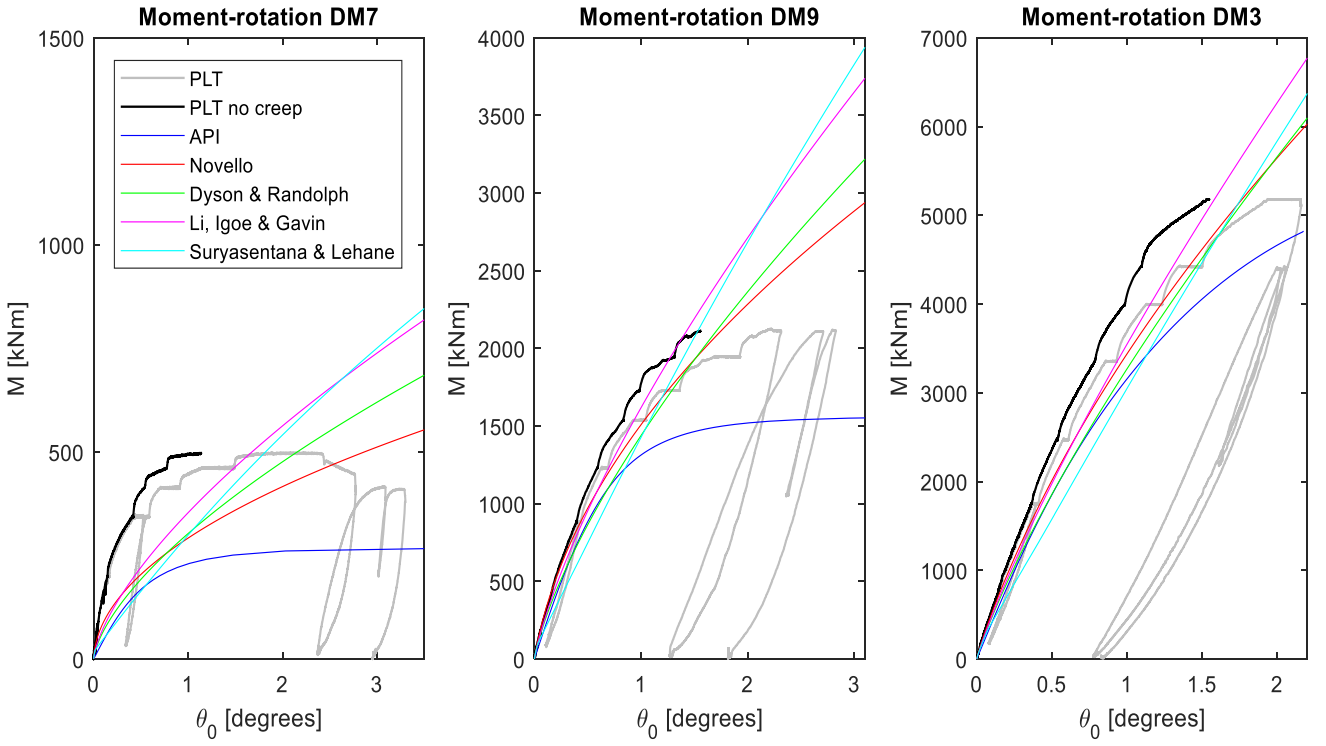

Figure 5-3: Moment-rotation response per p-y method for short, medium and long pile

5.2 Observations and discussion

5.2.1 Observations

Regarding the API method, a clear trend between accuracy and *L/D* ratio can be observed: with increasing *L/D* ratio the predicted pile response becomes stiffer and shows a better match with the PLT measurements. Based on the results of DM7, where the API method clearly overestimates the pile displacement, it can be concluded that the API method is not sufficient for predicting the behaviour of a short pile.

For all pile geometries, the CPT-based *p-y* methods predict a stiffer pile response than the API method and have a better match with the PLT measurements. Though, when comparing the results for DM7, the predicted response is still not stiff enough, certainly not when comparing the predictions to measurements where creep is ignored. When looking at DM7 and DM9, the predictions by CPT-based *p-y* methods have a closer match to the measurements with increasing *L/D* ratio. But predictions for the pile with the largest *L/D* ratio, DM3, do not necessarily show a better match to the measurements than the pile with medium *L/D* ratio, DM7.

It is interesting that the CPT-based methods tend to underestimate the soil stiffness under small loads, however, for large loads, the incremental stiffness (secant slope) of the CPT-based *p-y* methods seems higher than in the PLT measurements. If the loads are increased further the CPT-based *p-y* methods give the impression to pick up stiffness without limitation. This latter phenomenon can be explained by the character of the CPT-based *p-y* curves. In Figure 5-4 the *p-y* curves of all the methods are plotted at a depth of 1/3 pile depth. The CPT-based *p-y* curves by Novello (1999), Dyson & Randolph (2001) and Li, Igoe & Gavin (2014) are not limited by an ultimate soil pressure, therefore the soil keeps gaining stiffness when the displacement increases. Although, the *p-y* formula by Suryasentana & Lehane (2016) is limited by an ultimate soil pressure, this pressure value is not reached yet for the modelled cases. On the other hand, API's soil pressure is constant beyond a certain displacement (ultimate soil pressure), which means that the soil stiffness gradually decreases with increasing applied load resulting into large displacements. This explains why the API method predicts a softer pile response than the CPT-based *p-y* methods

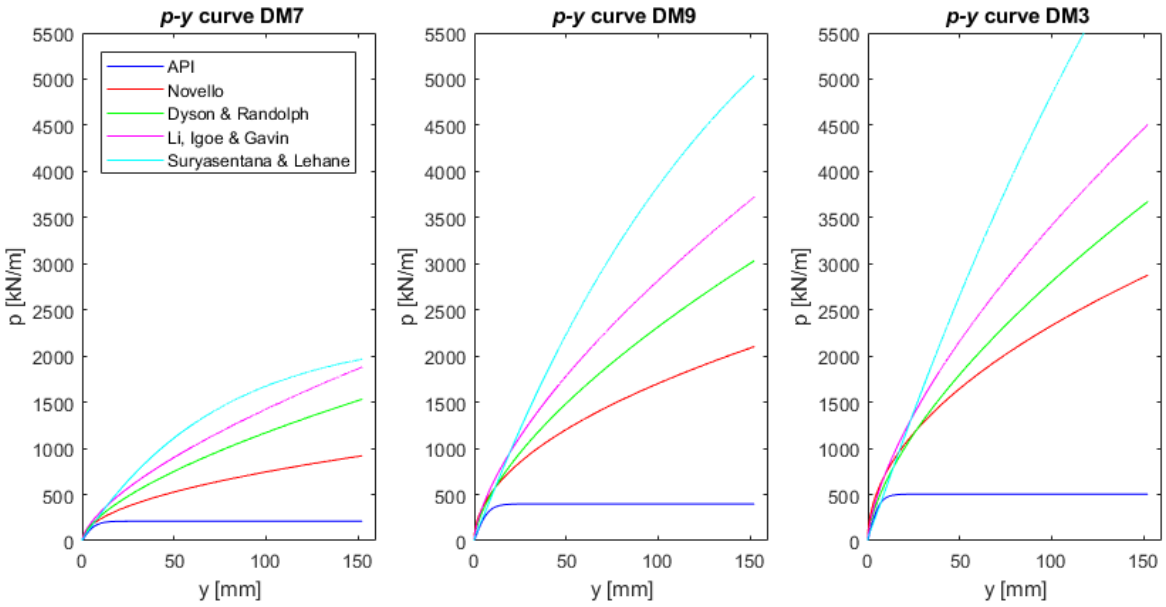

Figure 5-4: p-y curve at L/3 per p-y method for short, medium and long pile

5.2.2 Discussion

That the soil stiffness is generally underestimated for the short pile for all methods is consistent with the theory, explained in Section 2.5, that other soil reaction terms additional to *p-y* curves play a role in short the pile behaviour.

As with measurements and assumptions in general, the analysed situation may be different from the real situation. Possible measurement errors or assumptions could have led to inaccuracies in the results. Besides, soil is a non-homogenous medium and therefore soil properties have a vertical and lateral variability. If the location of the CPT measurements differed from the location where the PLT measurements were taken, it is possible that the assumed soil parameters have inaccuracies. Figure 5-5 shows the minimum, maximum and average CPT profiles that were measured among all pile locations in Dunkirk. In Appendix C, the pile response per *p-y* method is modelled with soil parameters that have a reasonable offset. The q_c profiles are varied with +/- 5 MPa and show that pile behaviour is highly dependent on the q_c parameter. Assumptions for the unit weight have influence on all *p-y* methods. The CPT-based *p-y* methods are less depended on variances in the unit weight than the API method (modelled for γ' = +/- 1 kN/m^3). The API method is also dependent on the friction angle, therefore the pile response is modelled with φ' = +/- 2^o, with a maximum of 42^o. As the soil initially is assumed to be very dense with high friction angles, the effect of lowering the friction angle is more clear. The friction angle is directly related to the initial stiffness and the ultimate soil pressure of the API *p-y* springs. Lowering the friction angle therefore has a severe influence on the soil stiffness and pile displacements.

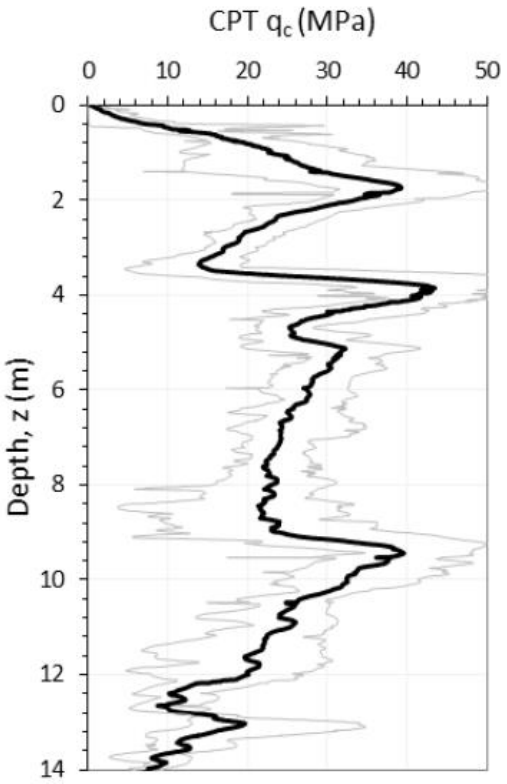

Figure 5-5: Minimum, maximum and average CPT profile at Dunkirk site

Part 3:

Investigation into a new CPT-based *p-y* method

This part of the research describes the investigation into a new *p-y* method based on PISA PLT data. For long and slender piles, the lateral distributed pressure *p* governs the lateral pile behaviour, hence, the total soil resistance that occurs under lateral pile loading is equal to the lateral pressure. The *p* and *y* components can therefore be derived from the PLT strain measurements. In this research part is described how PISA PLT data is interpreted and processed and what pitfalls are encountered during the process. A curve fitting assessment on 'simple' MATLAB curve fitting techniques is carried out in order to derive the soil pressure.

6. PLT data processing

6.1 Raw measurement data

In Subsection 2.3.1 is explained how PLT data can be used to derive *p-y* curves. In this Chapter, the same approach will be adopted to obtain the displacement and pressure profiles. As explained before, the *p-y* components should be derived from a pile that is such long that the *p-y* term is the only soil reaction term that dominates the pile displacement. The longest pile from the pile load test database is DM3 with an *L/D* of 8. This pile was subjected by 8 load increments, but before the load was increased further, the load was held constant until a desired displacement was reached. In the PISA report is mentioned that the last load step led to inaccurate strain data at some depth levels, therefore the eighth load step is ignored in further analysis of the PLT data.

During the pile load test the following measurements were taken:

- Applied load at e=10.062m, measured by means of a load cell.
- Ground- rotation and displacement, measured and derived from above ground LVDT instruments.
- Vertical strain, measured by means of fibre optic strain gauges that were mounted below ground at bot passive and active side of the pile. The strain was measured at 13 points along the pile length, from which one was above ground. No exact measurements were taken at ground level or pile toe.
- Rotation, measured by means of inclinometers above and below ground at the neutral line of the pile (both sides). The inclination was measured at 12 points along the pile length from which one was above ground. No exact measurements were taken at ground level or pile toe.

The raw results of these measurements are displayed in Figure 6-1 and Figure 6-2.

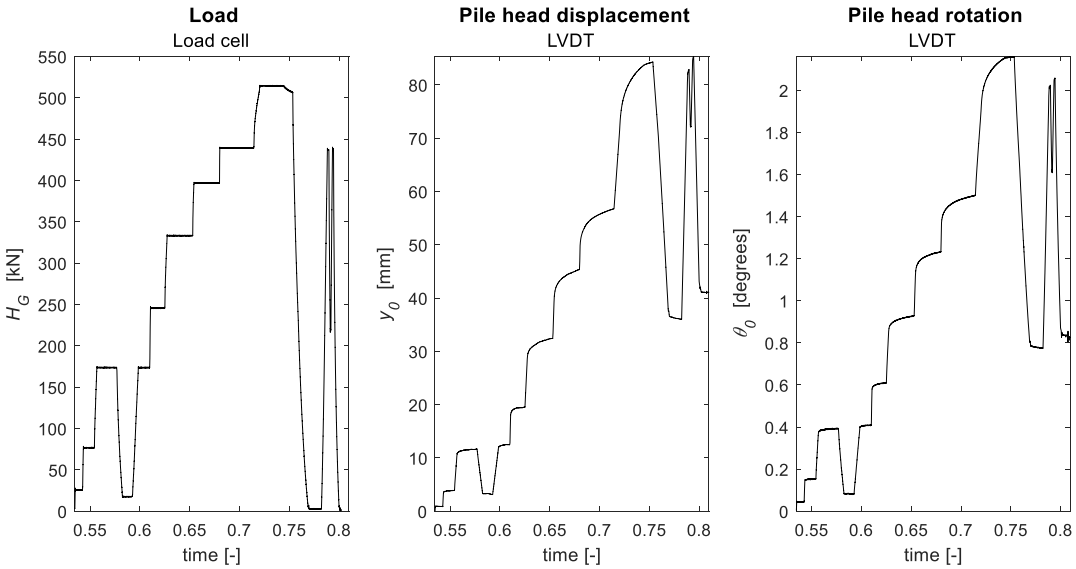

Figure 6-1: Above ground PISA PLT measurements taken from the DM3 pile

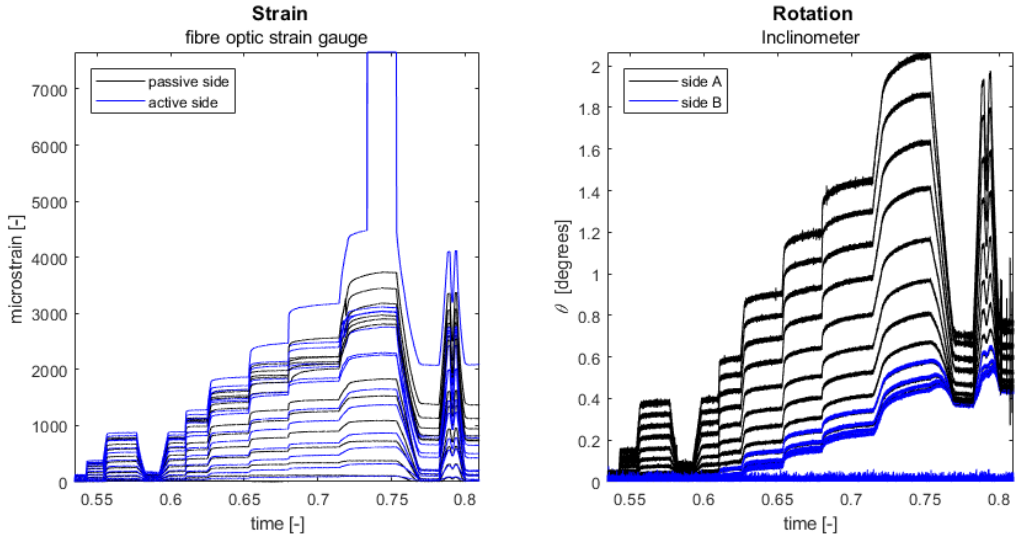

Figure 6-2: Below ground PISA PLT measurements taken from the DM3 pile

6.2 Data per load step

To determine the pile's behaviour per load step, raw PLT data is extracted at the time period just before the load was held constant. In this approach, the PLT measurements are altered as little as possible, but it should be noted that in all previous load steps the pile was allowed to displace while the load was not increased (creep effect) and in the extracted data thus is accounted for creep displacements. In Figure 6-3 is shown which load steps are considered together with the corresponding ground displacement and -rotation. In Figure 6-4 the raw strain and inclinometer data along the pile depth are extracted for the same load steps.

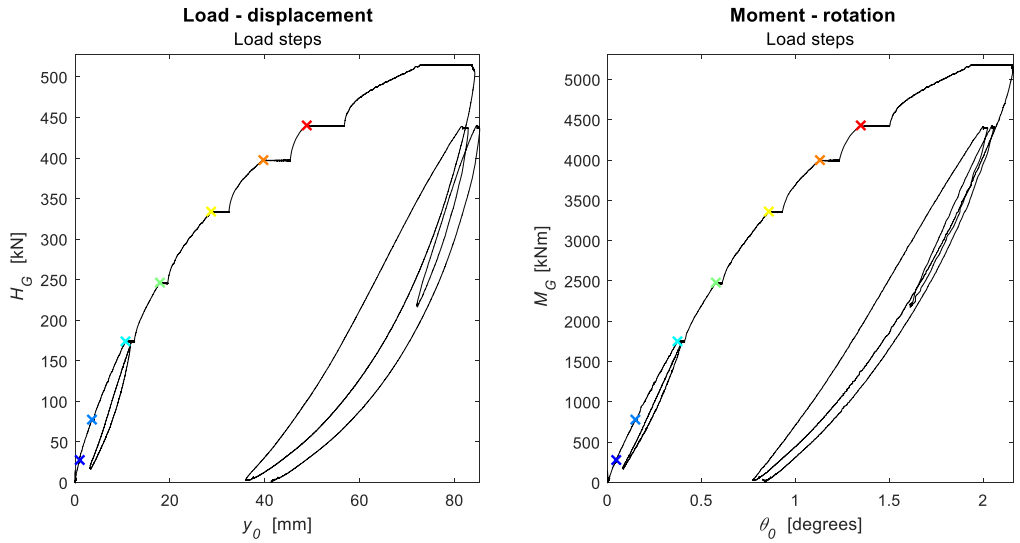

Figure 6-3: Ground- displacement and rotation per load step

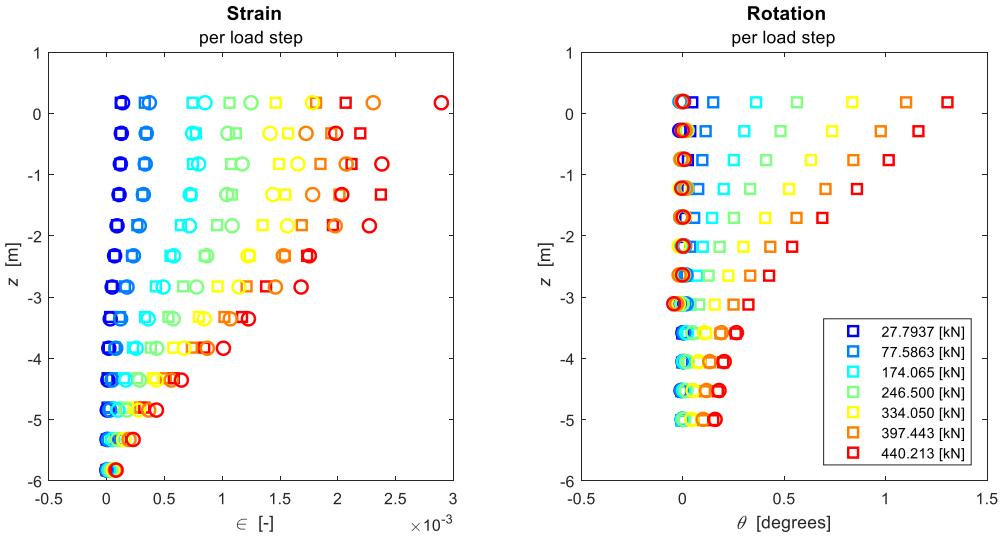

Figure 6-4: Strain and rotation data per load step, (squares correspond to passive side and rotation A, circles correspond to active side and rotation B)

In Figure 6-2 and Figure 6-4 can be seen that at some depths, the inclinometer data at one side (blue and circles) is not measured correctly. This data is discarded in further analysis and the resulting rotation is shown in Figure 6-5 with coloured crosses. For the strain data some variance between the pile sides can be seen too, especially above ground level. In Figure 6-6, the strain data is converted into moment data by means of the approach explained in Subsection 2.3.1. In the figure, also a straight line is drawn that represents the linear applied moment as function of depth: $H_G \cdot (e - h)$, where e is the eccentricity and h the height above ground level (negative h, means locations below ground level). At ground level, the moment should approximately be equal to $M_G = H_G \cdot e$. Below ground level, the soil acts with a force on the pile in opposite direction to the applied load, therefore it is not be possible that the pile bending moment exceeds the linearly extrapolated moment. As a result, the measured moments that exceed the black line are discarded. Subsequently, the remaining moments measured at each side are averaged to obtain the moment per depth level. When both of the measured moments exceeded the line, the value of the extrapolated moment was selected. The coloured crosses in the figure show the resulting moment profile that is used for further analysis.

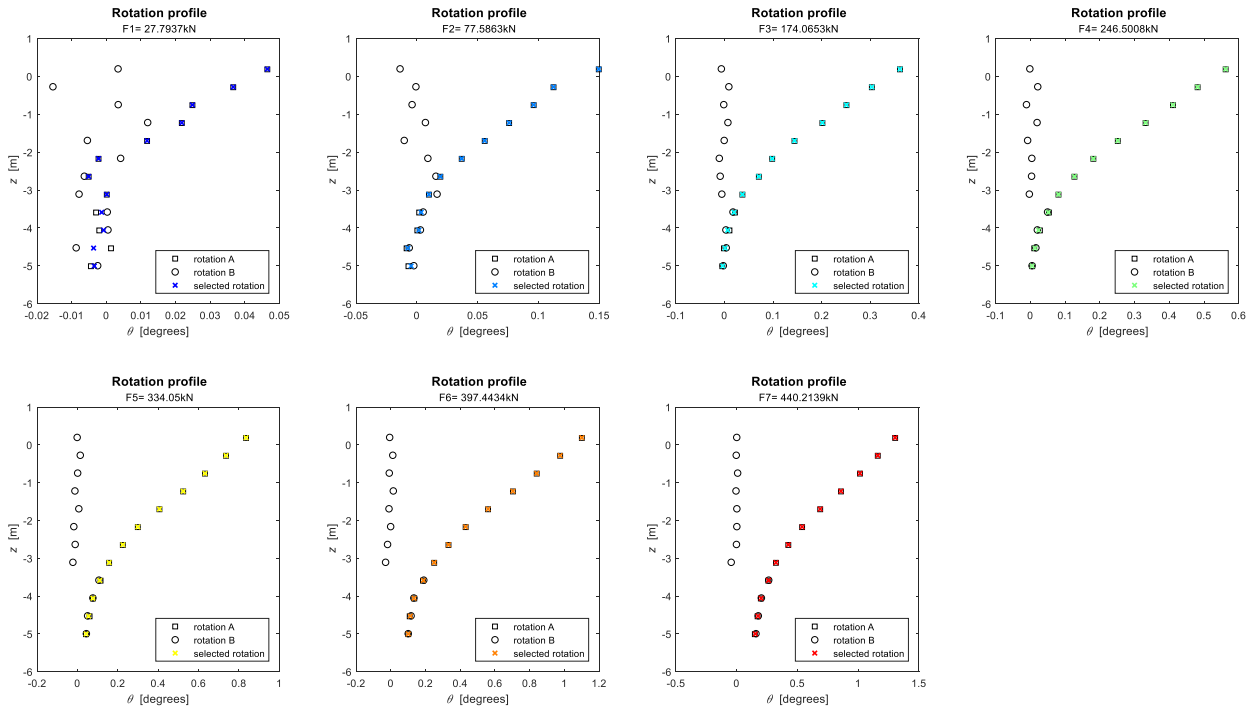

Figure 6-5: Measured rotation vs. selected rotation data

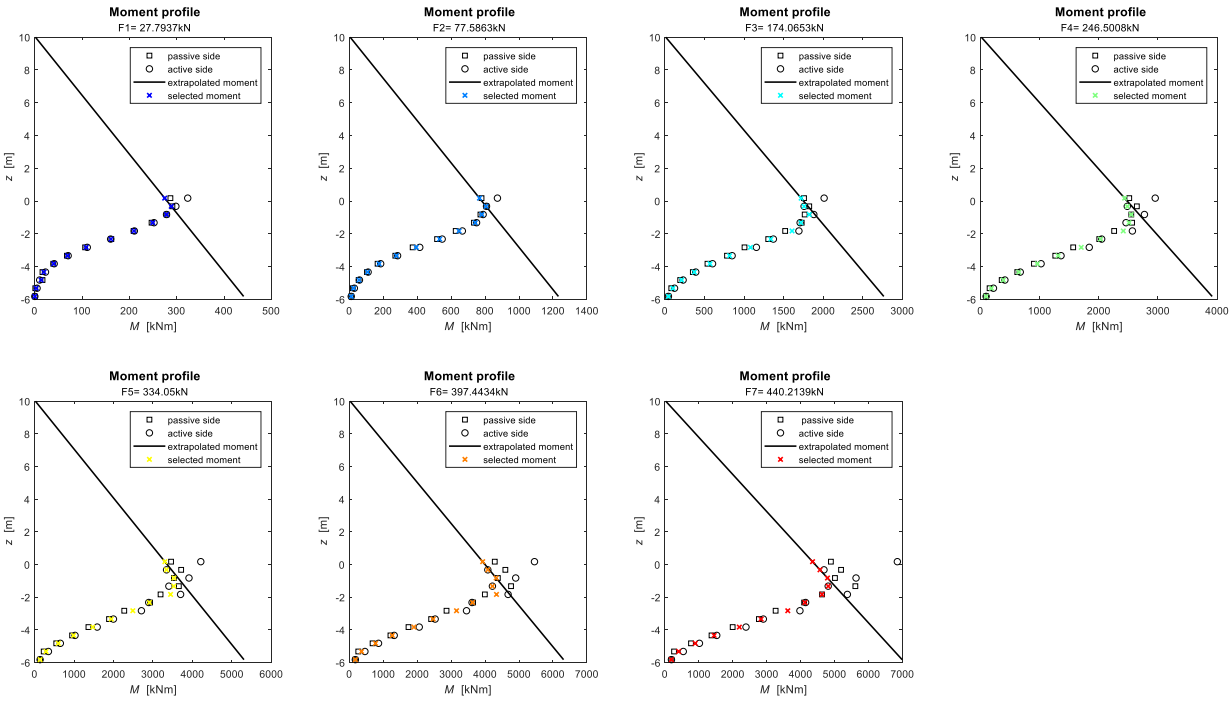

Figure 6-6: Measured moments vs. selected moment data

6.3 Data processing

In Subsection 2.3.1 is described how the soil pressure and displacement can be obtained from the moment. Following these steps directly results into the pile displacement and soil pressure profile shown in Figure 6-7 and Figure 6-8. The ground displacement and -rotation from Figure 6-3 are used as boundary conditions in Equation (2.3).

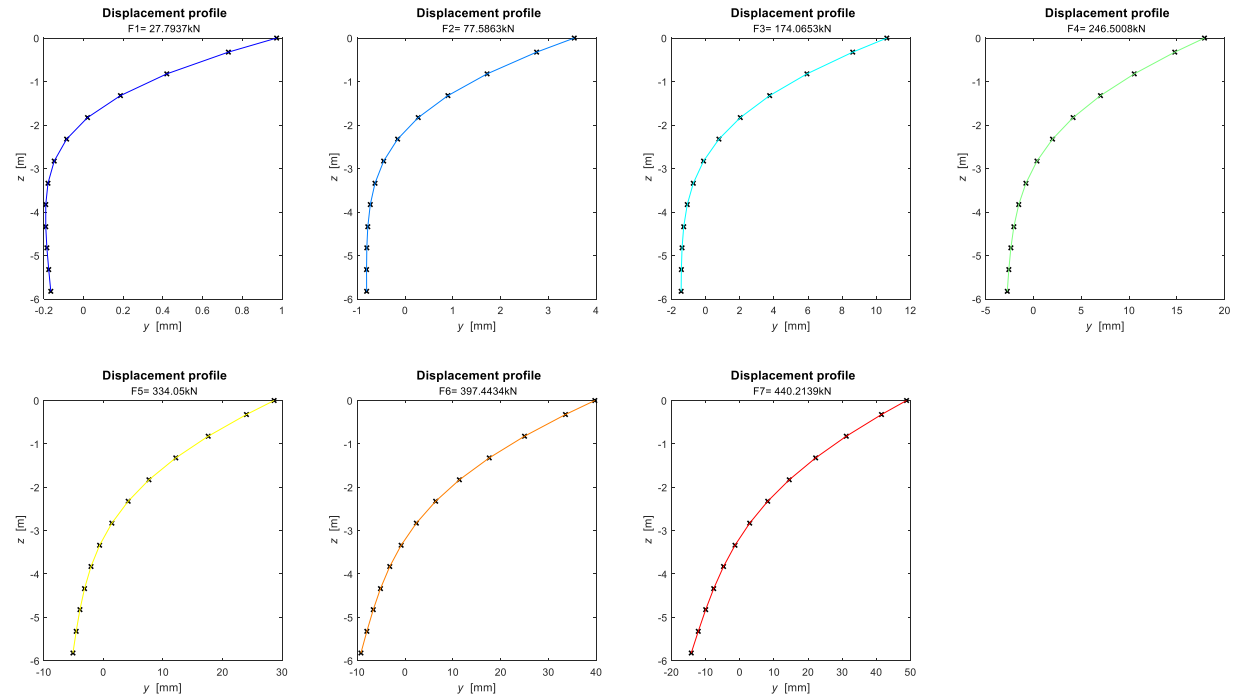

Figure 6-7: Displacement profile obtained after integrating the rotation profile

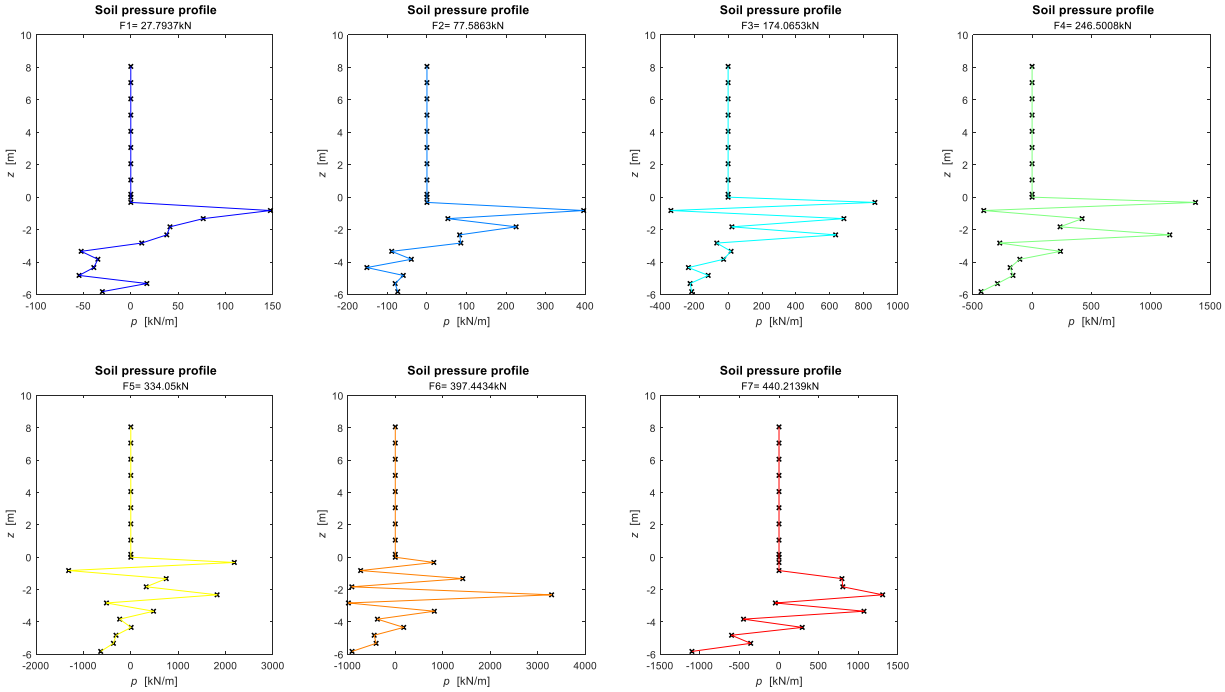

Figure 6-8: Soil pressure profile obtained after double differentiating the moment profile

Generally, taking a (double) integral is relatively accurate, however, a (double) derivative is more error prone as small changes in the data lead to relatively large changes in the slope. When data is not relatively smooth or accurate, problems can occur when the data is differentiated. Because the strain data is recorded at discrete depths, the resulting moment profile is discontinuous. Differentiating raw measurement data can therefore result into wiggly soil pressure profiles, this can be seen in Figure 6-8. Constructing a continuous curve that fits the strain data points in an approximate way may overcome this problem.

For the completeness also the shear profile and rotation profile according to the approach of section are shown in Figure 6-9 and Figure 6-10. In Figure 6-9 can be seen that there is a small offset between the measured rotation and the rotation that is obtained after integration with the measured ground displacement and rotation used as boundary conditions.

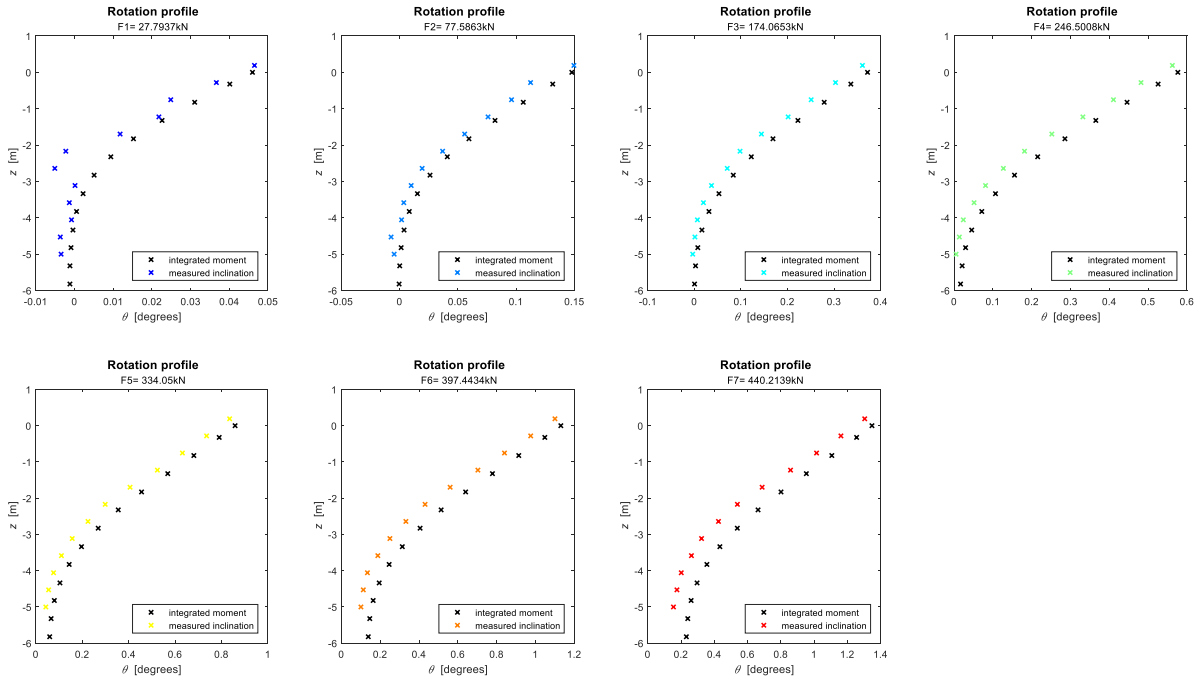

Figure 6-9: Rotation profile obtained after integrating the selected moment data vs. measured rotation from inclinometers

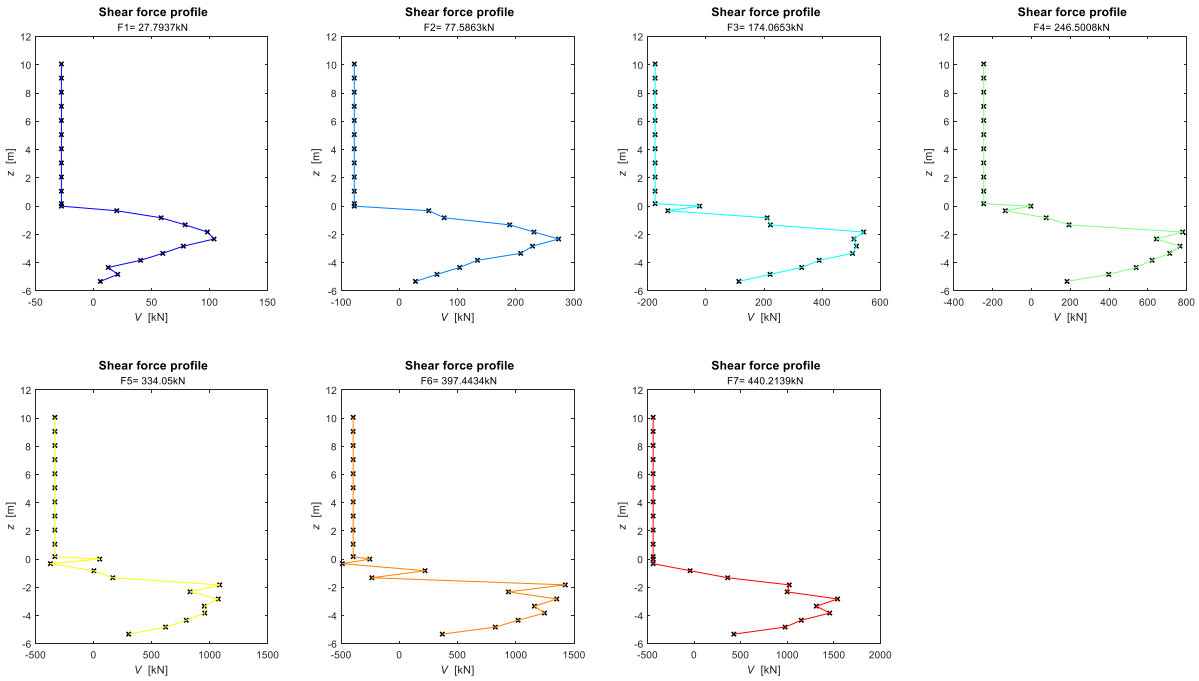

Figure 6-10: Shear profile obtained after differentiating the selected moment data

7. Curve fitting assessment

The use of discontinuous and relatively unsmooth data leads to inaccuracies when differentiated. This could be seen in the previous chapter, where double differentiation of the measured moment profile results in wiggly and unpractical soil pressure curves for all load steps. By means of curve fitting it is possible to create a continuous profile from a given set of data points. Curve fitting is a process in which a curve is constructed through the data points and an estimation is given for intermediate values. In this chapter, four types of curve fitting techniques that are available in MATLAB, are analysed to find a proper fit for the moment profile of DM3, and to derive the pile displacement and soil pressure.

7.1 Curve fitting techniques

In Figure 7-1 an overview of the construction codes in MATLAB for a global polynomial and piece wise polynomials (splines) is given. In MATLAB, splines can either be created by means of the MATLAB spline tool box ('simple spline fitting') or built from scratch ('advanced spline fitting'). Because of time limitation, the advanced method is not investigated in this thesis. This section gives a brief summary on the characteristics and construction of the curve fitting techniques displayed in Figure 7-1. More details about these curve fitting techniques or for example about 'advanced' curve fitting techniques, can be found in the online available MATLAB manual (The MathWorks, Inc, 2018).

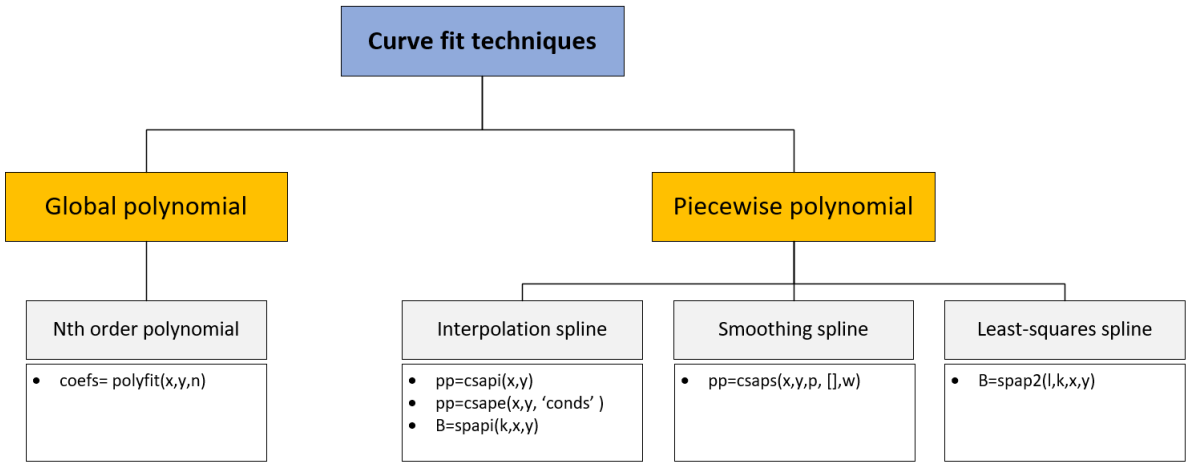

Figure 7-1: MATLAB curve fit construction codes

7.1.1 Global polynomial

Sometimes it is sufficient to describe the trend in a dataset just by means of one simple equation, for example by an exponential formula or an n^{th} order polynomial. In the MATLAB curve fitting toolbox (`cftool`), several of these regression models are already predefined and can be selected to find suitable regression coefficients for a given dataset.

In literature, n^{th} order polynomials are mentioned as a possible technique to fit strain gauge data (Haiderali & Madabhushi, 2016). When a dataset is described by one polynomial, it is called a global polynomial. In MATLAB, the polynomial coefficients of an n^{th} order polynomial that is fitted through input data *x* and *y* can be found with `polyfit(x,y,n)`.

7.1.2 Piecewise polynomials

Sometimes it is less convenient to fit an n^{th} order global polynomial, for example when a large set of (irregular) data points is stretched over an interval. To follow the trend in such a dataset, the degree of the polynomial 'n' has to be chosen large and this can lead to a wiggly effect. Alternatively, the interval can be divided in a few subintervals in which each subinterval is described by a separate polynomial. This is called a piecewise polynomial or a spline. In literature, also this type of curve fitting is mentioned (Yang & Liang, 2006).

With the MATLAB spline tool box (`sftool`) the following splines can be created:

1. Interpolation splines
2. Cubic smoothing spline
3. Least-squares spline

Instead of using `sftool`, the commands from Table 7-1 can be used to program the splines in the command window. The splines are represented using two forms: the ppform and the B-form. The pp-form describes the local polynomial coefficients for the spline in each break interval between two data points. With the B-form it is possible to construct break intervals outside of the given data points.

Table 7-1: MATLAB commands for spline construction

cs...	construct cubic splines (in ppform)
sp...	construct splines in B-form
..api	construct an approximation by interpolation
..aps	construct an approximation by smoothing
..ap2	construct a least-squares approximation

7.1.2.1 Interpolation splines

Csapi

Three types of interpolation splines are available in MATLAB. The default interpolation spline, `csapi`, is a cubic polynomial that is constructed in-between each two data points (break intervals) and fits the given input data exactly (except for the end points). It fulfils the not-a-knot end conditions, meaning that it has two continuous derivatives with breaks at all interior data points except for the end points. `pp=csapi(x, y)`, or `pp= spline(x, y)`

Csape

Alternatively, `csape` is a cubic interpolation spline for which it is possible to define more specific boundary conditions at the end points. In MATLAB one can choose from the end conditions displayed in Table 7-2 and construct a spline with `pp = csape(x, y, 'conds')`. `csape(x, y, 'not-a-knot')` gives the same results as the function above: `csapi(x, y)`.

Table 7-2: MATLAB end conditions

'clamped'	Matches the end slopes
'not-a-knot'	Make second and second-last sites inactive knots
'periodic'	Match first and second derivatives at left end with those at right end.
'second'	Match end second derivatives
'variational'	Set end second derivatives equal to zero

Also, custom end conditions can be specified by means of `csape([x],[a y b],[A B])`. This code constructs a cubic polynomial p for which *Dp(A) = a, p(x(i)) = y(i), D2p(B) = b.* A and B are either 1 (1st derivative), 2 (2nd derivative) or 0, which means that the end condition is neglected.

Spapi

With the third spline type, `spapi` , the order of the spline can be changed, and breaks at other points than at the given data points can be chosen. The breaks of a spline are also called knots.

`B = spapi(knots,x, y)` or `spapi(k,x, y)`

In the latter case, by default, `knots= aptknt(x,k)`, in which automatically an acceptable knot sequence is generated based on input data *x*. *k* is the order of the desired spline (*n + 1*). In this case, `B = spapi(aptknt(x,k),x, y)`, leads to the same results as `spapi(k,x, y)`.

An alternative for the knot distributions is to use `optknt`, that automatically generates the optimal knot distribution based on the given data.

7.1.2.2 Cubic smoothing spline

Csaps

A smoothing spline is a cubic spline that approximates the input data by means of a smoothing factor, rather than fitting it exactly. The cubic smoothing spline approximates the data with `pp = csaps(x,y)` in which the smoothing factor is automatically chosen by the program.

With `pp= csaps(x,y,p, [], w)`, the amount of smoothing can be controlled by means of a smoothing factor, p. It is also possible to give extra weight to some of the data points with the smoothing factor, w.

7.1.2.3 Least-squares spline

Spap2

A least-squares spline approximation can be obtained with the spap2 function `B= spap2(knots,k,x,y) or B= spap2(l,k,x,y)`. Break intervals and spline order can be specified by the user.

In the latter function `l` represents the desired number of spline pieces and automatically generates a knot sequence based on given input. If the generated knot distribution is not satisfying, a potentially better knot distribution can be obtained by `sp = spap2(newknt(sp),k,x,y)` Repetition of this procedure can lead to more improved knot distributions.

7.2 Curve fitting results for PISA data

In this section, the curve fitting techniques from Figure 7-1 are used to fit a curve through the moment data points that were derived from strain measurements of the DM3 pile. For reasons of clarity, this is shown only for the moments that were measured in the 7th loading step.

Expectations

Because pile DM3 has an *L/D* of 8, the pile is expected to be long enough to have fixed pile toe conditions. Therefore it is assumed, that the base moment-, shear- and pressure values are zero. At ground level, the shear force is expected to be as large as the applied load. The moment and shear profiles can thus be used to check whether the PLT data has the right requirements for the derivation of accurate profiles for the pile displacement and soil pressure.

Input data

Input `x` contains the average pile depth values at which strain measurements were recorded and input `y` contains the moment data points from load step 7, shown in Figure 6-6. The deepest depth where strain has been measured (-5.814m) is located at a higher position than the depth of the pile toe (-6.02m). Because it is expected that the pile has fixed pile toe conditions, an extra moment of zero was assumed and added to the data set.

Table 7-3: Input data

x [m]	0	0.323	0.82	1.323	1.828	2.323	2.828	3.338	3.828	4.338	4.823	5.323	5.823	6.02
y [MN]	4.428	4.571	4.791	4.812	4.630	4.125	3.621	2.835	2.192	1.450	0.892	0.404	0.092	0

Post-processing

The codes that are required for post-processing the polynomial and spline structures into moment-, displacement-, shear- and pressure profiles are displayed in Table 7-4. The codes follow the principles of Subsection 2.3.1. The integration constants, *C1* and *C2*, are equal to the rotation and displacement at ground level: $\theta_0 = 1.3480^o$ and $y_0 = 0.0489$m.

Table 7-4: codes for post-processing polynomials and splines (valid for pp-form and B-form)

Result	Polynomial	Spline
Moment	`polyval(coefs, x)`	`fnval(pp, x)`
Displacement	`polyint(polyint(coefs, C1), C2)`	`fnint(fnint(pp,C1), C2)`
Shear	`polyder(coefs)`	`fnder(pp)`
Pressure	`polyder(polyder(coefs))`	`fnder(pp, 2)`

7.2.1 Global polynomial

A global polynomial is fitted though the data set by means of `polyfit(x,y,n)` for n= 4, 5, 6, 10 and 11. The higher 'n', the more bends will appear in the curve. The high order polynomial with n=11, therefore results in an oscillating profile. The best prediction for the shear- and soil pressure curve is derived from a 5th order polynomial, although it is not possible that the pressure at ground level is negative (meaning that the soil reaction force acts in the same direction as the applied load) and the base shear force is rather high (same value as applied load).

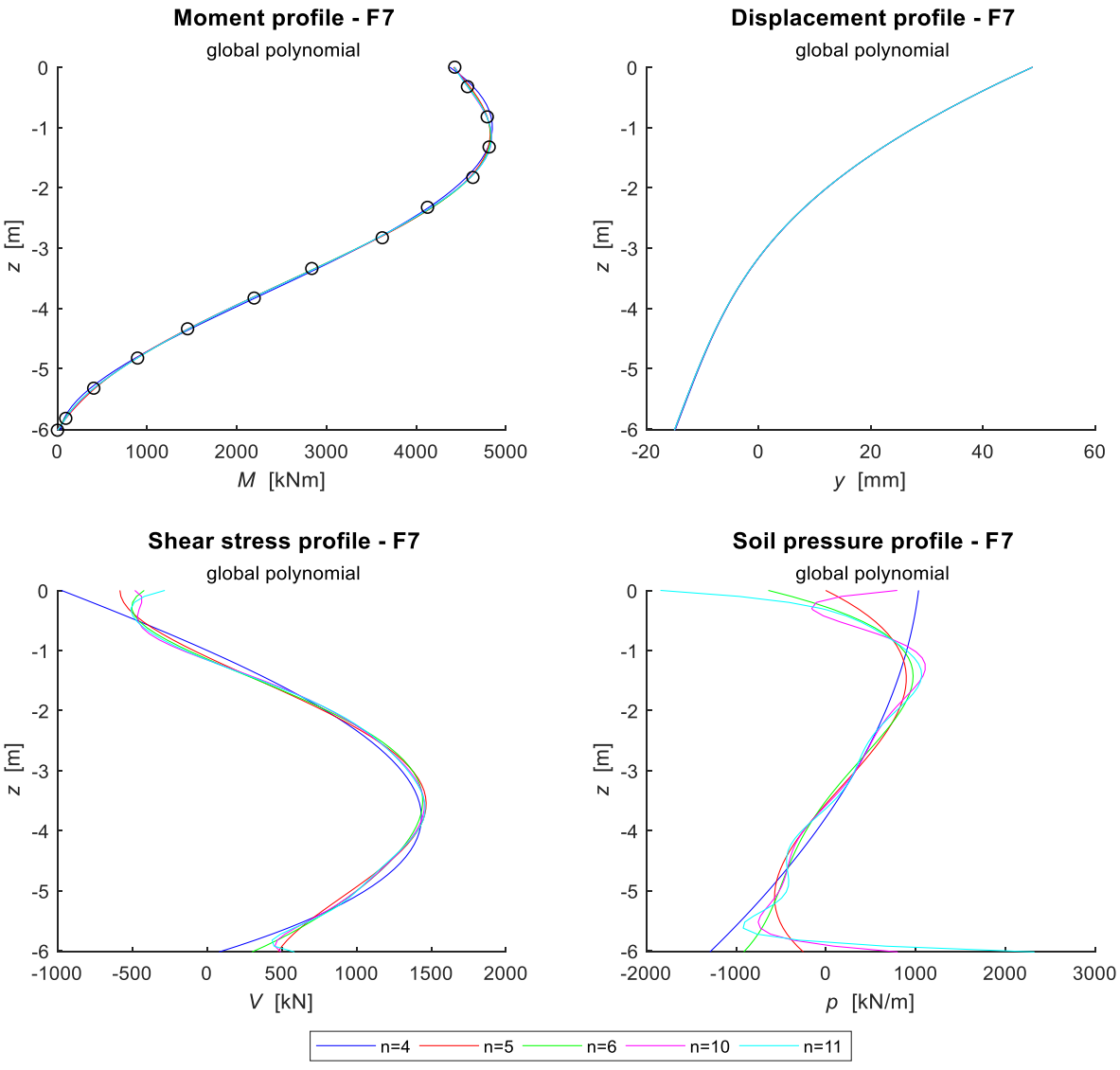

Figure 7-2: Global polynomial of degree 'n'

7.2.2 CSAPI & CSAPE

Because `csapi(x,y)` is an interpolation spline with not-a-knot end conditions and gives the same results as `csape(x,y, 'not-a-knot')`, this curve fitting technique is treated together with `csape`. To show the possible outcomes of the `csape` function with the standard end conditions provided by MATLAB, the end conditions from Table 7-2 have been plotted in Figure 7-3.

Boundary conditions that are expected for a long pile are programmed by means of `p_custom=csape(x,[Applied_load y 0],[1 1])` in which the the spline has the 1st derivative equal to the applied load at 0m depth and equal to zero at 6.02m depth.

The `csape` function is an interpolation method, which means that it passes exactly through all data points, except for (the end points) and thus has a break at each data point, which explains the wiggly effect in the soil pressure profile. Although the approximation for the moment profile looks accurate, the data does not appear to be smooth enough when the profile is differentiated twice. In the top two figures it can be seen that the various end conditions hardly have any effect on the displacement and moment profile.

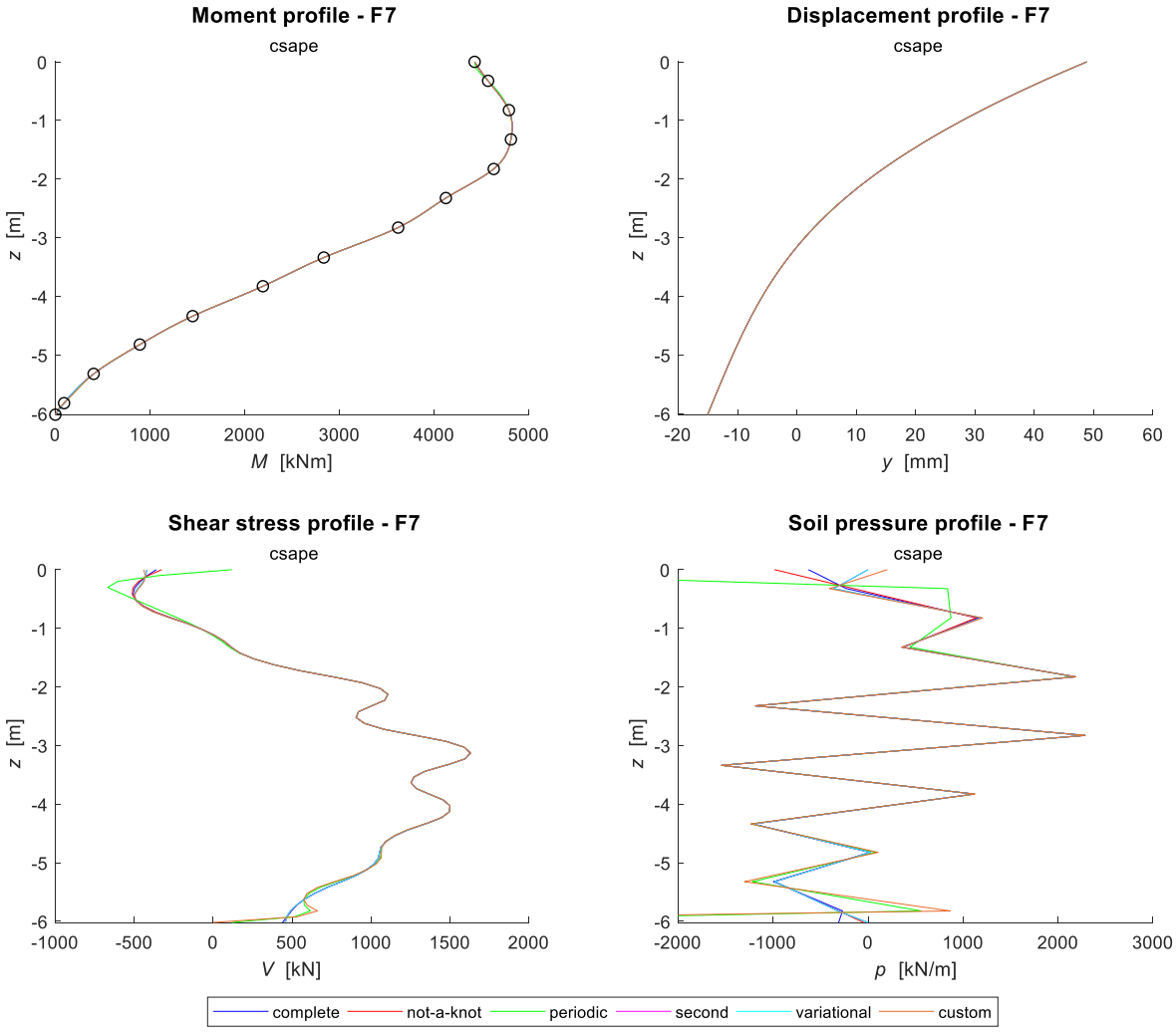

Figure 7-3: Interpolation spline with end conditions

7.2.3 SPAPI

With `knots= aptknt(k, x)` and `knots= optknt(k,x)` (k=4 and k=5), acceptable and optimum knot distribution were obtained for the interpolation spline `spapi(knots, x, y)`. Again, the interpolation spline results into a wiggly profile for the soil pressure. The cubic interpolation spline (*k=4*) has vertices at the breaks, while the quartic spline has smoother bends. For the given data set, there does not seem to be much difference in the results fitted by means of an optimum knot distribution or acceptable knot distribution. All `spapi` variants result into the same displacement profile, which is comparable to the displacement profiles of the `csape` variants as well.

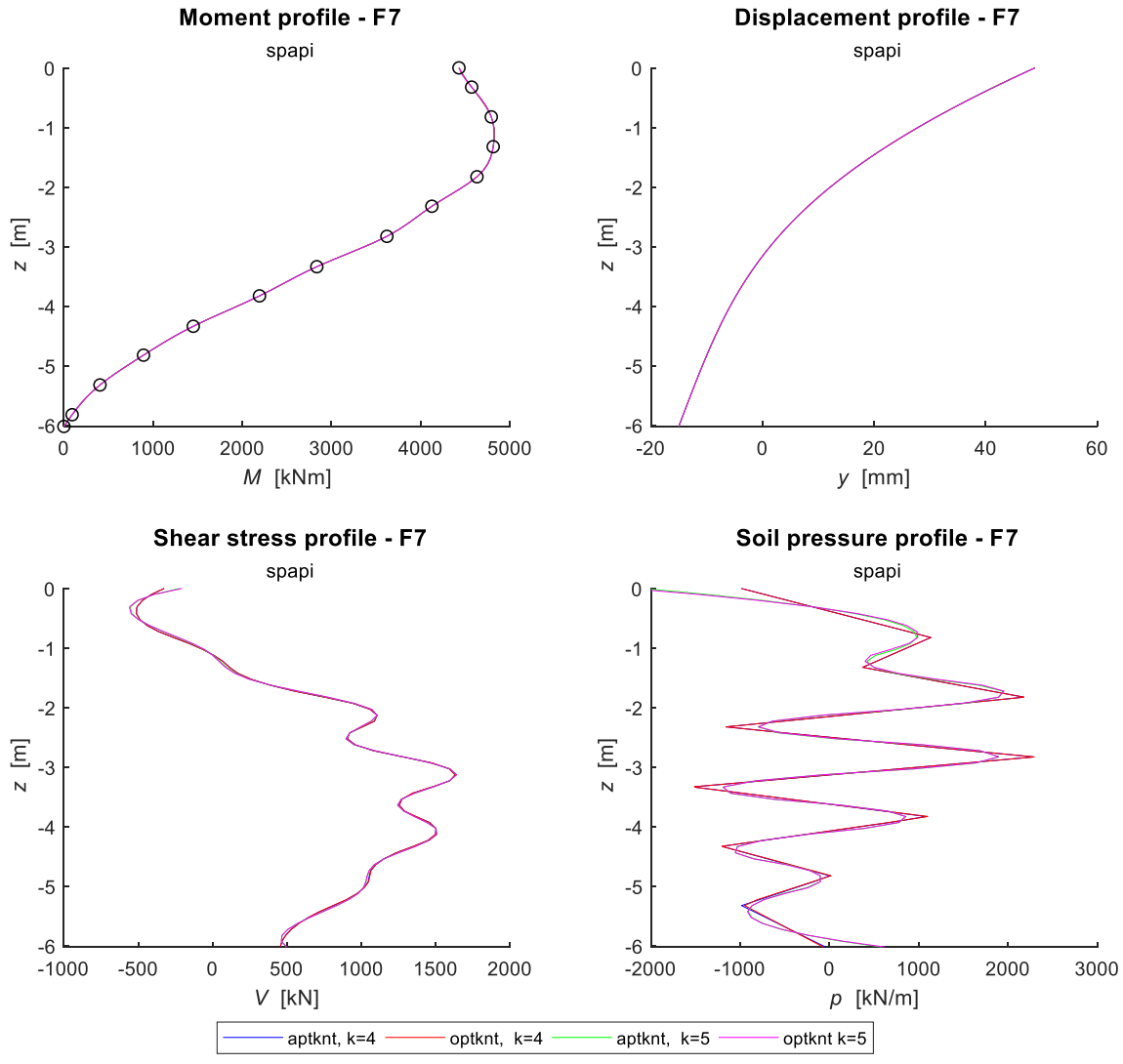

Figure 7-4: Interpolation spline with special knots

7.2.4 CSAPS

The `csaps` function approximates the given data with a certain tolerance represented by the smoothing factor *p*. In figure X the two extremes *p=1* and *p=0* are plotted together with the default smoothing factor *p** (in this case *p*= 0.9834) and three smoother approximations p= 0.75, 0.85 and 0.95. The default smoothing factor can be extracted with the following code: `csaps(x, y).`

The curves fitted with *p=1*, *p=0* result in inaccurate profiles for the soil pressure. p^* results again in a wiggly profile. The other soil pressure curves are quite smooth and have a reasonable shape for the soil pressure. All curves have a zero second derivative at ground level and pile toe, which is expected for an infinitely long pile. However, the base shear is as large as the load that is applied, which does not correspond at all with values expected for a long pile. On the other hand, the shear force at ground level is almost similar to the applied load, especially for *p=0.95*.

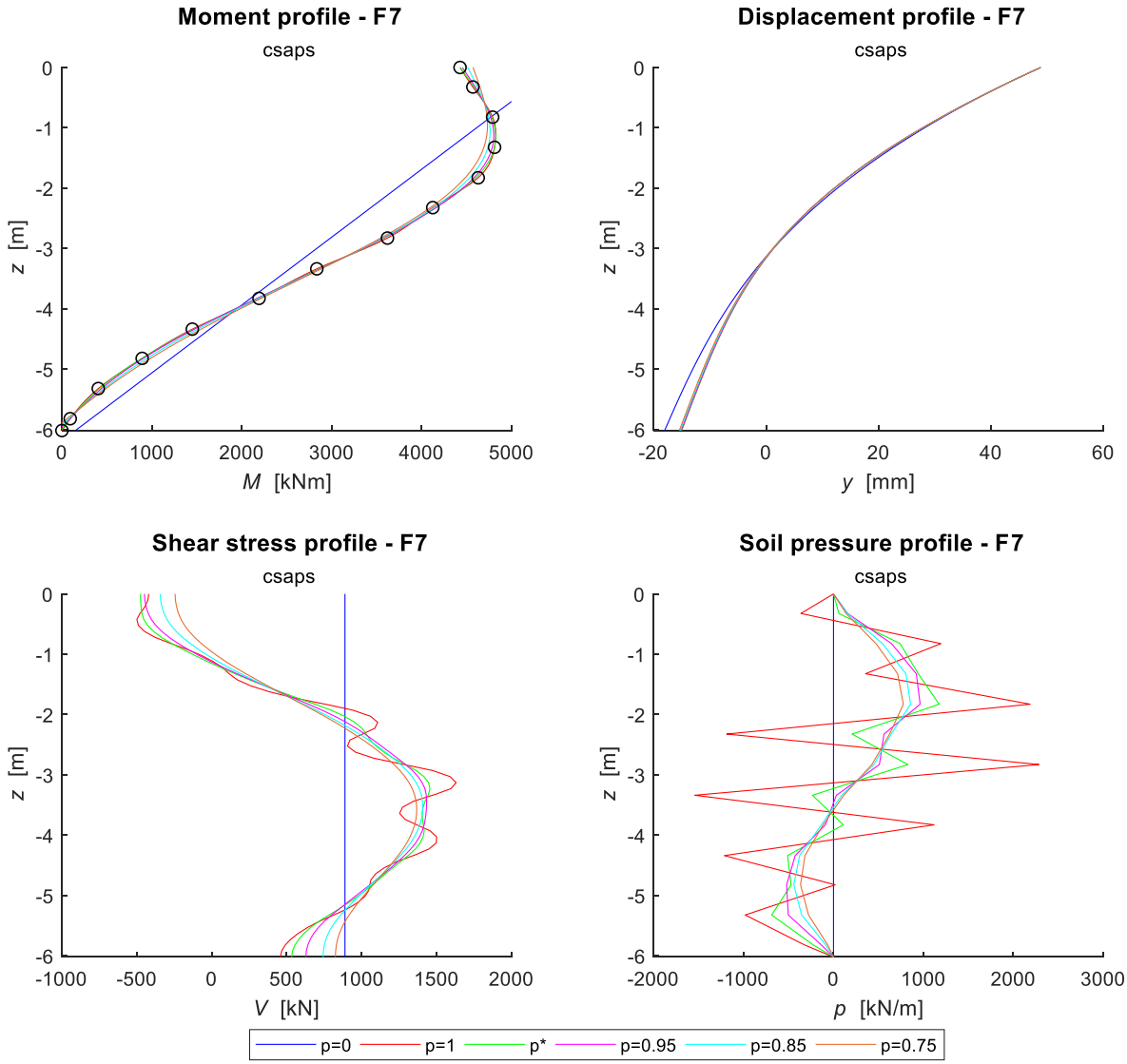

Figure 7-5: Smoothing spline with smoothing factor 'p'

7.2.5 SPAP2

With the least-squares approximation, splines are fitted with `spap2(l,k,x,y)`, for *l=3,4,5* and *k=4* after which the knots are updated for a possibly better knot distribution by `spap2(newknt(B),k,x,y)`. In the figure this is denoted by *l=3*,4*,5**. The `newknt` function does not necessarily lead to a better result for the shear- and pressure profile for the given dataset. The least-squares approximation spap2 gives a reasonable soil pressure for some variants, although the pressure profile is not a smooth profile. Though, just as for the other curve fitting methods, the base shear at the pile toe is too large to belong to a long pile.

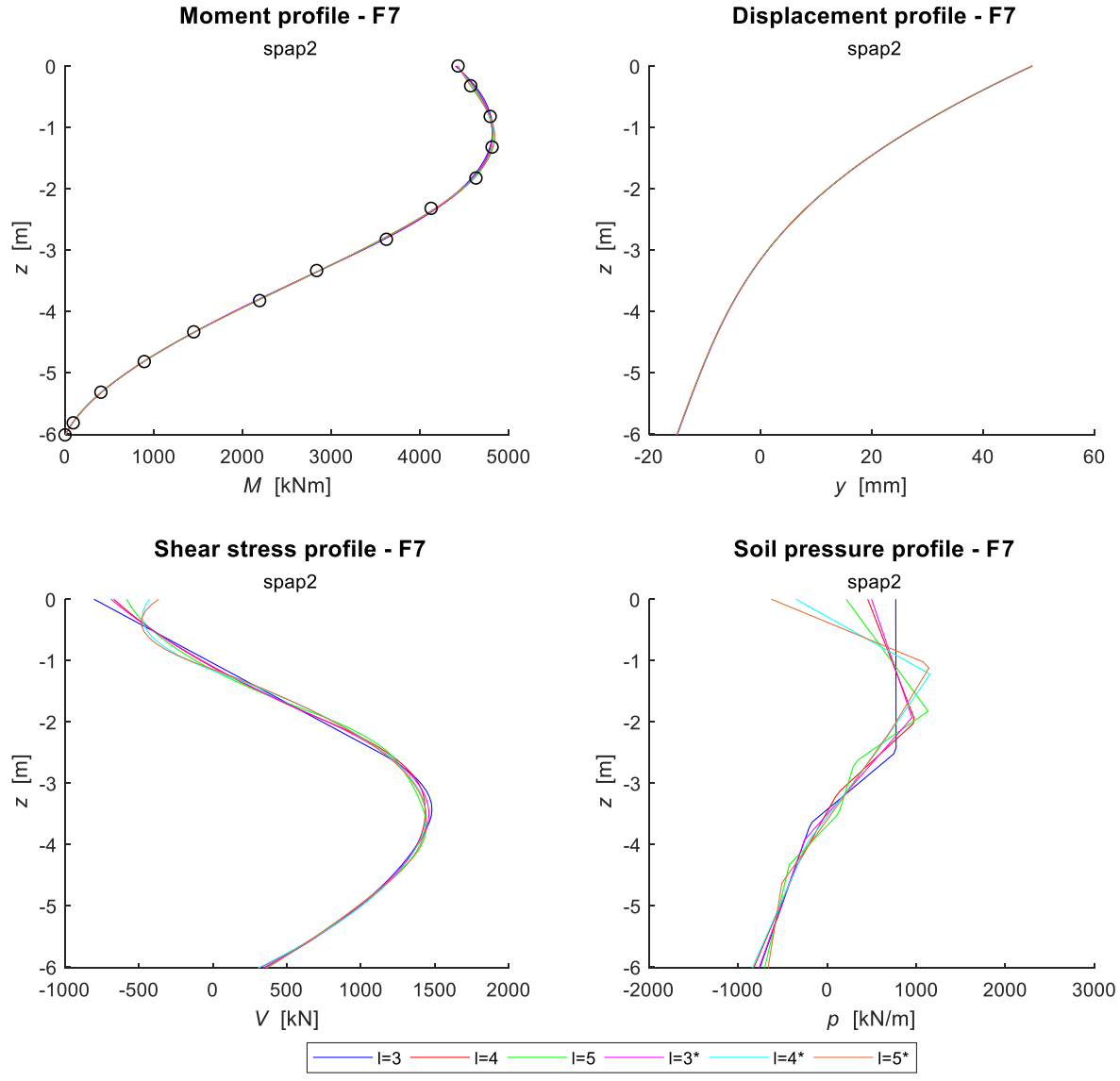

Figure 7-6: Least-squares spline

7.3 Curve fitting results for known pressure profile

To see how well the curve fitting techniques match to the 'real' soil pressure, the curve fitting techniques are also used to fit a curve through moment data, for which soil pressure data is known. In the figure below, the most optimal variant of each spline method is shown for a fictive pile. This pile has an *L/D* of 12 and its moment and pressure profile are predicted according to Suryasentana & Lehane's (2016) *p-y* relation by means of the pile-response model from Chapter 4. The spline methods are used to fit a curve through the calculated moment profile after which the curve is differentiated twice and compared with the pressure profile is calculated with the pile-responde model. The results are shown in Figure 7-7: the pressure profile generated by the pile response model (circles) is compared to the pressure profile obtained by curve fitting (solid line). For the mid-section, all curve-fitting methods predict similar good results for the soil pressure. The end-conditions however, are hard to control for most of the methods. `csaps` and `csape` give overall good predictions, because the pile used in this analysis is such long that the boundary conditions at the ends of the pile can assumed to be fixed. This analysis shows how well the curve fitting techniques perform for generated smooth data of a long pile in order to give a general conclusion per curve fitting technique. An overall summary and conclusion per curve fitting method that is investigated in this thesis, is shown in Table 7-6

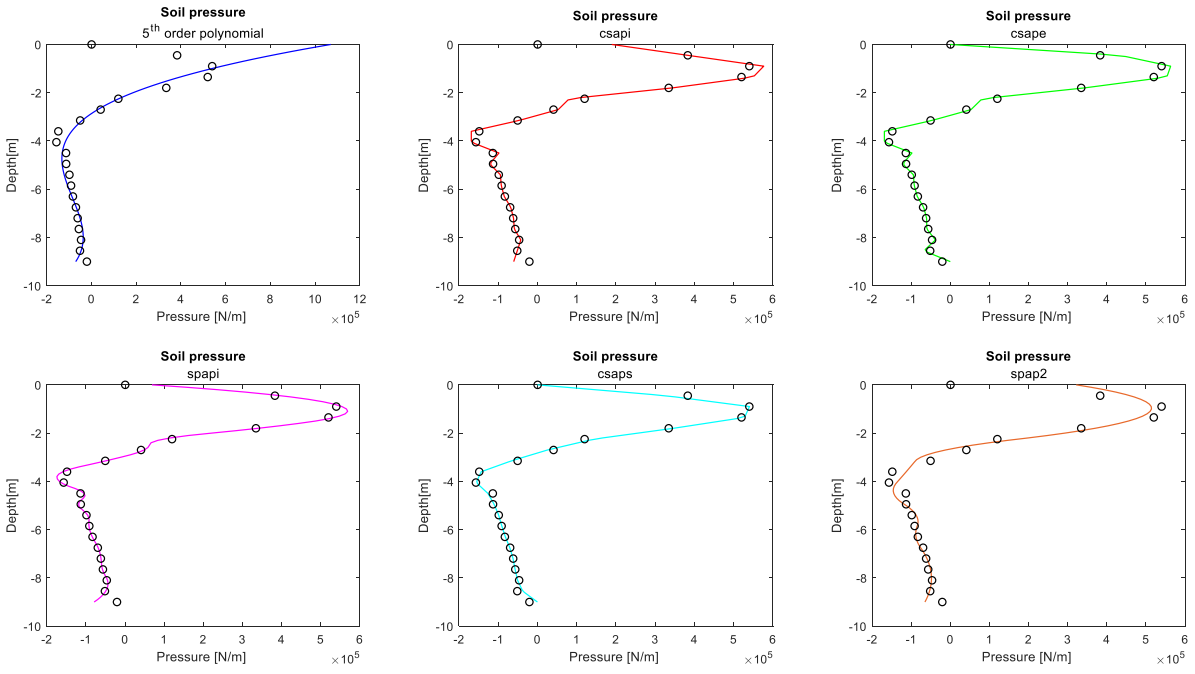

Figure 7-7: Long pile pressure profiles

The codes that were used to fit the data are displayed in Table 7-5. The soil pressure was obtained by using the double derivative functions from Table 7-4.

Table 7-5: Spline fitting functions used for comparison with known pressure profile

`polyfit(x,y, 5)`	`csapi(x,y)`	`csape(x , [0 y 0], [2 2] )`
`spapi(optknt(x, 5), x,y)`	`csaps(x,y, 0.98)`	`spap2(7, 5, x,y)`

Table 7-6: Conclusion curve fitting methods

Curve fit method	Fitting data	Description	Appropriate for soil pressure?
Global polynomial	`polyfit(x, y, n)`	Approximation by n^{th} order polynomial	No. Oscillates for high order polynomial, end-conditions cannot be controlled
	`csapi(x, y)`	Fits input data with not-a-knot end conditions (inactive ends)	Not when input data is inaccurate, end-conditions cannot be controlled
Interpolation spline	`csape(x, y, 'conds')`	Fits input data with custom end conditions	Only when input data is accurate and pile boundary conditions are known
	`spapi(knots, x, y)`	Fits input data with custom knot sequence	Only when input data is accurate, and only for mid-section
Smoothing spline	`csaps(x, y, p, [], w)`	Approximation by means of smoothing- and weighting factor 'p' and 'w'	Only when pile toe is 'fixed'
Leas-squares spline	`spap2(l, k, x, y)`	Approximation by least-squares with number of spline pieces 'l' and order ' k'.	Not when input data is inaccurate, end-conditions cannot be controlled

7.4 Conclusion and discussion

7.4.1 Conclusion

It can be concluded that neither of the MATLAB curve fitting codes that were investigated for the PLT data of DM3, lead directly to soil pressure curves that would be expected for a long pile. For all fitting techniques the base shear is too large. With the `csape` function, the end conditions can be manipulated so that they fulfil the assumptions for a long pile, but the curve itself is rather wiggly with sharp bends implicating that an interpolation spline might not be suitable for the differentiation of unsmooth data. The smoothing spline `csaps` gives a reasonable smooth shape for the soil pressure and good estimations for the shear force at ground level. Despite having zero pressure at the pile toe, the base shear is quite large, which could mean that the data might not represent a pile that is long enough for this particular boundary conditions.

7.4.2 Discussion

Apart from curve fitting limitations and the pile length, other possible pitfalls are strain data quality and interpretation of the PLT data in general. As can be seen in all the graphs from Section 7.2, a small change in the input data leads to big differences in the derivatives. Specifically, assumptions for the base moment and the moments just below the ground level and at which points of time the strain data is extracted could have influenced the results. As explained before, during the tests is accounted for creep (horizontal parts in Figure 6-1), therefore ‘many’ rotation, displacement and strain values correspond to a load increment. The data measured over the horizontal part can be extracted at either the start or end of the time interval or even averaged over the whole time interval, all resulting in totally different strain input. Ultimately, there is too little information to state whether the data, pile dimension or curve fitting techniques is or are the limiting factors in this research.

8. Conclusions

8.1 Evaluation of existing *p-y* methods

In part 2, the performance of CPT-based *p-y* methods is compared to the API method and pile load test measurements from a respectively short, medium and long pile. The analysis showed, that the API method generally underestimates the soil stiffness and predicts larger pile head displacements than the CPT-based *p-y* methods and PLT measurements. Especially for the short pile, the API method seems not sufficient for predicting ultimate resistance.

For the short pile, and for small displacements especially, the CPT-based *p-y* methods underestimate the soil stiffness as well, but show a considerably better fit with the PLT measurements than the API method. The accuracy of CPT-based *p-y* methods increases with increasing *L/D* when looking at the short and medium pile.

Based on this analysis it can be concluded, the current API standard needs a revision and that a CPT-based design method is a promising method for the prediction of pile behaviour.

8.2 Investigation into new *p-y* method

In part 3, the research continues with the investigation into a new CPT-based *p-y* method based on pile load test data. The available strain data was not accurate enough to derive the soil pressure directly by means of differentiating. It is tried to generate a smoother strain profile by means of curve fitting. 'Simple' curve fitting techniques that were available in MATLAB are analysed and used to obtain the soil pressure. Neither of the derived soil pressure curves showed results that were expected for a pile that is long enough to have its behaviour governed only by lateral soil pressure, hence it was not possible to continue the development of a new method based on the current dataset.

From this research part it can therefore be concluded that it may not be possible to develop a new *p-y* method, by using DM3 strain data in combination with MATLAB's 'simple' curve fitting techniques.

Part 4:

Future work

In this part, a future work approach is presented that can be used as a guideline for further research into the development of a new CPT-based design method for large diameter monopiles. First discussed are all pitfalls that have been encountered during this research along with recommendations on how to avoid them. Then a step by step approach is given in which is elaborated on data gathering, PLT testing, PLT data processing, curve fitting and on how to the link *p-y* curves to *qc* data. Also the first preliminary steps for the derivation of the additional soil reaction springs are proposed here.

9. Recommendations & Future work approach

In the development of a CPT-based design method for large diameter piles by means of PLT data, the contributions of all soil reaction terms have to be determined in a first stage, starting with the *p-y* term. The *p* and *y* components are obtained by double integrating and respectively differentiating the moment profile that is measured during a pile load test that has been performed on a long pile. By means of a regression analysis on *qc* data and the derived *p-y* data, a CPT-based *p-y* formula can be developed after which the distributed moment and base- shear and moment can be investigated .

In Chapter 7, it is concluded that the available pile load test data in combination with the 'simple' MATLAB curve fitting techniques are not suitable for the derivation of the *p-y* term. Hence, further investigation into the contribution of the additional soil reaction terms and developing spring relations was not feasible based on the approach that is followed in this thesis.

This chapter addresses the pitfalls encountered in this research along with recommendations for further research on a new CPT-based method based on pile load test data. The chapter ends with recommendations for a new approach.

9.1 Soil reaction terms from PLT data

In the subsections below, it is described how problems regarding data quality, data interpretation and curve fitting can be mitigated and what further steps could be taken once an accurate soil pressure and pile displacement profile are obtained. This future work approach is summarized in Figure 9-1.

9.1.1 Data selection and processing

This thesis uses a database consisting of PLT data of several piles that have been tested in Dunkirk. For a few piles, also below ground strain data was made available from which only one pile is possibly long (*L/D*=8) enough to consider the *p-y* term as only governing soil reaction. The strain data is quite scattered and has not been recorded at the pile ends exactly. As explained in Chapter 0, the pile toe does hardly displace in the case of a long pile, therefore it is assumed that the pile has fixed pile toe condition in the further analysis of this pile. Though, it is not certain that the pile is indeed long enough to fulfil fixed pile toe conditions. Hence the analysis is error prone. For further research, it is recommended to use strain -and or inclination data that is measured from ground level to the very end of the pile. This way, it can be easily checked whether the pile end conditions are fixed and, which avoids that the derivation of *p-y* curves is based on assumptions. A simple and efficient way to gather strain data, is to use strain data from history PLTs.

Another point of interest is that during the PISA PLTs was accounted for creep displacements which also have effect on strain readings. Usually, *p-y* curves describe the load-displacement relationship under instantaneous loading instead of under creep. Therefore the strain data, in this research, is extracted just before the load was held constant in each load step. Though, in all previous load steps the pile was allowed to displace while the load was held constant, the extracted strain per load step is thus affected by the creep effect. In this approach, the PLT data is altered as little as possible and the results are true to the measured situation. However, for further research based on PISA PLT data, it can be interesting to alter the PLT data such that creep is ignored entirely. In Chapter 5 this was done already for the pile head rotations and -displacements in order to compare the existing *p-y* methods to PLT data (Figure 5-2and Figure 5-3). In Appendix D is shown what the effect is of ignoring creep is on strain measurements. Also the moment profile with and without creep is compared to moment profiles that are generated by the *p-y* methods from Equation (2.8), (2.10), (2.11), (2.14) and (2.16). Because of time constraint, the influence of creep effect on the soil pressure profiles could not be investigated further, but it is recommended to investigate this in future research.

Better even, is to perform rapid-load tests on piles in which the instantaneous response is captured directly. This avoids the radical modification (and along coming inaccuracies) of PLT measurements that is necessary when creep parts have to be removed from the data.

9.1.2 PLT tests

When it is desired to derive *p-y* curves from new PLTs, then the following recommendations are given regarding the execution of the tests itself:

9.1.2.1 Instrumentation

To avoid inaccuracies that come with curve fitting and differentiating the moment twice to get the soil pressure, it can be useful to explore instruments that measure the soil pressure directly. For example, the soil force could be measured by means of load cells that are distributed along the buried pile depth. The soil pressure is then simply the measured load divided by the vertical distance in-between the load cells. For all below-ground measurements, it is advised to record the data at regularly distributed depths and at least at ground level and at the pile tip.

9.1.2.2 Pile geometries

As explained earlier, pile load tests should be performed on piles that are long enough to have fixed conditions at the pile toe. In this research, a pile with *L/D* of 8 seemed not long enough to fulfil these conditions, therefore it is recommended to test piles that have an *L/D* of 10 or higher. To establish a relationship that accounts for the diameter effect, it is also advisable to vary the pile diameters.

For the development of short pile soil reaction terms and validation of the newly developed method, also pile load tests on piles with lower *L/D* ratios should be performed. For example an *L/D* of 3 and *L/D* of 5.25 which were tested in the PISA project.

9.1.3 Curve fitting

As with measurements in general, it is likely that strain data comes with noise in the data, taking the double derivative directly then leads to an irregular soil pressure profile. The smoothing spline in MATLAB, `csaps`, can be used to smoothen the data but is only applicable to piles that have fixed toe and tip conditions.

If strain data of such piles is not available, it might be useful to research the more advanced pp-form and B-form splines in MATLAB. Although the approach to construct these types of splines is not straightforward, it is possible to indicate the order of the spline, break points, coefficients and smoothing specifically. More information about curve fitting in MATLAB can be found in the online available 'user's guide for curve fitting' (The MathWorks, Inc, 2018).

9.1.4 CPT-based *p-y* formula

Once accurate soil pressure, displacement and *qc* profiles are obtained, a CPT-based relation for the *p-y* curve can be developed. Start with research into a parameterized equation that is capable of emphasizing the relation between the cone resistance *qc*, effective vertical stress σ_v' depth *z*, and diameter *D*. A good example is the updated relation of Suryasentana & Lehane (2016). Extensive research has been conducted prior to their publication and it is also the most recent CPT-based *p-y* method that has been published. By means of regression analysis, the coefficients making the closest fit to the input data can be derived. Ideally, soil pressure and displacement profiles of piles with varying diameters are used to relate *p, y* and *qc* to *D*.

A newly developed CPT-based *p-y* relationship can be validated by simulating the pile response of other (long) piles by means of the new CPT springs, and compare the calculated pile head displacements with measurements.

9.1.5 CPT-based short pile reaction terms

Once the CPT-based *p-y* formula is validated, the contributions of the short pile reaction terms can be investigated. The following steps can be used to derive a relation for the base shear spring, $F_b(y)$, base rotation spring, $m_b(\theta)$, and distributed rotation springs, *t-z*.

As explained in Subsection 2.5.4, preliminary assumptions for these spring relations can be found in the DNV (2017) and API (2011). The distributed rotational springs presented in Equation (2.22), (2.23), and (2.25) are already *qc* dependent. To make the base shear and rotation *qc* dependent as well, it is advised to study the relation between *qc* and *G0* and the relation between *qc* and the vertical base shear first.

The extra soil reaction terms can be incorporated in the soil response model of Chapter 4, by adding rotational springs with an extra rotational and translational spring at the base. The performance of the springs can be checked by modelling the pile response for several short piles and comparing the calculated internal moments with the measured moments (from strain gauge readings).

Future work approach

Data selection and processing

1. PLT on long pile (pile toe is fixed)
2. Measure soil pressure directly by means of load cells or:
    2. Measure strain from ground level to pile toe

↓ $\phi = \frac{\varepsilon_{compression} - \varepsilon_{tension}}{D}$

$M = \phi EI$

    3. Discrete moment

↓ *Curve fitting: research into advanced spline fitting*

    4. Continuous moment profile

↓ $y = \iint M/EI + \theta_0 z + y_0$

$p = -\frac{d^2M}{dz^2}$

CPT-based *p-y* formula

5. *p* and *y* values along pile depth + parameterised equation + *qc*, σ_v', *z*, *D*

↓ *Regression analysis*

6. *p-y* formula long pile

↓ *Simulation with pile-response model*

7. Check modelled vs. Measured ground displacement

↓ *Update p-y relation*

8. Updated formulation *p-y*

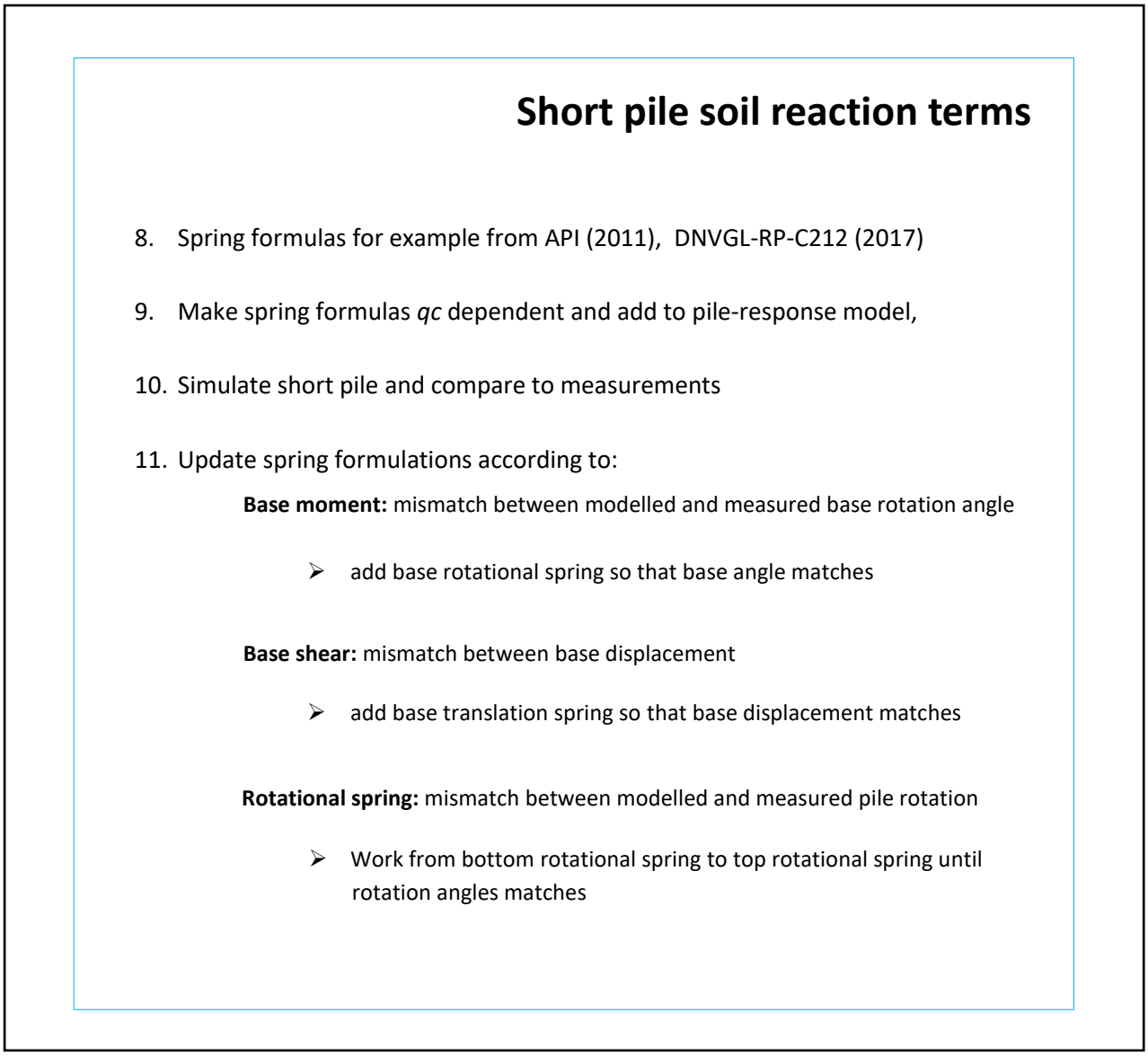

Figure 9-1: Approach for further research into the development of a CPT-based design method based PLT data

9.2 Soil reaction terms from 3D FEM

The steps presented in the work approach described in this chapter, follow each other up like a chain in which if one of the steps leads to inaccurate results, the succeeding steps would be inaccurate too (garbage in, is garbage out). Hence, the success of the approach taken in this thesis is highly dependent on data availability, quality of the data and curve fitting limitations.

Therefore it might be useful to perform further research into other approaches that can be used to extract soil reaction terms. Problems regarding data availability and quality can be avoided by means of numerical analysis in which pile deformations are simulated in a soil continuum model. From a FEM model much more information about pile deformation can be extracted than with PLT measurements. For example, 3D FEM analysis was used to derive the soil springs for short pile behaviour in the PISA Project. This is discussed in Subsection 2.5.3.

References

4 C Offshore, 2018. *4 C Offshore.* [Online] Available at: https://www.4coffshore.com/windfarms/turbines.aspx

Andersen, K. & schjetne, K., 2013. Database of Friction Angles of Sand and Consolidation Characteristics of Sand, Silt, and Clay. *Journal of Geotechnical and Geoenvironmental Engineering*, 139(7), pp. 1140-1155.

API, 2011. Geotechnical and foundation design considerations, ANSI/API RP 2GEO. In: Washington, DC: API Publishing Services..

Arany, L., Bhattacharya, S., Macdonald, J. & Hogan, S. J., 2014. *Simplified critical mudline bending moment spectra of offshore wind turbine support structures.* Bristol, UK, John Wiley & Sons.

Ardalan, H., Eslami, A. & Nariman-Zahed, N., 2009. *Piles shaft capacity from CPT and CPTu data by polynomial neural networks and genetic algorithms.* Comput. Geotech., 2009, 36, 616–625.

Baguelin, F., Frank, R. & Said, Y. H., 1977. Theoretical Study of Lateral Reaction Mechanism. *Geotechnique,* Volume Vol. 27, No. 3, pp. 405-434.

Borgard, D. & Matlock, H., 1980. Simplified Calculation of p-y Curves for Laterally Loaded Piles in Sand. *Proceedings, 5th Offshore Technology Conference,* Volume OTC, Paper 4501, 495-502..

Broms, B., 1964. Lateral Resistance of Piles in Cohesionless Soils. *Journal of the Soil Mechanics and Foundations Division, Proceedings of the ASCE ,* Volume 90, No.SM3, 123-156.

Burd, H. et al., 2017. Design aspects for monopile foundations. *Proceedings of TC 209 workshop 19th ICSMGE*, pp. 35-44.

Bussel, G. J. v., 2008. *http://mstudioblackboard.tudelft.nl.* [Online] Available at: http://mstudioblackboard.tudelft.nl/duwind/Wind%20energy%20online%20reader/

Byrne, B. & Houlsby, G., 2004. Foundations for offshore wind turbines. *Philosophical Transactions of The Royal Society A Mathematical Physical and Engineering Sciences*.

Byrne, B. et al., 2015a. New design methods for large diameter piles under lateral loading for offshore wind applications. *Proc 3rd International Symposium on Frontiers in Offshore Geotechnics (ISFOG 2015),* Oslo, Norway.

Byrne, B. et al., 2015b. Field testing of large diameter piles under lateral loading for offshore wind applications. *Proc 15th European Conf on Soil.*.

Byrne, B. et al., 2017. PISA: NEW DESIGN METHODS FOR OFFSHORE WIND TURBINE MONOPILES. *OSIG 2017,* pp. 142-161.

Chen , J., 2016. *Oil Field Development Engineering.* [Online] Available at: https://www.ofdeng.com/offshore.html [Accessed 2018].

Chow, F., 1997. *Investigations into the behaviour of displacement piles for offshore foundations.* PhD thesis, Imperial College, University of London.

Corbetta, G., Ho, A. & Pineda, I., 2015. *Wind energy scenarios for 2030,* s.l.: the European Wind Energy Association.

Davidson, H. L. & Donovan, T. D., 1983. DESIGN OF LATERALLY LOADED DRILLED PIERS. *IEEE Transactions on Power Apparatus and Systems,* Volume PAS-102, No. 1.

DNV, 1992. Foundations. *Classification notes 30.4.*

DNV, 2017. Offshore soil mechanics and geotechnical engineering. *DNVGL-RP-C212.*

DNV-OS-J101, 2014. *Design of Offshore Wind Turbine Structures,* s.l.: DET NORSKE VERITAS AS.

Dyson, G. J. & Randolph, M. F., 2001. Monotonic lateral loading of piles in calcareous sand. *J. Geotech. Geoenviron. Engng,* 127(4), p. 346–352.

EUCO 169/14, 2014. *Conclusions on 2030 Climate and Energy Policy Framework,* Brussels: European Council.

Eurocode7, NEN-EN 1997-1. Geotechnisch ontwerp - Deel 1: Algemene regels.

Gavin, K., Igoe, D. & Kirwan, L., 2013. The effect of ageing on the axial capacity of piles in sand. *Proc. Inst. Civ. Eng. – Geotech. Engng,* 166(2), p. 122–130.

Haiderali, A. E. & Madabhushi, G., 2016. Evaluation of curve fitting techniques in deriving p-y curves for laterally loaded piles. *Geotechnical and Geological Engineering,* 34(5).

Hald, T. et al., 2009. Revisiting monopile design using p–y curves – results from full scale measurements on Horns Rev. *Proceedings of the Europeanoffshore wind conference and exhibition,* Stockholm, Sweden.

Houlsby , G. T. & Hitchman, . R., 1988. Calibration chamber tests of a cone penetrometer in sand. *Géotechnique,* 38(1), pp. 39-44.

Hoving, J., 2016. *OE44095 Bottom founded offshore structures, Offshore Foundation Design Theory.* Delft, TU Delft.

Hoving, J., 2016. *OE44095 Bottom founded offshore structures, Offshore Foundation Design Theory.* Delft, TU Delft.

Huang, J.-w., 2011. *Development of modified p-y curves for Winkler Analysis to characterize the lateral load behavior of a single pile embedded in improved soft clay.* Iowa: Iowa State University.

Igoe, D., Gavin, K. & B., O., 2011. Shaft capacity of openended piles in sand. *J. Geotech. Geoenviron. Engng,* 137,(No. 10).

Jamiolkowski, M., Lo Presti, D. & Manassero, M., 2003. Evaluation of relative density and shear strength of sands from CPT and DMT. *Soil behavior and soft ground construction: proceedings of the symposium,* 19(Geotechnical Special Publication), pp. 201-238.

Janoyan, K. D. & Whelan, M., 2004. Interface Stresses Between Soil and Large Diameter. *ASCE Geotechnical Special Publication No. 124, "Drilled Shafts, Micropiling, Deep Mixing, Remedial Methods, and Specialty Foundation Systems"*.

Kulhawy, F. & Mayne, P., 1990. Manual on estimating soil properties for foundation design. *Electric Power Research Institute (EPRI),* Volume (EPRI Report ; EL-6800).

Lemnitzer, A., 2013. *www.findapile.com.* [Online] Available at: http://www.findapile.com/p-y-curves/definition

Liingaard, M., 2013. Pile Soil Analysis (PISA) Project. *Join-industry project: improved design methods for laterally loaded piles*.

Li, W., Igoe, D. & K., G., 2014. Evaluation of CPT-based P–y models for laterally loaded piles in siliceous sand. *Géotechnique Letters,* Issue 4, p. 110–117.

Lourens, E.-M., 2016. *OE5662 Offshore Wind Farm Design, Support Structure Design.* Delft, TU Delft.

Luff, B., 2007. Back Analyses of Pile Behaviour in Perth Dune Sand. Honours. *Thesis, School of Civil and Resource Engineering, University of Western Australia.*

Lunne, T., Robertson, P. & Powell, J., 1997. *Cone Penetration Testing in Geotechnical Practice.* New York, Blackie Academic/Routledge Publishing.

M.I., R., D., B. S. & Popescu, R., 2013. Offshore anchor piles under mooring forces: centrifuge modelling. Canadian Geotechnical Journal , 50, No. 1, 373–381..

Mayne, P., 2007. In-Situ Test Calibrations for Evaluating Soil Parameters. *Engineering Properties of Natural Soils,* Volume 3.

Mayne, P., Christopher, B. & DeJong, J., 2002. Subsurface Investigations: Geotechnical Site Characterization: Reference Manual: NHI Course No. 132031",National Highway Institute, Washington, Report / Federal Highway Administration, No. FHWA-NHI-01-031..

Mayne, P., Peuchen, J. & Bouwmeester, D., 2010. Soil Unit Weight Estimated from CPTu in Offshore Soils. *Frontiers in Offshore Geotechnics II: Proceedings of the 2nd International Symposium on Frontiers in Offshore Geotechnics,* pp. 371-376.

McClelland, B. & Focht, J. A., 1958. *Soil Modulus for Laterally Loaded Piles.*. ASCE, No. 2954, 1049-1063.

Novello, E., 1999. *From static to cyclic P–y data in calcareous.* Perth, Proc. 2nd Int. Conf. on Engineering for Calcareous, p. 17–27.

Novello, E., 1999. From static to cyclic P–y data in calcareous. In: *Proc. 2nd Int. Conf. on Engineering for Calcareous.* Perth: s.n., p. 17–27.

O'Neill, M. W. & Murchison, J. M., 1983. *An evaluation of p–y relationships in sands,* report to American Petroleum Institute. Houston, TX, USA: University of Houston.

Pando, M. et al., 2006. A Laboratory and Field Study of Composite Piles for Bridge Substructures. *Report to VirginiaTransportation Research Council, March 2006.*

Peralta, P., 2010. *Investigations on the Behavior of Large Diameter Piles under Long-Term Lateral Cyclic Loading in Cohesionless Soil,* Hannover: Institut für Geomechanik (IGtH) Leibniz Universität Hannover.

Prendergast, . L., 2015. *Monitoring of scour around structures using changes in natural frequency of vibration.* PhD thesis, University College Dublin.

Reese, L. C., Cox, W. R. & Koop, F. D., 1974. Field Testing of Laterally-Loaded Piles in sand.. *Sixth Annual Offshore Technology Conference,* Volume OTC Paper 2080, 473-483.

Robertson, P., 2009. Interpretation of Cone Penetration Tests - a unified approach. *Canadian Geotechnical Journal,* Volume 64, pp. 1337-1355.

Suryasentana, S. K. & Lehane, B. M., 2014a. Numerical derivation of CPT-based p-y curves for piles in sand. *Géotechnique,* 64(No. 3), p. 186–194.

Suryasentana, S. & Lehane, B., 2016. Updated CPT-based p–y formulation for laterally loaded piles in cohesionless soil under static loading. *Géotechnique 66, No. 6,* p. 445–453.

Suryasentana, S. & Lehane, B. M., 2014b. Verification of numerically derived CPT based p-y curves for piles in sand. *3rd International Symposium on Cone Penetration Testing,* vol. 1(3rd International Symposium on Cone Penetration Testing, Las Vegas, Nevada, United States, 13/05/14), pp. 1013-1020.

The MathWorks, Inc, 2018. *Curve Fitting Toolbox™ User's Guide.* R2018a ed. Natick: The MathWorks, Inc.

Titi, H. H. & Abu-Farsakh, M. Y., 1999. *EVALUATION OF BEARING CAPACITY OF PILES FROM CONE PENETRATION TEST DATA,* Baton Rouge, LA: Louisiana Transportation Research Center.

Venville, C. S., 2004. Lateral Loading of Grout Piles – Testing & Interpretation. *Honours Thesis, School of Civil and Resource Engineering, University of Western Australia.*

Wesselink, B. et al., 1988. Analysis of centrifuge model test data from laterally loaded piles in calcareous sand. In Jewell and Andrews (eds). *Proc. of Engineering for calcareous sediments,* pp. 261-270. Balkema, Rotterdam..

Williams, A. et al., 1988. The performance and analysis of lateral load tests on 356 mm dia piles in reconstituted calcareous sand. *In Jewell and Andrews (eds), Proc. of Engineering for calcareous sediments:,* pp. 271-280.Balkema, Rotterdam..

Windeurope, 2018. Annual combined onshore and offshore wind energy statistics. *Wind in power 2017,* February.

Wrana, B., 2015. *PILE LOAD CAPACITY – CALCULATION METHODS.* Studia Geotechnica et Mechanica, Vol. 37, No. 4, 2015.

Yang, K. & Liang, R., 2006. Method for derivinfg p-y curves from instrumented lateral load tests. *Geotechnical Testing Journal,* 30(1).

Appendix

A. Soil parameters PISA project

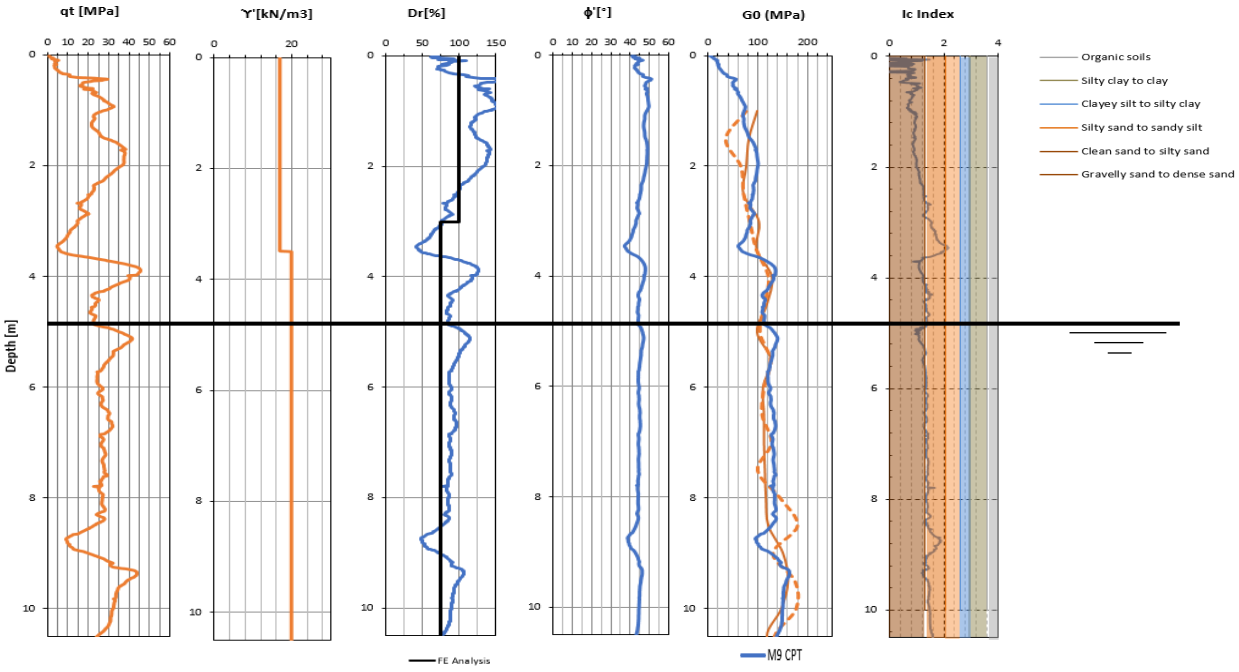

Figure 0-1: Soil parameters derived in PISA Project for location DL2

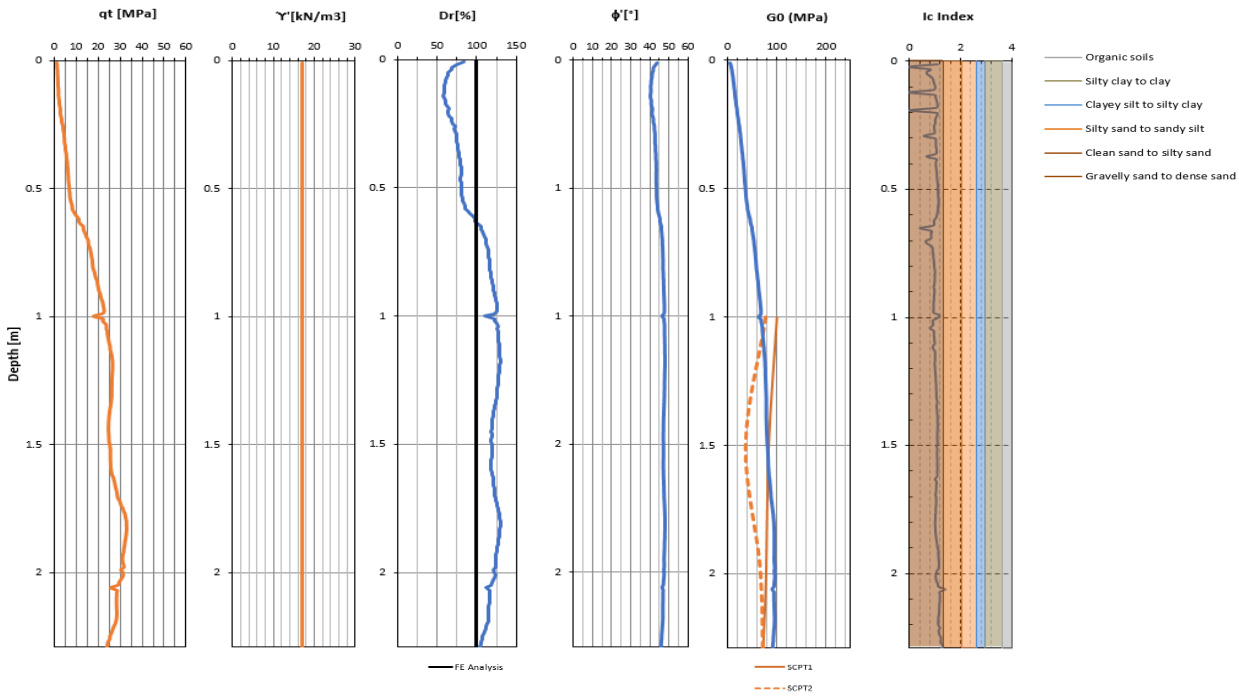

Figure 0-2: Soil parameters derived in PISA Project for location DM7

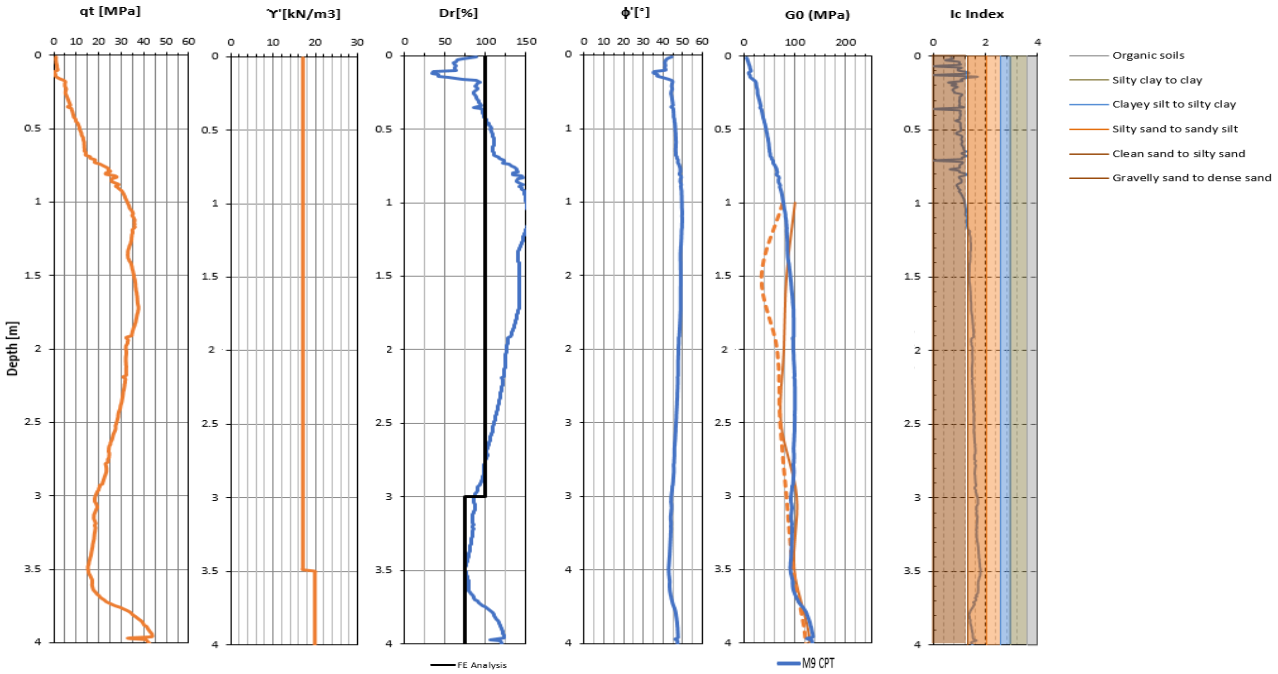

Figure 0-3: Soil parameters derived in PISA Project for location DM9

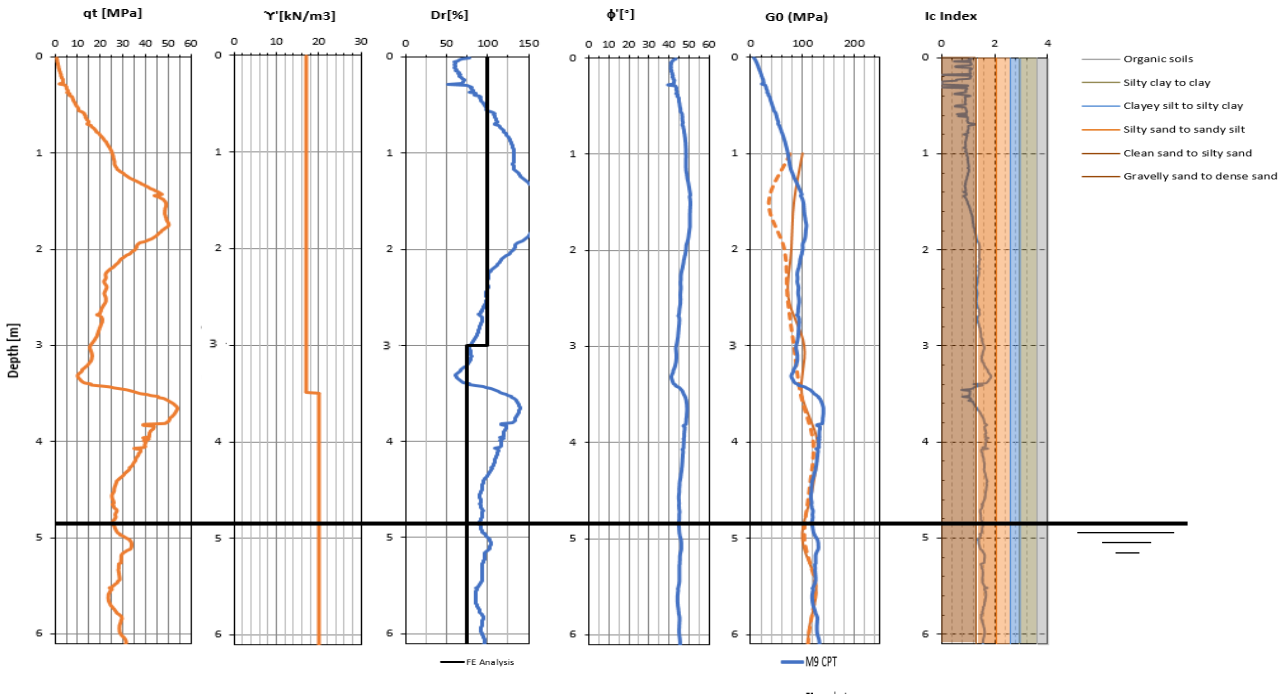

Figure 0-4: Soil parameters derived in PISA Project for location DM3

B. Soil parameters for *p-y* evaluation

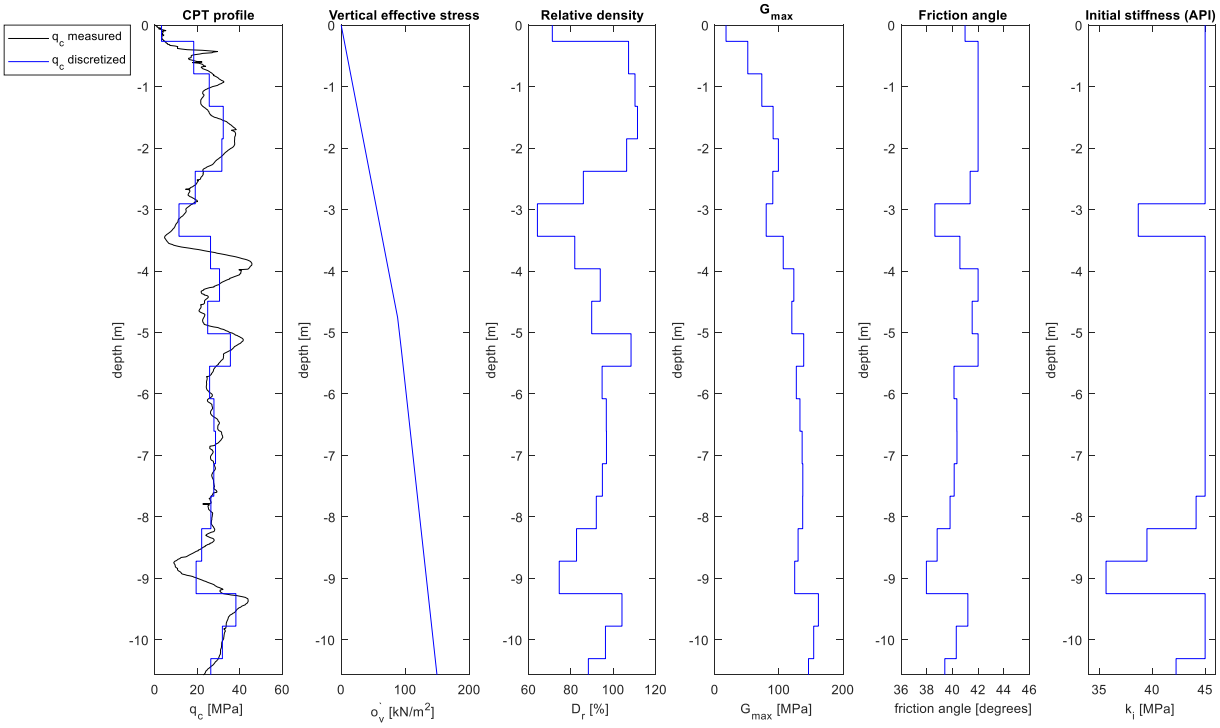

Figure 0-5: Soil parameters used for DL2 in pile-response model

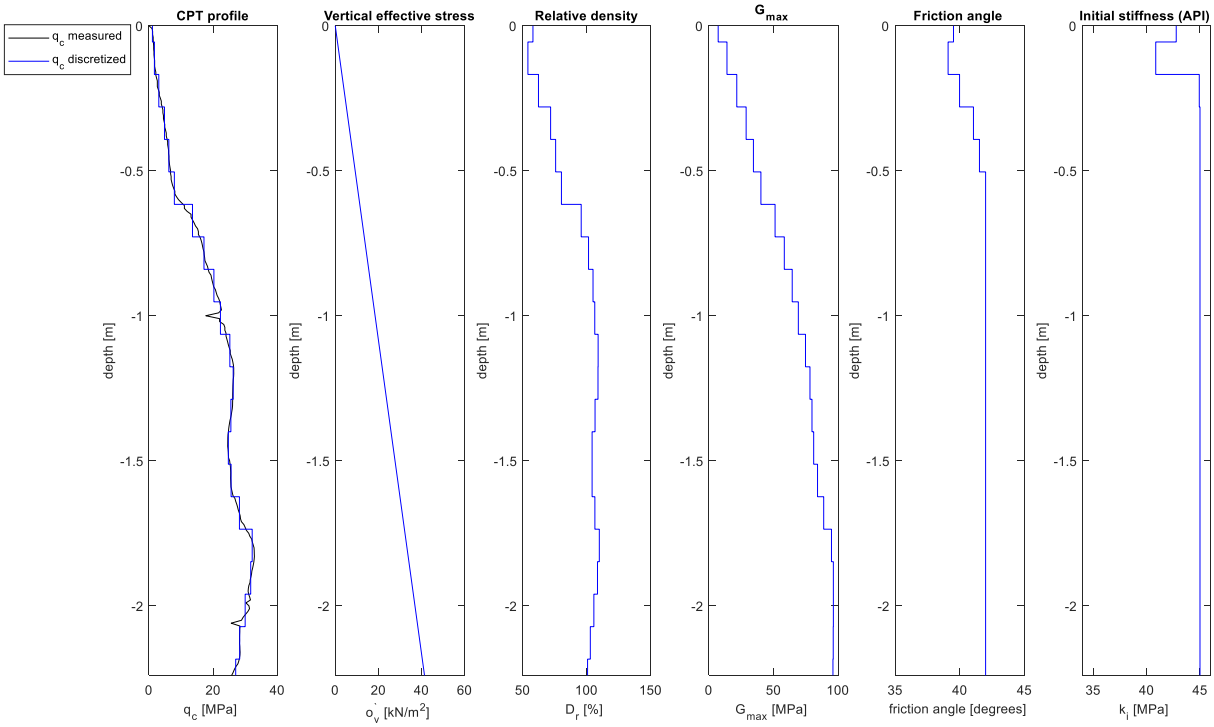

Figure 0-6: Soil parameters used for DM7 in pile-response model

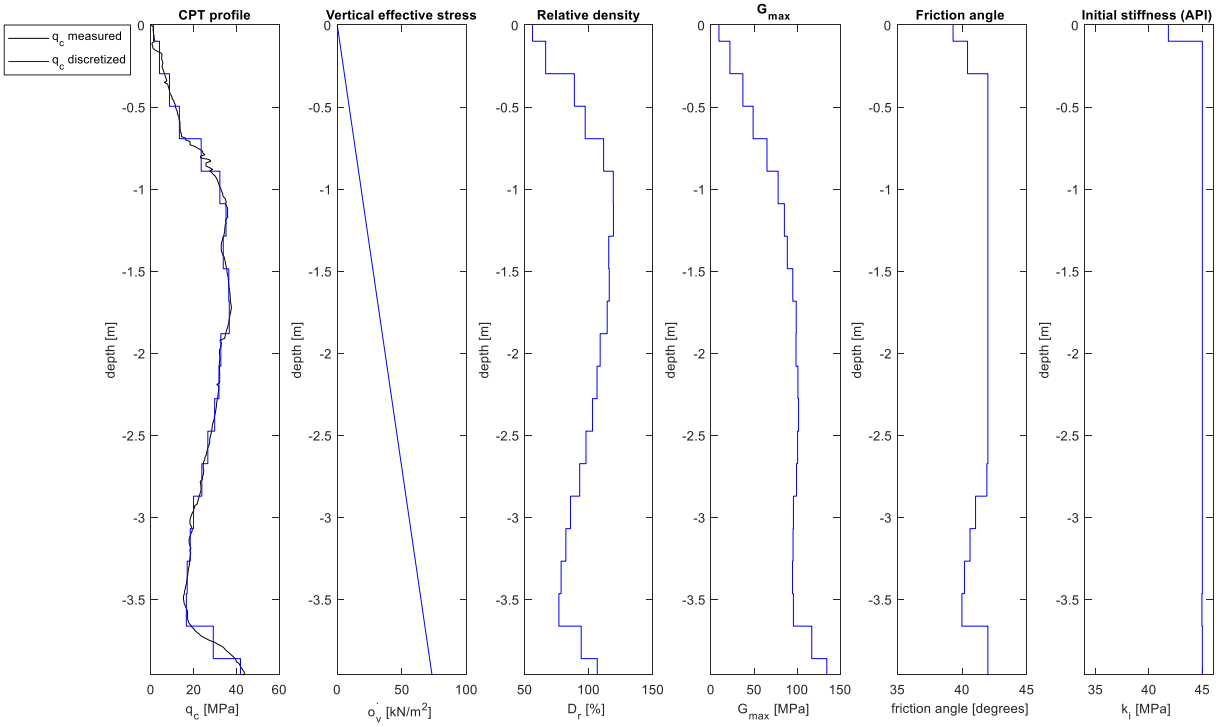

Figure 0-7: Soil parameters used for DM9 in pile-response model

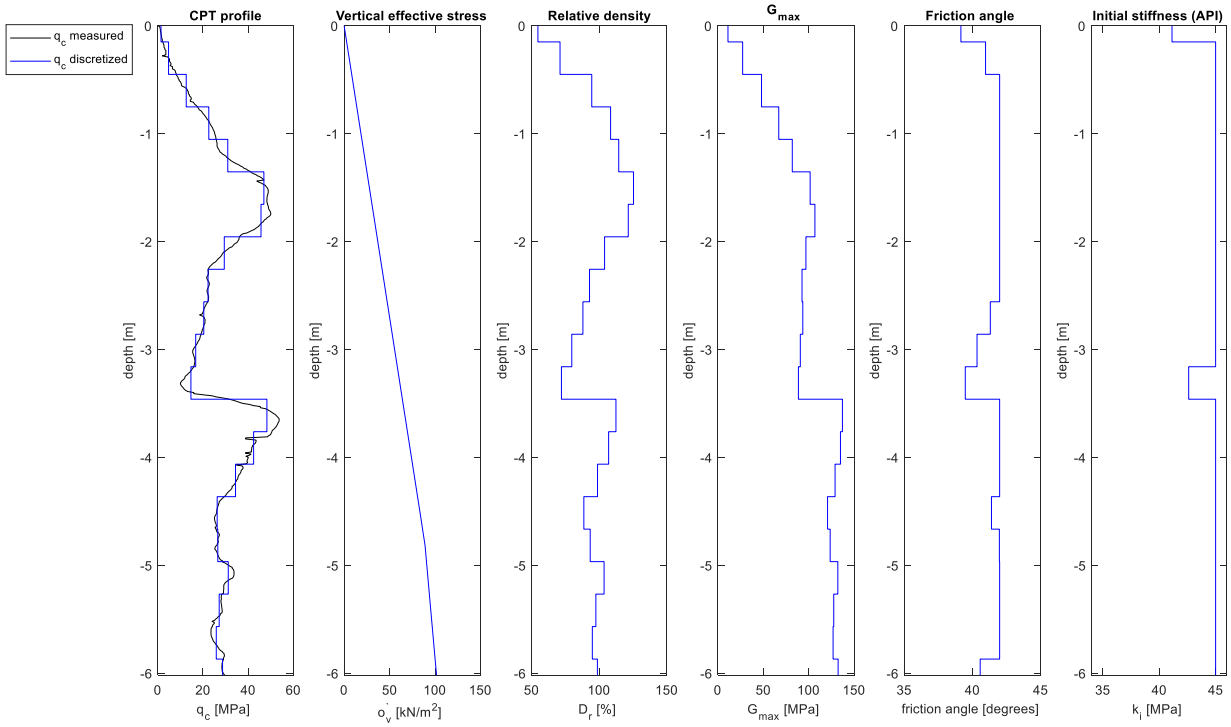

Figure 0-8: Soil parameters used for DM3 in pile-response model

C. Influence of soil parameters on pile response per *p-y* method

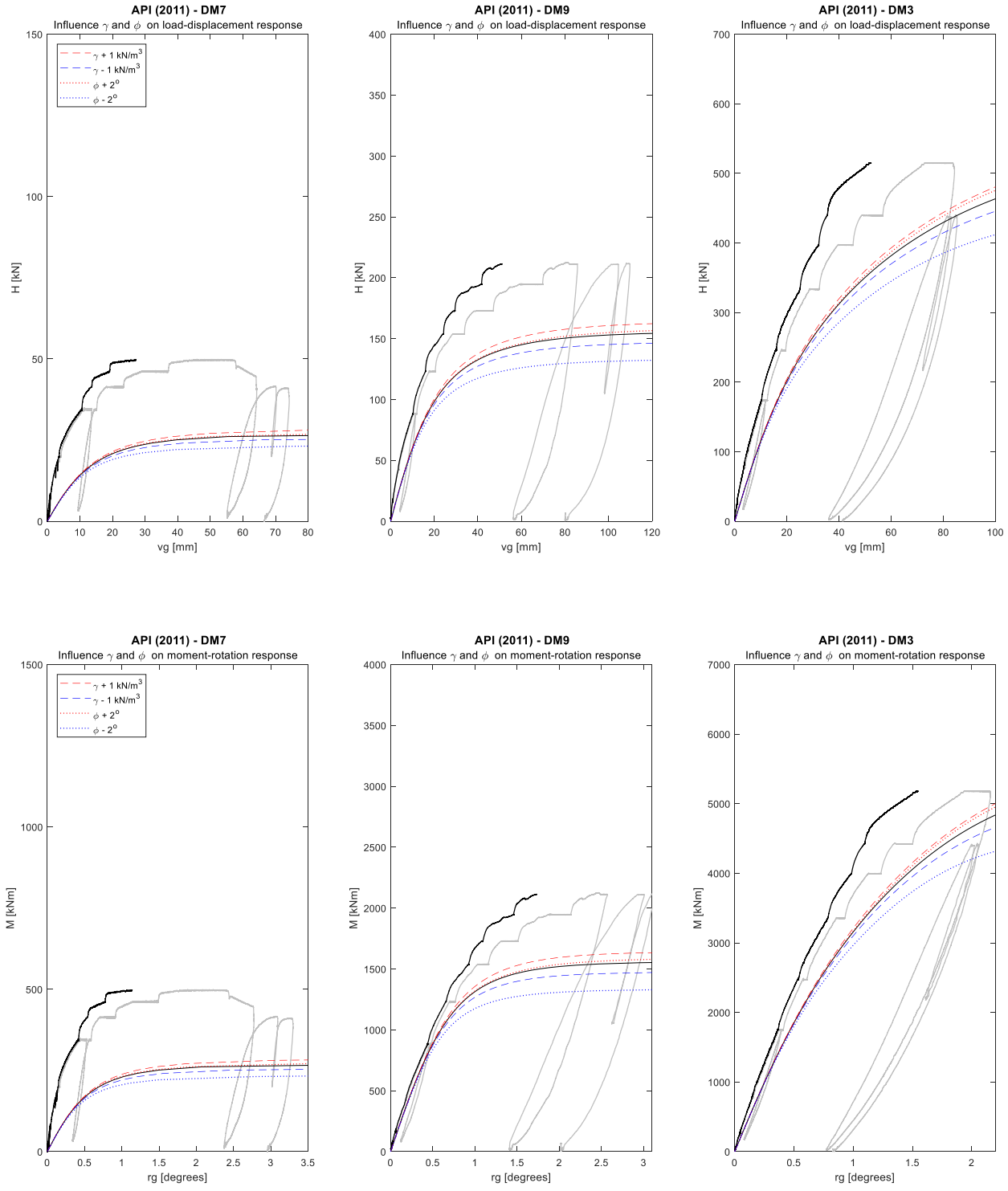

Figure 0-9: Influence variance in soil parameters on pile behaviour modelled according to API (2011)

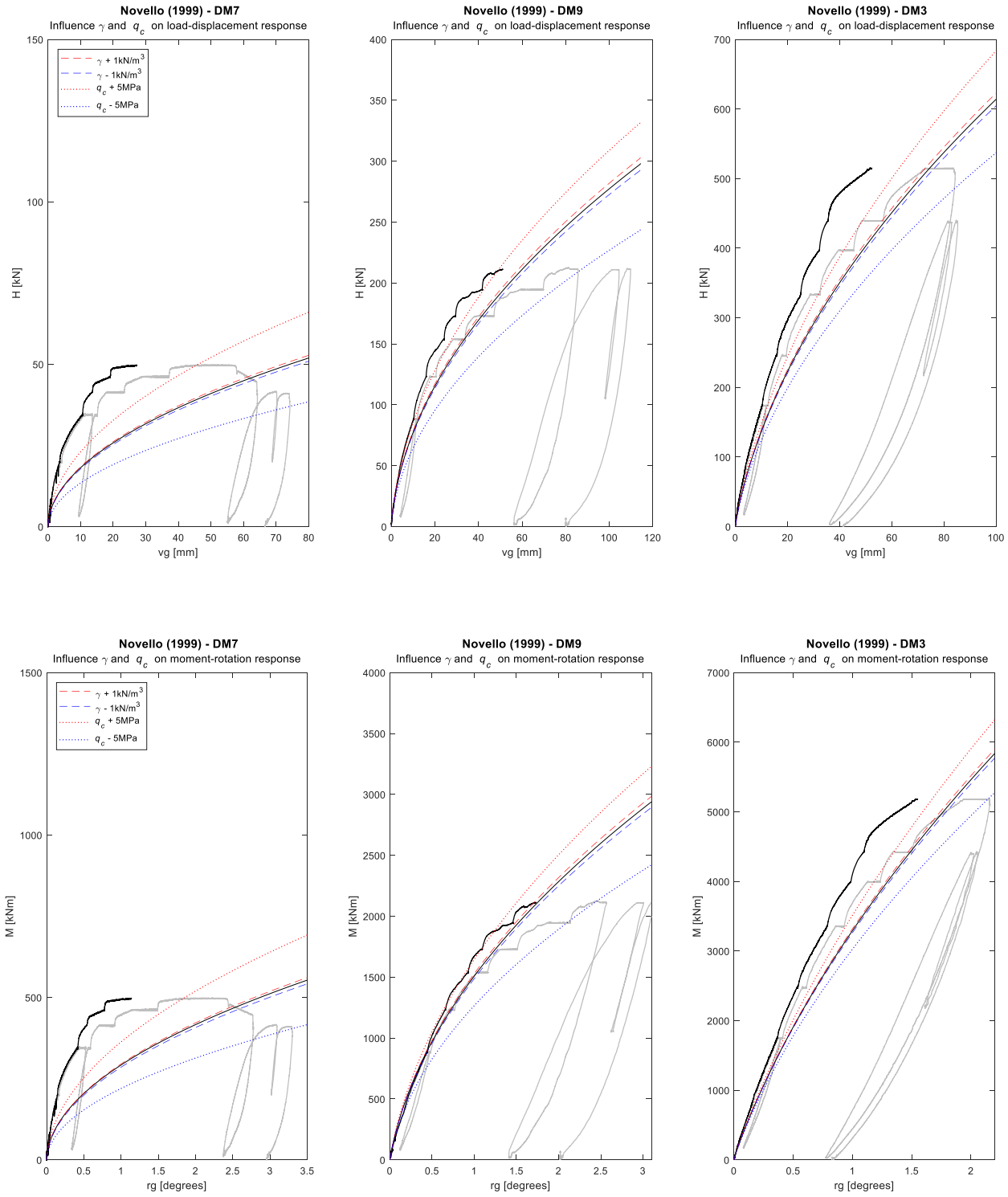

Figure 0-10: Influence variance in soil parameters on pile behaviour modelled according to Novello (1999)

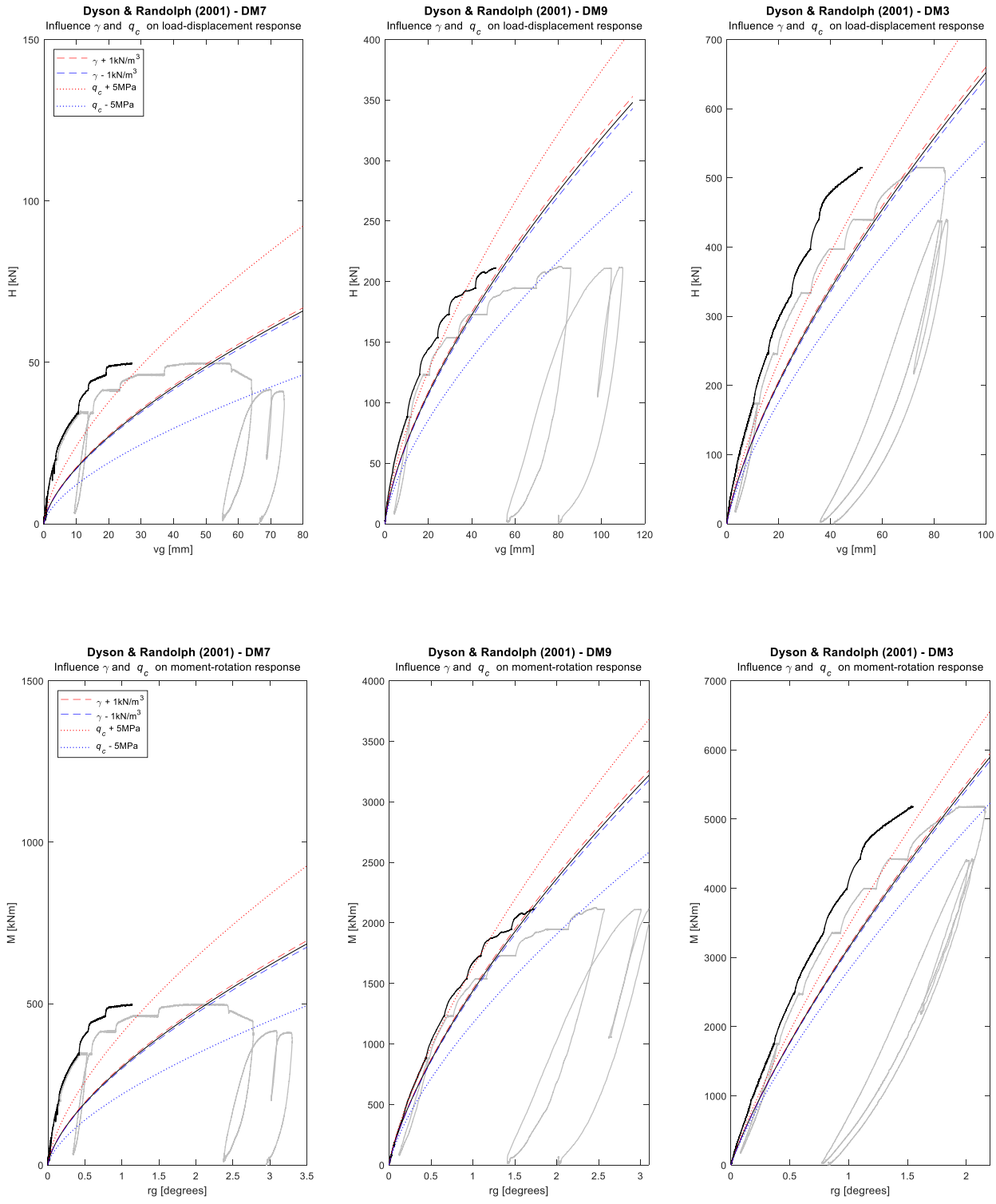

Figure 0-11: Influence variance in soil parameters on pile behaviour modelled according to Dyuson & Randolph (2001)

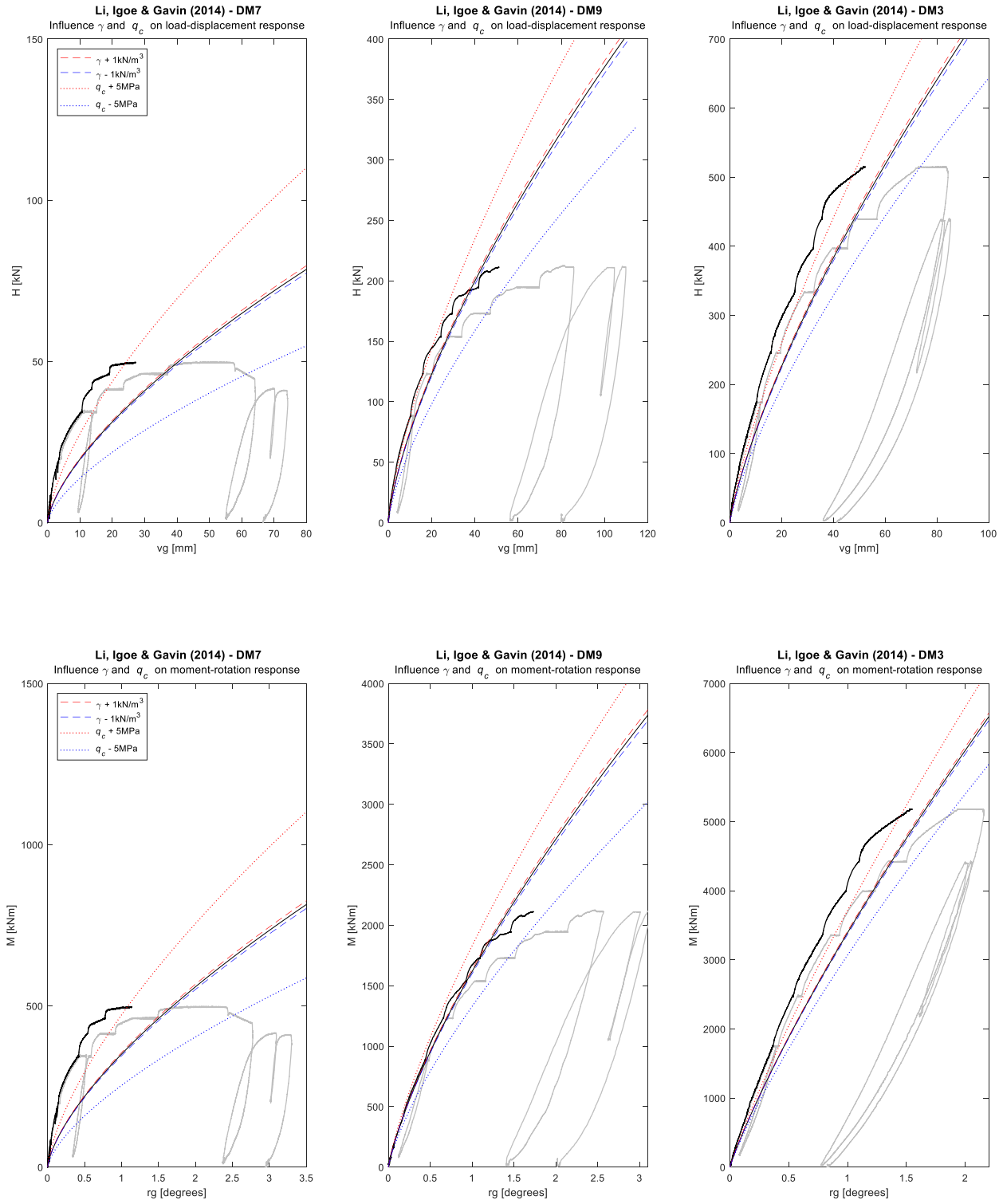

Figure 0-12: Influence variance in soil parameters on pile behaviour modelled according to Li, Igoe & Gavin (2014)

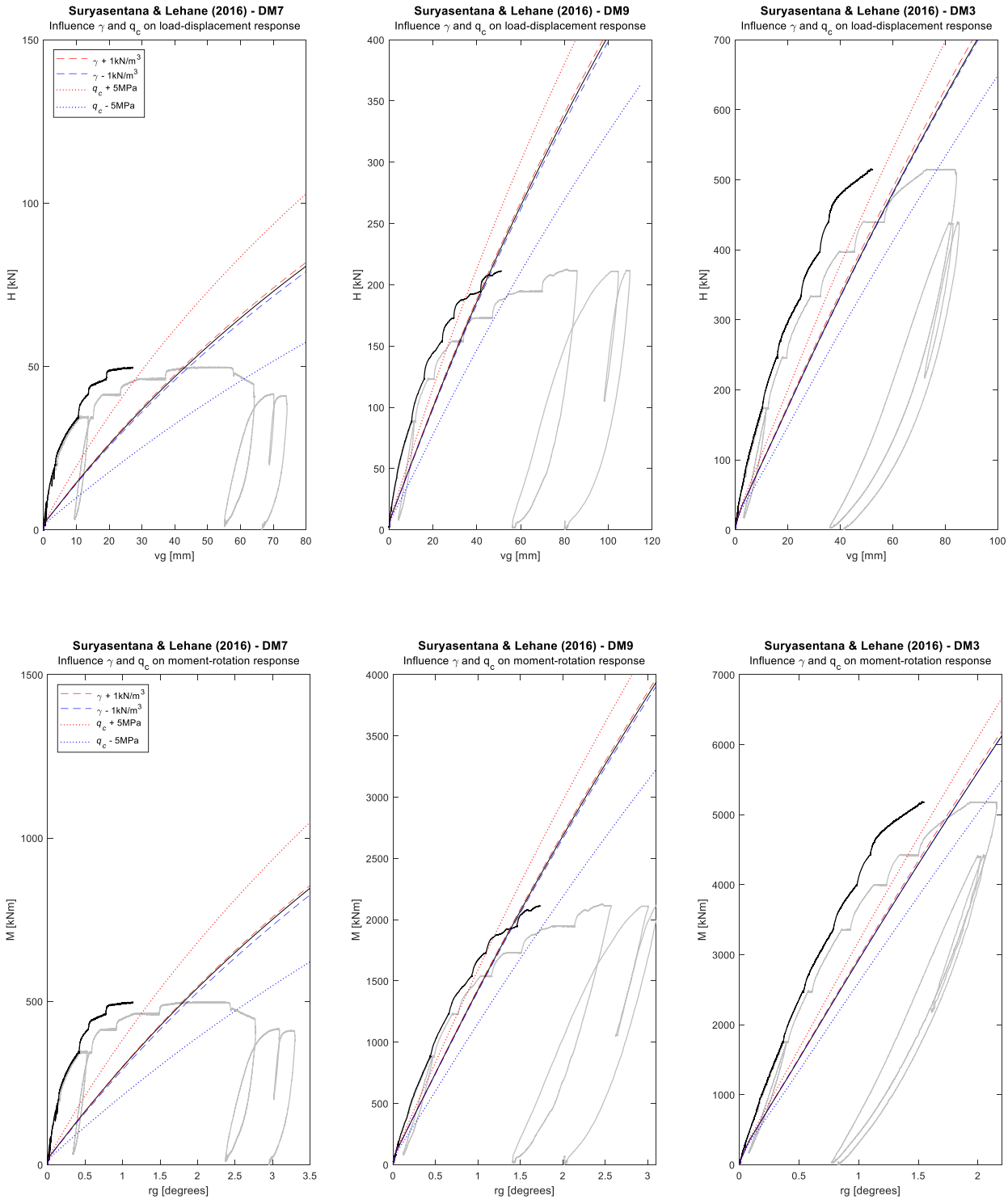

Figure 0-13: Influence variance in soil parameters on pile behaviour modelled according to Suryasentana & Lehane (2016)

D. Influence of creep on PLT strain data

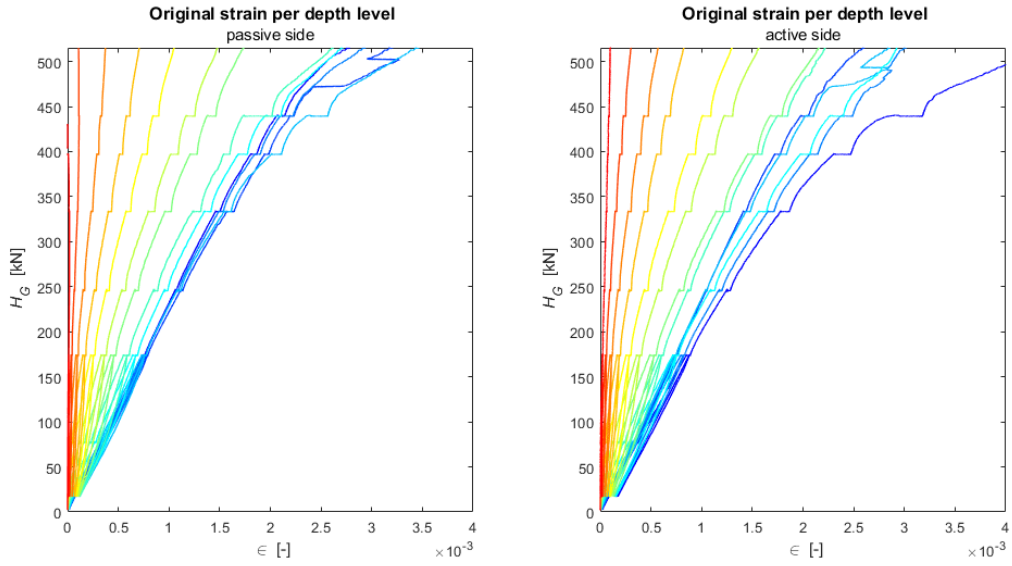

Figure 0-14: Original PLT strain data per each depth level

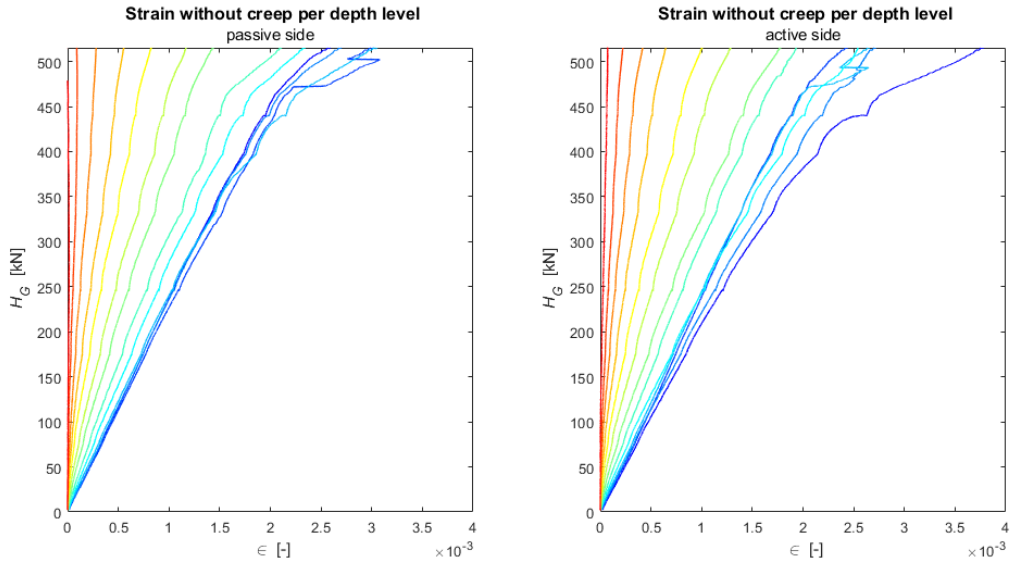

Figure 0-15: PLT strain data per each depth level with creep removed

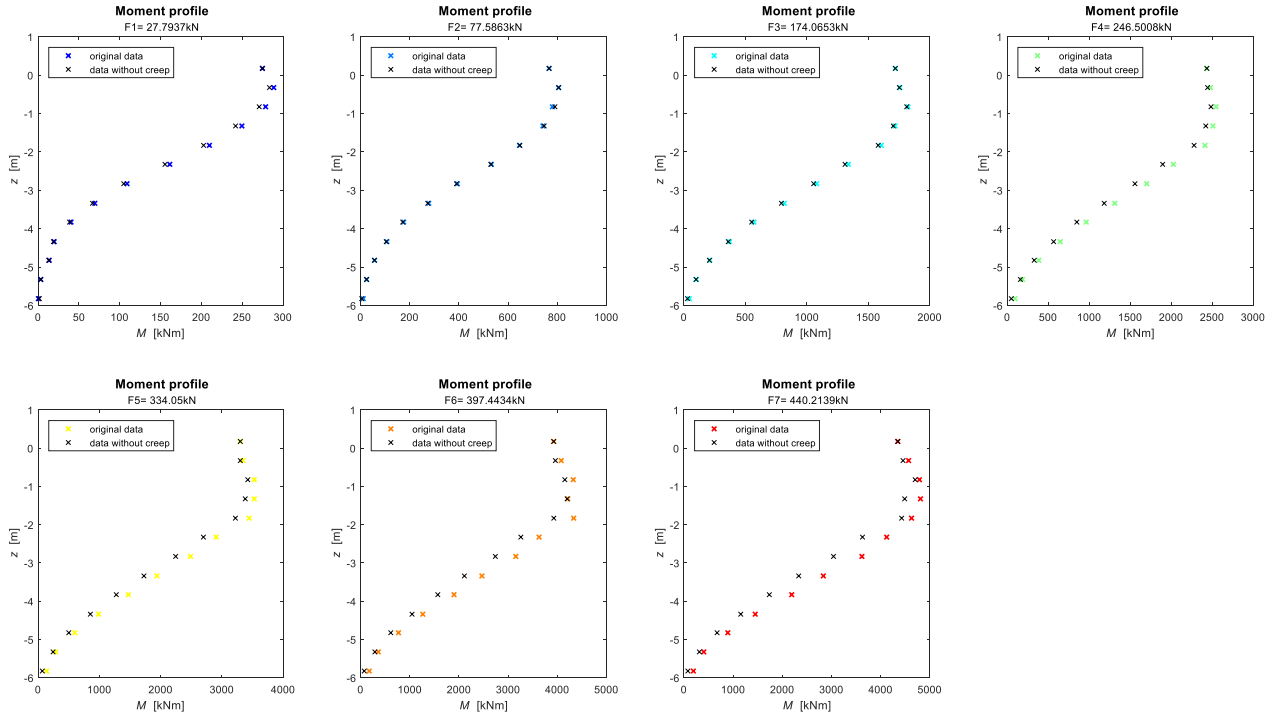

Figure 0-16: Influence of creep effect on moment profile per load step

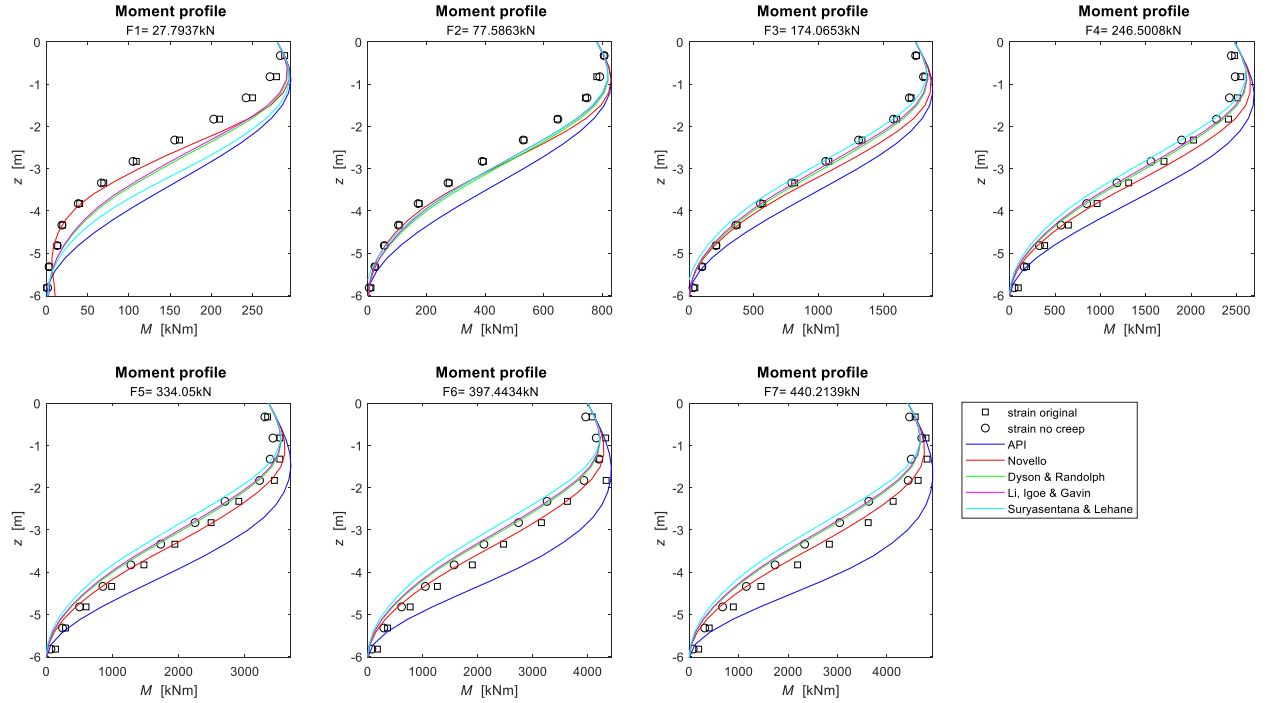

Figure 0-17: PLT moments compared with moments calculated by means of p-y methods

List of tables and figures